THE POTENTIAL FOR EMULATING THE HUMAN FOOTSTRIKE USING A SIX DEGREES-OF-FREEDOM INDUSTRIAL ROBOT

A Doctoral Thesis Submitted in Partial Fulfilment of the Requirements for the Award of Doctor of Philosophy of Loughborough University

By

James Allen Jones

Wolfson School of Mechanical and Manufacturing Engineering

Loughborough University

United Kingdom

July, 2014

CERTIFICATE OF ORIGINALITY

This is to certify that I am responsible for the work submitted in this thesis, that the original work is my own except as specified in the acknowledgements or footnotes, and that neither the thesis nor the original work contained therein has been submitted to this or any other institution for a higher degree.

……. (Signed)

……. (Date)

For Grandma,

'You were barely ten minutes old when I held you in my arms. Your large blue eyes looked straight into mine and from that moment on I was sentenced to do your bidding.'

ACKNOWLEDGEMENTS

There have been times in the last five years when writing this page seemed a long way off… It certainly has been a long and interesting journey, which has had its many ups and downs. There are a number of people that I have to thank for all of the help and support that I have received during my time in Loughborough. First of all I would like to say a huge thank you to my PhD supervisors; Dr Steph Forrester, Professor Roy Jones, Dr Paul Leaney and Dr Andy Harland. Your advice and expertise has been invaluable throughout the process. I would also like give a big thanks to the Sports Tech Institute technician team, both past and present; Steve, Max, Rue and Simon – your help has been invaluable! Thanks for putting up with my when I break things/cant get them to work properly.

To Mum and Dad, you have been there for me every step of the way, you've never stopped believing in me and your constant support and encouragement has gotten me through every challenge I've ever faced– thank you. To my Grandparents, I know how proud this would make you – thank you for everything!

I'd also owe a huge thanks to all of my friends, the majority of you left me behind as you went off into the real world and got a 'proper job', but never the less you were always there for me offering support, encouragement and most importantly distractions. The whole team at the STI have helped to make my PhD that little bit easier be it through technical advice or one of our many tea breaks and of course not forgetting Christmas golf! Finally to the Haze family – you have been a massive part of a defining moment in my life, new friends and a new sport to love have been without a doubt the highlight of my time in Loughborough. Through happy times and sad, these bonds can never be broken.

ABSTRACT

Part of the testing process for athletic footwear is exposing the shoes to realistic wear conditions; this can be in the form of user trials or, as is becoming more common place, the use of mechanical test devices. However, current mechanical test devices tend to be somewhat simplistic and fail to expose the footwear to the realistic loading environment. Thus, the aim of this thesis was to investigate the potential of using an off the shelf 6 Degrees-of-Freedom industrial robot to emulate the ground contact phase of human gait. This was achieved through addressing four research questions.

The first research question aimed to outline the biomechanical features that were to be emulated and what their typical values were. Kinematics and kinetics of the real human gait were then collected, for use in programming the robot and evaluating its outputted movements. This was complemented by a comprehensive review of relevant literature.

Previous investigations had highlighted the need for understanding of the robot's capabilities. This was taken further and input parameters such as level of robotic smoothing, programme velocity and the number of three dimensional co-ordinate points used were found to have an effect on the output kinematics of the robot. These features were also found to be part of the accompanying programme software (RoboGuide). Despite this, the differences were not identical and it was concluded that the software could only have a limited use in supporting the wider thesis aim.

Prior to emulation, there was a need for robot set-up and its environment to be optimised. A new robot end-effector, with improved biofidelity, was developed which incorporated a new way of generating the robot motion that intended to aid kinetic and kinematic emulation. Further to this, analysis on robot movements in various locations identified the optimal location for the ground contact phase to be achieved.

Using all of the gathered knowledge the robot was programmed to complete a footstrike for human walking using two types of programming method. When the robot is programmed directly with the human kinematic data the emulation of the footstrike is relatively poor; ground contact time is too long with an increased footprint size and poor ground reaction force profiles replication. Using a rotation about a fixed point on the footform led to improved, although not complete, emulation of the human gait parameters.

The developed system has been shown to improve on previous work at Loughborough University and is also comparable with what is being used in industry and developed within academia. The concept remains in the early phases but the current study indicates that future work can move the robot further towards being able to produce a more biofidelic emulation that can be used in the footwear testing industry.

TABLE OF CONTENTS

Chapter 1 - Introduction **1**
1.1 Background 1
1.2 Mechanical Testing in the Footwear Industry 2
1.3 Thesis Aims and Research Questions 3
1.4 Thesis Structure 5

Chapter 2 – Literature Review **7**
2.1 Functional Anatomy of the Foot 8
2.1.1 Bones of the Foot 8
2.1.2 Joints of the Foot 10
2.1.3 Arches of the Foot 12
2.1.4 Muscles and Soft Tissue 12
2.2 Foot-Ground Interaction During Gait 15
2.2.1 Stages of the Ground Contact Phase 15
2.2.2 Walk to Run Transition 18
2.2.3 Ground Reaction Forces 18
2.2.4 Centres of Pressure 20
2.2.5 Gait Kinematics 21
2.3 Athletic Footwear 23
2.3.1 Footwear Anatomy 23
2.3.2 Footwear Properties 24
2.3.3 Development Process 26
2.4 Mechanical Footwear Testing Devices 27
2.4.1 Existing Robotic Test Devices 28
2.4.2 Other Robot Applications in Sport 35
2.5 The Robot Footform 36
2.5.1 Blatchford Elite 2 36
2.5.2 The Otto Bock Trias 37
2.5.3 The elite Vector Thrust (VT) 38
2.5.4 Ossur Ceterus 39
2.5.5 Rigid Last 40
2.6 Summary 41

Chapter 3 – Kinematics and Kinetics of Human Walking and Running **42**
3.1 Introduction 42
3.1.1 Aims 43
3.1.2 Objectives 43
3.2 Methodology 44
3.2.1 Subject 44
3.2.2 Equipment 44
3.2.3 Data Collection 48
3.2.4 Data Processing 49
3.3 Results 51
3.3.1 Foot Angle 51
3.3.2 Positions 52
3.3.3 Heel Velocity 54
3.3.4 Ground Contact Times 55
3.3.5 Ground Reaction Forces 55
3.3.6 Centre of Pressure 57
3.4 Discussion 58
3.4.1 Robot Inputs 58
3.3.5 Robot Outputs 59
3.5 Conclusions 61

Chapter 4 – The FANUC R2000*i*-B Industrial Robot **62**
4.1 Introduction 62
4.2 Robot Specification 63
4.2.1 Specification 63
4.2.2 The Robot End-Effector 65
4.2.3 Safety Features and robot cell 66
4.3 Programming the Robot 67
4.3.1 Instructing Robot Movement 67
4.3.2 Tool Centre Points and Coordinate Frames 69
4.4 Previous Footstrike Emulation 70
4.5 Summary 71

Chapter 5 – Initial Characterisation of the Robot Movement **72**
5.1 Introduction 72
5.1.1 Aims 74
5.1.2 Objectives 74
5.2 Methodology 75
5.2.1 Equipment and set up 75
5.2.2 Robot Programmes and Trials 77
5.2.3 Data Collection and Processing 79
5.2.4 Data Analysis 79
5.3 Results 80
5.3.1 Vertical and Horizontal Movements 80
5.3.2 Corner Movements 84
5.4 Discussion 87
5.4.1 Vertical and Horizontal Movements 87
5.4.2 Corner Movements 89
5.4.3 Implications for the emulations of sporting movements 89
5.5 Conclusions 90

Chapter 6 – Evaluation of RoboGuide to Simulate the Footstrike in A Virtual Environment **91**
6.1 Introduction 91
6.1.1 Aims 92
6.1.2 Objectives 92
6.2 Methodology 93
6.2.1 Creating the Virtual Robot Environment 93
6.2.2 Data Collection 95
6.2.3 Data Processing 97
6.3 Results 98
6.3.1 Set 1 – Simple Linear Movements 98
6.3.2 Set 2 –Human Heelstrike Running 103
6.4 Discussion 105
6.5 Conclusions 107

Chapter 7 – Design and Characterisation of A New End-Effector **108**
7.1 Introduction 108
7.2 Original End-Effector Characterisation 110
7.2.1 Visual and technical analysis 110
7.2.2 Ground contact emulation using the original end-effector 111
7.2.3 Biofidelic footform characterisation 111
7.3 Conceptual Design 114
7.3.1 Design Specification 114
7.3.2 Design Concepts 114
7.3.3 Design Concept One 118
7.3.4 Design Concept Two 120
7.4 Design Selection 122
7.4.1 Design Alteration 122
7.4.2 Design Validation 127
7.5 Conclusions 129

Chapter 8 – Robot Cell Design and Optimal Force Platform Location **130**
8.1 Introduction 130
8.1.1 Aims 131
8.1.2 Objectives 131
8.2 Methodology 132
8.3 Results 136
8.4 Discussions 143
8.5 Conclusions 147

Chapter 9 – Emulation of the Shoe-Ground Interaction During the Ground Contact Phase of Human Walking **148**
9.1 Introduction 148
9.1.1 Aims 150
9.1.2 Objectives 150
9.2 Methodology 151
9.2.1 Footstrike Data 151
9.2.2 Equipment 151
9.2.3 Data Collection 152
9.2.4 Robot Programmes 152

9.2.5 Data Processing 156
9.3 Results 157
9.3.1 Ground Reaction Forces 157
9.3.2 Centres of Pressure 159
9.3.3 Footform kinematics 160
9.3.4 Footform angles 162
9.4 Discussion 165
9.4.1 Ground Reaction Forces 165
9.4.2 Ground Contact Times 168
9.4.3 Centre of Pressure 170
9.4.4 Footform Kinematics 171
9.5 Conclusions 173

Chapter 10 - Conclusions **175**
10.1 Introduction 175
10.1.1 Aims 175
10.1.2 Objectives 175
10.2 Research Question 176
10.2.1 Research Question One 176
10.2.2 Research Question Two 177
10.2.3 Research Question Three 178
10.2.4 Research Question Four 179
10.3 Summary 180
10.4 Future Work 181

References **183**

Appendix 1 ..... **191**

LIST OF FIGURES

CHAPTER 1

Figure 1.2.1: The scale of biofidelic emulation between mechanical testing and human gait.

Figure 1.4.1: Flow diagram illustrating the interaction between thesis chapters and how they relate to each individual research question.

CHAPTER 2

Figure 2.1.1 – The 3 regions the foot (the forefoot, midfoot and hindfoot), reproduced from Floyd 2007.

Figure 2.1.2 – A summary of the different joint of the foot, reproduced from Cole *et al* (2001).

Figure 2.1.3 – The three primary arches of the foot, reproduced from Cheung *et al* 2006.

Figure 2.1.4 – Soft tissue on the plantar aspect of the foot

Figure 2.2.1. – An example of the ground preparation phase for shod heelstrike running

Figure 2.2.2 – An example of the midstance phase

Figure 2.2.4 – An example of the ground push off phase

Figure 2.2.5 – Figures illustrating the three different force profiles, for **(a)** running and **(b)** walking; reproduced from (Mara 2007, Hunt *et al* and Giakas 1996)

Figure 2.2.6 – An interaction between the foot and the ground during walking. **(1)** Heelstrike, **(2)** foot flat, **(3)** midstance and **(4)** toe-off. Reproduced from Rodgers, 1988.

Figure 2.2.7 – The centre of pressure path during barefoot running. Reproduced from De Cock *et al* (2008).

Figure 2.2.8 – A summary of joint motions during the different phases of gait. Reproduced from Rodgers, 1988.

Figure 2.3.1 – The anatomy of the running shoe, Chase *et al* (2009)

Figure 2.4.1 – The adidas wheel wear machine. Reproduced from Mara (2007)

Figure 2.4.2 – Typical Ground Reaction Force (a) WWM when running (Mara, 2007) & (b) Human heelstrike running

Figure 2.4.3 – The Pedatron – SATRA, reproduced from SATRA test equipment catalogue.
Figure 2.4.3 The KUKA 6 DoF industrial robot used by De Raeve *et al* (2014), reproduced from De Raeve *et al* (2014)

Figure 2.4.4 The ABB 6 DoF industrial robot used by Starker *et al* (2013), reproduced from Starker *et al* (2013)

Figure 2.4.5 The ground reaction forces for **(a)** the human subject and **(b)** the ABB robot, reproduced from Starker *et al* (2013)

Figure 2.4.6 – The Stewart platform .

Figure 2.4.7 The tilt table used by Starker *et al* (2014), reproduced from Starker *et al* (2014)

Figure 2.8.4 – Results reproduced from Ronkainen *et al* (2010). **(a)** The vertical ground reaction force for heel strike running for the robot (R) and human (H) and **(b)** The heel marker trajectories for heel strike running for the robot (R) and human (H).

Figure 2.5.1 – The Blatchford elite2 and its configuration as a prosthetic device.

Figure 2.5.2 – The Otto Bock Trias – www.ottobock.co.uk

Figure 2.5.3 – Walking vertical GRF for the Otto Bock TRIAS, for the three different force profiles

Figure 2.5.4 – The eliteVT – www. endolite.co.uk

Figure 2.5.5 – The Ossur Ceterus - http://www.oandp.com

Figure 2.5.6 – A rigid last, traditionally used in footwear manufacturer but could have applications as an end-effector footform.

CHAPTER 3

Figure 3.2.1: An example of a VICON T-series camera.

Figure 3.2.2: A schematic of the test set up used in the data collection process, showing the force plate and location of the VICON cameras. The timing gates are positioned at the locations marked (*).

Figure 3.2.3: An example of a Photron Fastcam High speed camera.

Figure 3.2.4: The Fusion sport smart speed light gates.

Figure 3.2.5: The wand used for static and dynamic calibration of the capture space within VICON.

Figure 3.2.6: The anatomical positions of the VICON markers (not all are visible) for (a) shod & (b) barefoot conditions. The locations were identified through palpitation and manual manipulation of the subject. The marker locations are as follows: 1. hallux 2. Medial metatarsal 3. Lateral metatarsal 4. Medial calcaneus 5. Lateral calcaneus 6. Medial malleolus 7. Lateral malleolus 8. Heel 9. Lateral aspect of the mid-shank 10. Medial femoral condyle (not shown) 11. Lateral femoral condyle (not shown).

Figure 3.2.7: A visual representation of the foot reconstructed within the VICON software. The markers correspond to those identified in Figure 3.2.6.

Figure 3.3.1: The angle of the foot throughout ground contact for walking and running under both barefoot and shod conditions. A positive angle at impact indicates a heelstrike.

Figure 3.3.2: The ground contact phase for both barefoot and shod walking. Starting prior to impact (pre-TD), moving through contact (TD) into the mid-stance (MS) and heel lift. The heel continues to rise to toe-off (TO) before the foot leaves the ground as part of the post contact phase.

Figure 3.3.3: The ground contact phase for both barefoot and shod running**.** Starting prior to impact (pre-TD), moving through contact (TD) into the mid-stance (MS) and heel lift. The heel continues to rise to toe-off (TO) before the foot leaves the ground as part of the post contact phase.

Figure 3.3.4: The velocity of the heel marker versus percentage of ground contact for walking under (a) barefoot and (b) shod conditions. The solid line represents the ground contact phase.

Figure 3.3.5: The velocity of the heel marker versus percentage of ground contact for jogging under (a) barefoot and (b) shod conditions. The solid line represents the ground contact phase.

Figure 3.3.6: The ground reaction force data versus ground contact time percentage for walking and jogging under barefoot and shod conditions.

Figure 3.3.7: The centre of pressure in the anterior-posterior and medial-lateral directions for walking and running under both barefoot and shod conditions. Both are presented relative to the position at impact.

CHAPTER 4

Figure 4.2.1 – The FANUC R2000*i*-B 6 Degrees-of Freedom industrial robot. Also shown is the location of each robot joint (J1-J6), moving from the proximal joint 1 (the attachment to the floor) to the most distal joint 6.

Figure 4.2.2 –The dimensions and potential Range-of-Motion (RoM) of the robot.
Figure 4.2.3 – SICK laser proximity sensor, used to emit a protective light curtain around the inside of the robot cell

Figure.4.3.1 - An example of how robotic smoothing level may affect the robot motion, reproduced from the FANUC programming manual.

Figure 4.3.2 – A screenshot from the teach pendant showing the required input parameters.

CHAPTER 5

Figure 5.1.1: An example of how robotic smoothing level may affect the robot motion (Reproduced from FANUC programming manual).

Figure 5.2.1: The end-effector spike used to provide a consistent reference point on the robot.

Figure 5.2.2: A schematic outlining the test area and equipment positions.

Figure 5.2.3: A real World representation of the schematic shown in figure 5.2.3.

Figure 5.2.4: The configuration of the simple linear (horizontal and vertical) motion paths; showing **(a)** no additional points, **(b)** one additional point and **(c)** two additional points.

Figure 5.2.5: The configuration of the 90° corner motion paths; showing **(a)** no additional points, **(b)** one additional point and **(c)** two additional points.

Figure 5.3.1: Downwards vertical displacement from the start point (programmed displacement was 400 mm, shown by the dashed line) to the turn point for the robot with different levels of robotic smoothing applied at different velocities; with **(a)** no additional co-ordinate points **(b)** one additional co-ordinate point and **(c)** two additional co-ordinate points programmed.

Figure 5.3.2: Horizontal displacement from the start point (programmed displacement was 400 mm, shown by the dashed line) to the turn point for the robot with different levels of robotic smoothing applied at different velocities; with **(a)** no additional co-ordinate points **(b)** one additional co-ordinate point and **(c)** two additional co-ordinate points programmed.

Figure 5.3.3: Total motion times and the time taken to reach the turn point for the robot moving in the simple vertical motion with different levels of robotic smoothing and velocity applied with **(a)** no additional co-ordinate pointes programmed and **(b)** two additional co-ordinate points programmed.

Figure 5.3.4: Total motion times and the time taken to reach the turn point for the robot moving in the simple horizontal motion with different levels of robotic smoothing and velocity applied with **(a)** no additional co-ordinate pointes programmed and **(b)** two additional co-ordinate points programmed.

Figure 5.3.1: The outputted velocities against the programmed velocities under all conditions for the vertical linear motion showing **(a)** the peak velocity attained and **(b)** the average velocity.

Figure 5.3.2: The outputted velocities against the programmed velocities under all conditions for the horizontal linear motion showing **(a)** the peak velocity attained and **(b)** the average velocity.

Figure 5.3.5: The corner movement trajectories for the robot with different levels of robotic smoothing applied and with different numbers of additional co-ordinate points (+ 0, +1 and + 2) at different velocities (500 mm/s, 1000 mm/s and 1500 mm/s). The movements start at the origin (0, 0) and the inputted trajectory is shown by the dotted line.

Figure 5.3.6: Total motion times and the time taken to reach the turn point for the robot moving in the corner motion with different levels of robotic smoothing and velocity applied with **(a)** no additional co-ordinate pointes programmed and **(b)** two additional co-ordinate points programmed.

Figure 5.3.7: The outputted velocities against the programmed velocities under all conditions for the corner motion showing **(a)** the peak velocity attained and **(b)** the average velocity.

CHAPTER 6

Figure 6.2.1: The FANUC robot cell environment was recreated within RoboGuide

Figure 6.2.2: (a) The imported CAD model of the Blatchford end-effector; (b) The imported CAD model of the Kistler Force Platform

Figure 6.2.3: A summary of the two sets of trials completed on both the robot and RoboGuide, showing input movements, robot and RoboGuide positions and the investigated parameters.

Figure 6.3.1: Vertical displacement from start point to turn point (programmed displacement was 400 mm, shown by the dashed line) for the robot and RoboGuide with **(a)** different levels of robotic smoothing and velocity (using no additional co-ordinate points) and **(b)** different numbers of additional co-ordinate points and levels of robotic smoothing (using a velocity of 1500 mm/s).

Figure 6.3.2: Horizontal displacement from start point to turn point (programmed displacement was 400 mm, shown by the dashed line) for the robot and RoboGuide with **(a)** different levels of robotic smoothing and velocity (using no additional co-ordinate points) and **(b)** different numbers of additional co-ordinate points and levels of robotic smoothing (using a velocity of 1500 mm/s).

Figure 6.3.3: Total motion times and the times taken to reach the turn point for the robot and RoboGuide at 1500mm/s with various levels of smoothing applied for **(a)** vertical and **(b)** horizontal linear movements.

Figure 6.3.4: The corner movement trajectories for the robot and RoboGuide with different numbers of additional co-ordinate points (+ 0 and + 2) at the extremities of applied level of smoothing and velocity respectively. **(a)** No smoothing at 500 mm/s, **(b)** Maximum smoothing at 500mm/s, **(c)** No smoothing at 1500 mm/s and **(d)** Maximum smoothing at 1500mm/s.

Figure 6.3.5: Time for the total movement and to reach the turn point for the robot and RoboGuide at a velocity of 1500mm/s with various levels of smoothing applied to the corner movement.

Figure 6.3.6: Heel trajectory data for heelstrike human running, the robot and RoboGuide throughout the ground contact phase, which starts at 0 mm in the vertical and horizontal plane, trials start 20 mm horizontally prior to initial contact, ending 150 mm after contact in the sagittal plane.

Figure 6.3.7: A comparison of running gaits for **(a)** a human, **(b)** the robot and **(c)** RoboGuide; both the robot and RoboGuide are programmed to run through 'mid-air'. Starting prior to impact (pre-TD), moving through contact (TD) into the mid-stance (MS). The heel continues to rise to toe-off (TO) before the foot leaves the ground as part of the post contact phase.

CHA#PTER 7

Figure 7.1.1 – The original end-effector used in previous footstrike emulations using the FANUC.

Figure 7.2.1 – An example of the original end-effector mounted onto the Instron mechanical test machine for characterisation.

Figure 7.2.2. . The compression information for each state of the Blatchford prosthetic; shod (a), barefoot (b) and blade(c) for the 1st and 20th cycles of 20 cycles. Stiffness was calculated from the slope of a straight line fitted to the loading data between 200N and 800N.

Figure 7.3.1 – A selection of potential design concepts, based on using the principle of a linear bearing and a slide. Each design is made up of a robot attachment, the linear slide and a footform.

Figure 7.3.2 – The two design concepts that were chosen to be taken forward to prototype phase.

Figure 7.3.3 – The prototype of design concept one.

Figure 7.3.4 – A visual analysis of the robots movements for design concept one, for **(a)** ground contact and **(b)** toeoff.

Figure 7.3.5 - The vertical ground reaction forces for a robot footstrike with design concept one.

Figure 7.3.6 – The prototype of design concept two.

Figure 7.3.7– A visual analysis of the robots movements for design concept two, for **(a)** ground contact and **(b)** toeoff.

Figure 7.3.8 - The vertical ground reaction forces for a robot footstrike with design concept two.

Figure 7.4.1 – An example of a foam sample on the Instron ElectroPuls, prior to mechanical testing.

Figure 7.4.2. A chart showing applied load against compression distances for the selected foam sample, at interval's of 100 cycles for a total of 1000 cycles.

Figure 7.4.3 – Technical drawings of the final design selection, consisting of robot attachment and linear slide bearing.

Figure 7.4.4 – The final design solution. Consisting of biofidelic sections (with applied pre-load), robot attachment and linear bearing.

Figure 7.4.5 - The vertical ground reaction forces for a robot footstrike with the final design solution.

CHAPTER 8

Figure 8.2.1: (a) The imported CAD model of the shod original end-effector; **(b)** The imported CAD model of the shod linear bearing end-effector and **(c)** The imported CAD model of the Kistler Force platform.

Figure 8.2.2: A schematic showing the layout of the potential force platform locations. The hatched area shows the original location of the force platform. In addition to the 49 locations illustrated, this was repeated at two further z values (+500mm and +1000mm from the original). The 147 (7 x 7 x3) potential new locations cover a volume of 1.5m x 1.5m x 1m.

Figure 8.3.1: Map of the run times (seconds) for the different force platform locations and the original end-effector. Green on the scale represents an improvement on the original location and red is slower. The solid rectangle at z + 0mm represents the original force platform location. Not all of the potential locations are covered

Figure 8.3.2: Map showing the percentage changes in run time for the different force platform locations against the original end-effector, a negative percentage means a slower time and a positive percentage represents a faster time. Green on the scale represents an improvement on the original location and red is slower.

Figure 8.3.3: Map of the run times (seconds) for the different force platform locations and the linear bearing end-effector. Green on the scale represents an improvement on the original location and red is slower.

Figure 8.3.4: Map showing the percentage changes in run time for the different force platform locations with the linear bearing end-effector, a negative percentage means a slower time and a positive percentage represents a faster time. Green on the scale represents an improvement on the original location and red is slower.

Figure 8.3.5: The location of each joint (1-6) on the FANUC robot. Joint 1 is the most proximal and joint 6 is the most distal.

Figure 8.3.6: Map showing cycle times (seconds) for various force platform locations using the original end-effector, for selected locations on the robot. Green on the scale represents an improvement on the original location and red is slower.

Figure 8.3.7: Map showing cycle times (seconds) for various force platform locations using the linear bearing end-effector, for selected locations on the robot. Green on the scale represents an improvement on the original location and red is slower.

CHAPTER 9

Figure 9.2.1: The anatomical positions of the VICON markers (not all are visible) for the robot fitted with the linear end-effector. The marker locations are as follows: 1. Hallux 2. Medial metatarsal (not shown) 3. Lateral metatarsal 4. Medial calcaneus (not shown) 5. Lateral calcaneus 6. Medial malleolus (not shown) 7. Lateral malleolus 8. Heel 9.Centre of the end-effector.

Figure 9.3.1: The vertical ground reaction forces for the real world human and the robot programmed with human kinematic data. The pink trace represents the adapted programme with increased impact offset.

Figure 9.3.2 – The vertical ground reaction forces for the real world human and the robot programmed with rotations about the MPJ and heel. The thinner rotation traces represent the different start and finish positions respectively, the thinner the trace the more removed the position. The vertical lines represent the two vertical ground reaction peaks (thick) and touchdown/toeoff (thin) for real human data.

Figure 9.3.3: The horizontal ground reaction forces for the real world human and the robot programmed with human kinematic data. The pink trace represents the adapted programme with increased impact offset.

Figure 9.3.4: The horizontal ground reaction forces for the real world human and the robot programmed with rotations about the MPJ and heel. The thinner rotation traces represent the different start and finish positions

respectively, the thinner the trace the more removed the position. The time of the maximum force (represented by the vertical line) for each phase have been offset to match the human

Figure 9.3.5: The centres of pressure as a percentage of the anterio-posterior distance for the real world human and the robot programmed with human kinematic data. The pink trace represents the adapted programme with increased impact offset.

Figure 9.3.6: The centres of pressure as a percentage of the anterio-posterior distance for the real world human and the robot programmed with rotations about the MPJ and heel. The thinner rotation traces represent the different start and finish positions respectively, the thinner the trace the more removed the position.

Figure 9.3.7: A schematic showing the position and orientation of the real human footform against each of the robot programmes at the main points of the ground contact phase; **TD –**touch down, **PK1 –** Peak 1 (impact peak), **MS –** Midstance, **PK2 –** Peak 2 and **TO –** Toeoff. The heel marker for each robot programme was matched to that of the real human at the initial point of ground contact.

Figure 9.3.8: The two dimensional position of the heel in the sagittal plane for the real world human and the robot programmed with human kinematic data. The pink trace represents the adapted programme with increased impact offset.

Figure 9.3.9: The two dimensional position of the heel in the sagittal plane for the real world human and the robot programmed with rotations about the MPJ and heel. The thinner rotation traces represent the different start and finish positions respectively, the thinner the trace the more removed the position.

Figure 9.3.10: A representation of the angle of the footform relative to the ground for the real world human and the robot programmed with human kinematic data. The pink trace represents the adapted programme with increased impact offset.

Figure 9.3.11 – A representation of the angle of the footform relative to the ground for the real world human and the robot programmed with rotations about the MPJ and heel. The thinner rotation traces represent the different start and finish positions respectively, the thinner the trace the more removed the position.

Figure 9.3.12: A representation of the angle of the MPJ for the real world human and the robot programmed with human kinematic data. The pink trace represents the adapted programme with increased impact offset.

Figure 9.3.13 – A representation of the angle of the MPJ for the real world human and the robot programmed with rotations about the MPJ and heel. The thinner rotation traces represent the different start and finish positions respectively, the thinner the trace the more removed the position.

LIST OF TABLES

CHAPTER 2

Table 2.1.1: A summary of the joints of the foot.

Table 2.1.2: The properties of the heel pads for the two groups (Mean +/- SD); reproduced from Challis *et al* (2008).

Table 2.2.2 – The frontal and sagittal plane kinematics of 9 subjects, reproduced from De Wit *et al* 2000.

CHAPTER 3

Table 3.2.1 The selected trials for data presentation for each of the locomotion conditions.

Table 3.3.1: The angle of the foot at impact and takeoff for walking and running under both barefoot and shod conditions. A positive angle at impact indicates a heelstrike.

Table 3.3.2: The ground contact time for walking and running under both barefoot and shod conditions for all trials.

Table 3.3.3: Vertical ground reaction force loading rates to the first main peak (taken as the slope of the line fitted to data for 20% and 80% of the peak force value).

CHAPTER 4

Table 4.2.1 – The specification sheet for the FANUC robot along with the specifications of two similar robots from ABB and KUKA respectively. The robot joints (J1-J6) are shown in figure 4.2.1.

CHAPTER 7

Table 7.2.1 - The compression information for each state (shod, barefoot and blade) of the Blatchford prosthetic footform for the 1st and 20th cycles of 20 cycles.

Table 7.4.1. The compression and stiffness data for the adequate foam samples that achieved stiffness values in the range 10-30 kN/m.

CHAPTER 8

Table 8.3.1 The angles in degrees of each robot joint relative to its neutral position for original, best and worst location for each end-effector. The position of each joint is shown in figure 8.3.5. The values shown are for those where the footform is in mid-stance.

CHAPTER 9

Table 9.2.1 – The robot programme and corresponding footform positions for the robot programmed with human kinematic data. Shaded cells represent the area of ground contact.

Table 9.2.2 – The robot programme and corresponding footform positions for the robot programmed with a fixed point of rotation at the heel. Shaded cells represent the area of ground contact.

Table 9.2.3 – The robot programme and corresponding footform positions for the robot programmed with a fixed point of rotation at the MPJ. Shaded cells represent the area of ground contact.

Table 9.3.1 – A summary of the remaining key kinematic and kinetic features for each of the robot and real human footstrikes. Values coloured in red represent a good emulation of the real human value.

NOMENCLATURE

2D	Two dimensional
3D	Three dimensional
6 DoF	6 Degrees of Freedom
CAD	Computer Aided Design
CNT	Continuous
CoP	Centre of Pressure
GCT	Ground Contact Time
GRF	Ground Reaction Force
H	Horizontal
J#	Joint Number
kg	kilogram
m	Metre
MPJ	Metatarsophalangeal joint
N	Newton
s	Second
TD	Touch Down
TO	Toe Off
V	Vertical
Vel.	Velocity

PUBLICATIONS ARISING FROM THIS WORK

Conference

J. A. Jones, P.G. Leaney, A.R. Harland, S.E. Forrester; *Validation of RoboGuide to Support the Emulation of Sporting Movements using an Industrial Robot.* Vol. 34, pp 307-312. Proceedings of the 9th Conference of the International Sports Engineering Association (ISEA). Lowell, MA

CHAPTER 1

INTRODUCTION

1.1 Background

Manufacturers of sports equipment are continuously striving to improve their product in relation to performance, comfort and/or safety. Part of this process is to test the equipment to ensure that it is fit for purpose, this may include mechanical testing intended to emulate the human interaction with the equipment. This typically complex multidimensional problem is generally simplified to a one or two dimensional approximation. Regardless, it can be assumed that the more accurately the test conditions represent real life use, the better the test is for product research and development.

A good example of where sports equipment testing is widely used is in the athletic footwear industry; which is one of the most lucrative and competitive markets in the world. Large amounts of money are dedicated to the research, development and marketing of the product - $185.2bn as of 2011 (PRWeb 2013). The importance of athletic footwear was highlighted by Bates *et al* 1983 where they stated the following: 'the foot shoe complex forms the dynamic base upon which the runner functions. What happens at the foot-surface interface affects the total functional mechanism.' When designing athletic footwear the main aim is to either improve performance and/or to decrease the injury potential whilst prioritising and maximising the users comfort. It is in these design features that companies are striving to achieve a competitive advantage over their rivals, to offer the customer the best possible product. One such tool that can be used to optimise this process is mechanical testing (Odenwald 2006), a process that is being pioneered by some of the World's largest companies, such as NIKE and adidas.

1.2 Mechanical Testing in the Footwear Industry

The purpose of mechanical testing is to subject the footwear to real world usage conditions whilst removing the variability of a real human subject. One of the main aims of testing is to evaluate its durability and to ensure that it can function for a sufficient time period. For this purpose applying the right force magnitudes, with adequate loading rates, at the correct location on the footwear are key. These tests can be very basic and not very biofidelic at all; one such example is a simple test which involves dropping a weighted metal cylinder onto a sole unit (ASTM F1614-99 (2006) 'Standard Test Method for Shock Absorbing Properties of Materials Systems for Athletic Footwear') to try and generate appropriate reaction forces. Although these types of tests have some benefit (to benchmark different types of shoe for example), it is very difficult to achieve an accurate emulation of the kinetics of the shoe-ground interaction and therefore the results may have limited validity. One of the most common methods used to assess the wear on athletic footwear is to conduct trials with human subjects, providing an understanding of the shoe under realistic use conditions. Traditionally, subjects are given some athletic footwear and asked to use them for a predefined distance (typically several hundred kilometres) before returning them for assessment. This method can be very time consuming and is not very controlled. Consequently, it can provide a wide range of results which can be heavily influenced by factors including subject weight, running style and activity levels as well as surface and weather.

A controlled mechanical test that can accurately emulate the human footstrike has advantages in terms of both time and repeatability and there are a number of prime examples where this approach has been adopted, e.g. adidas, SATRA and NIKE all use their own systems (Chapter 2). As yet these techniques have been quite poor in their emulation of the kinetics (ground contact times, ground reaction forces and loading rates) of the ground contact phase. In 2008, Loughborough University purchased a FANUC R2000*i*B six degrees-of-freedom (6 DoF) industrial robot (FANUC robotics; Mount Fuji, Japan) with the intention of investigating its use within a sports application. Using this type of robot has the benefit over creating a bespoke system in-house, of an established control system and support network and the flexibility to be applied widely within the sports equipment

industry beyond footwear testing. Ronkainen *et al* (2010) used the robot to attempt to emulate the kinetics and kinematics of the running gait with limited levels of success. The ground contact time and the footprint were both too large while the impact peak was absent and the horizontal forces were braking throughout. Issues were also identified in how the robot is programmed; the effect of robotic smoothing has revealed the difficulty in emulating human kinematics on the robot.

Mechanical testing is increasingly being used in footstrike emulation, but as yet with only limited success. This thesis follows on from the aforementioned robot emulation study conducted at Loughborough University. The main emphasis is on moving emulation as close to the human end of the scale as possible (figure 1.2.1) as well as evaluating its longer term potential for moving even closer:

Figure 1.2.1 – The scale of biofidelic emulation between mechanical testing and human gait.

1.3 Thesis Aims and Research Questions

This thesis aims to investigate the use of using a FANUC R2000*i*-B six degrees-of-freedom (6 DoF) industrial robot to emulate human gait, with a specific interest on the ground contact phase. The work documented in the thesis addresses this aim whilst laying the foundations for the robot to be used as an accelerated wear device for testing footwear. Robotic testing of footwear remains in its infancy, with many of the techniques being basic and un-refined. The novelty of this thesis lies in the observation that the use of an off the shelf six DoF industrial robot for footwear testing has not previously been explored. The following chapters generate the knowledge required to achieve the above aim and address the following four research questions:

1 **What are the biomechanical features that need to be emulated and what are typical values for them?**

To be able to both programme and evaluate the output of the robot an understanding of the kinematics and kinetics of human gait is required. Studying literature and collecting human trial data will help to address this.

2 **What are the capabilities of the robot and what are the intricacies of its operation?**

Before being able to use the robot to emulate a complex sporting motion it is important to gain an understanding of its basic operating principles and performance capabilities. The findings of Ronkainen *et al* (2010) showed the ground contact time to be too long and the effects of robotic smoothing have not previously been fully examined. Understanding these features and how best to accommodate them is critical in moving forward. Basic movement analysis is an ideal starting point for this task.

3 **How can the robot set-up be configured to emulate the ground contact phase of the human gait?**

The robot is located within a cage/cell that restricts robot movement and maintains the safety of the user. When attempting to emulate footstrike, the ground interaction will occur with a force plate located on a platform in the middle of the robot cell. The design and layout of the furniture within the cell can influence the robot movement required and potentially the success of the emulation. An evaluation of potential robot movements for associated force plate locations is essential for optimising the output. Similarly, the design and orientation tool/end-effector of the robot can have a significant role on the ground interaction and should be considered accordingly. These points can be addressed in part with the help of RoboGuide – an accompanying computer software package that allows for quick and easy alterations to the robots physical interactions whilst outputting meaningful data.

4 **To what degree can the robot be used to accurately emulate human gait?**

The outcomes from the previous research questions can be combined to develop a protocol that can explore the potential of emulating the ground contact phase of the human gait. An understanding of how the robot works and how it can be programmed alongside knowledge relating to the optimal physical environment will

lead to the best opportunity of an accurate emulation. Kinematic and kinetic data collected from human trials were used to both programme the robot motions and evaluate their outcome. This process involves comparing key kinetic features (ground reaction forces, loading rates, ground contact times and centres of pressure) of the robots interaction with the ground to those of the human.

1.4 Thesis Structure

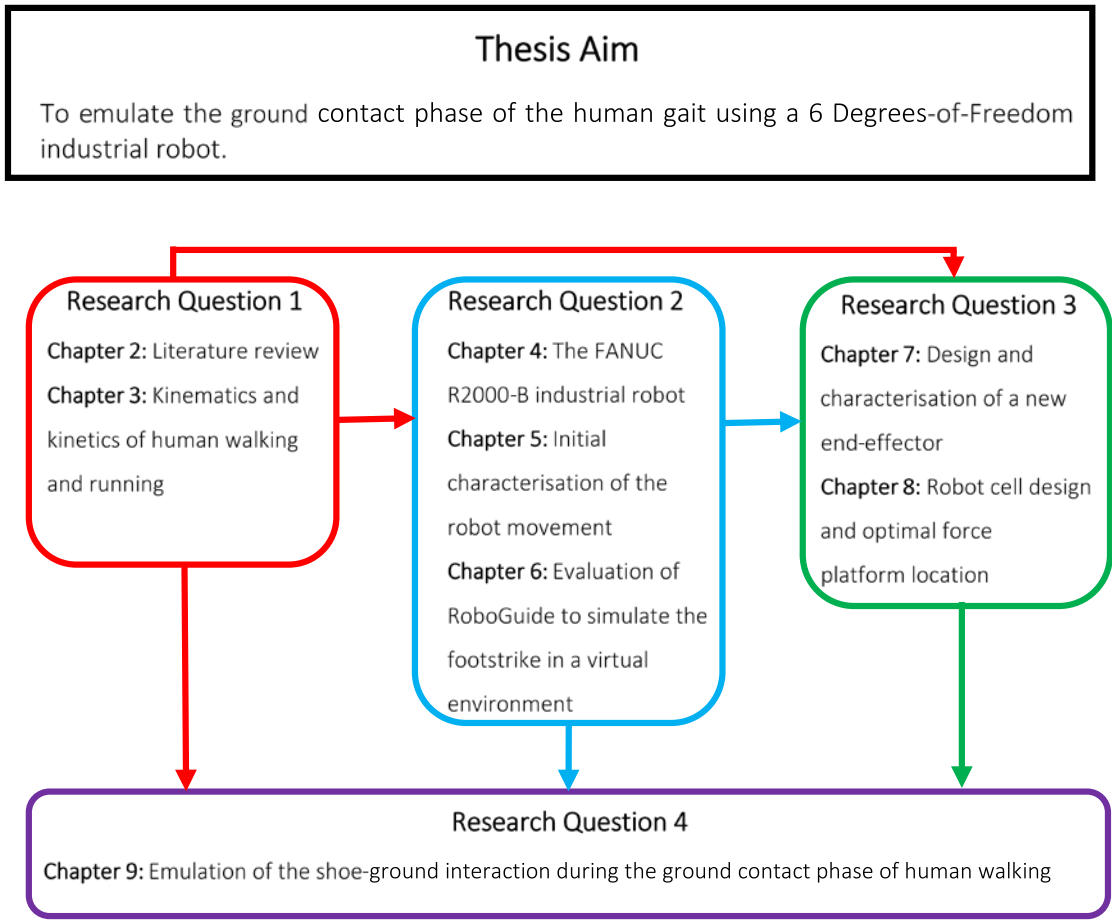

Figure 1.4.1: Flow diagram illustrating the interaction between thesis chapters and how they relate to each individual research question.

Figure 1.4.1 demonstrates how each of the subsequent chapters relate to the aforementioned research questions and how they work towards the overall thesis aim. *Research question one* is to be addressed by Chapter 2 which presents a review of the relevant literature and Chapter 3 which aims to measure typical kinematics and kinetics of human gait. The information gathered in addressing research question one is also used to support the other three research questions. *Research question two* is primarily answered by Chapters 4, 5 and 6. The general introduction to the robot in Chapter 4 compliments the whole of the thesis. Chapter 5 aims to investigate the effects of the programmable inputs to the robot and Chapter 6 assesses the relationship between the robot and the computer software RoboGuide. As well as identifying the capabilities and intricacies of robot operation, the knowledge gained here will also help in addressing research questions three and four. *Research question three* is centred around the robot set-up and how it can be optimised to best emulate footstrike. This is addressed in Chapter 7 which aims to design, develop and test a new robot end-effector and Chapter 8 which aims to identify the optimal position for the force platform within the root cell. Research questions one, two and three all assist in addressing *Research question four*, however the main focus for this is from Chapter 9 which aims to use the robot to emulate the ground contact phase of human gait.

CHAPTER 2

LITERATURE REVIEW

The aim of this chapter is to present a comprehensive review of the current literature relevant to robotic emulation of the human footstrike.

Initially the basic anatomy of the foot is presented followed by the biomechanics of the foot-ground interaction during walking and running gaits. The focus then turns to athletic footwear industry including shoe anatomy and how they are made and tested. The testing of athletic footwear is expanded on further in the next section with a specific emphasis on mechanical testing in the footwear industry and how robotic testing is increasingly being used as a tool for gait emulation. The final topic is the range of commercially available prosthetic feet reviewed with respect to their potential for use as the end-effector in robotic emulation of the footstrike.

The chapter concludes with a summary of the key outcomes from the literature review most relevant to the focus of the thesis.

2.1 FUNCTIONAL ANATOMY OF THE FOOT

The work undertaken in this thesis requires a basic understanding of the anatomy of the human foot. This section provides a brief summary of the functional anatomy of the human foot covering bones, joints, muscles and soft tissue.

2.1.1 Bones of the Foot

Without bone, varying human posture would not be possible and they work together with muscles to transfer muscle forces into joint torques lever systems. Both cortical (hard outer shell) and trabecular (soft inner region) bone provide support for the soft tissues and for the skeletal body (Nigg and Herzog 2005). The 26 bones of the foot, expanded upon below, can be grouped as the forefoot, midfoot and hindfoot (Figure 2.1.1) (Floyd 2007).

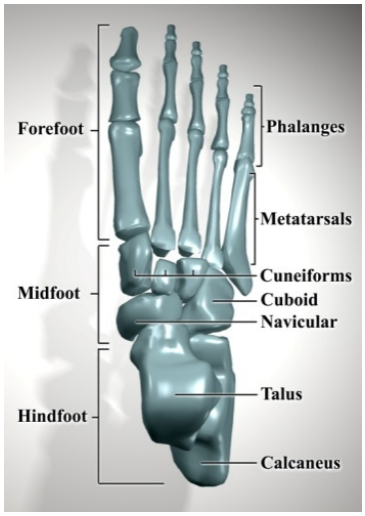

FIGURE 2.1.1 – The 3 regions the foot (the forefoot, midfoot and hindfoot), reproduced from Floyd 2007.

2.1.1.1 The Forefoot

The **metatarsals and phalanges** are the primary bones of the forefoot, they are important because of their load-bearing role (Graaff 1998). There are five **metatarsals**, numbered 1 to 5 from the medial side. Each metatarsal has a distal head, an elongate shaft in the middle, and a proximal base. The head of each metatarsal articulates with the proximal phalanx of a toe and the base articulates with one or more of the distal group of midfoot bones.

Metatarsal 1 (the great toe) the shortest and thickest, due to its load bearing role, has an articulation with two small **sesamoid** bones on the plantar surface. The metatarsals also articulate with each other at the sides, the base of the 5th metatarsal has a tuberosity, for attachment for the tendon of the fibrous brevis muscle (Graff 1998, Drake *et al* 2005 and Standring *et al* 2005).

The **phalanges**, or toes of the foot, are made up of three bones called a phalanx (proximal, middle and distal). Each phalanx consists of a base, a shaft and a distal head; the hallux only has a proximal and distal phalanx. The proximal phalanx articulates with the head of the related metatarsal. The non-articular head of each distal phalanx is flattened into a crescent-shaped plantar tuberosity under the plantar pad (Drake *et al* 2005).

2.1.1.2 The Mid Foot

The midfoot is made up of the **navicular, cuneiform** and **cuboid** bones. The navicular articulates between the talar head proximally and the cuneiform bones distally, there is a rounded tuberosity on the medial side for tendon attachment (Standring *et al* 2005 & Drake *et al* 2005). The cuneiform bones also articulate with the first to third metatarsals distally. The cuboid is located between the calcaneus and the fourth and fifth metatarsals (Standring *et al* 2005).

2.1.1.3 The Hindfoot

The hindfoot, made up of the **talus** and **calcaneus** is the primary articulation with the lower leg and is the initial point of contact with the ground during heel strike. The talus, a link to the leg, has a rounded head for articulation with the navicular, calcaneus and ligaments. The superior aspect of the talus forms the ankle joint with the distal ends of the tibia and fibula (Drake *et al* 2005 and Standring *et al* 2005). It is short in order to provide strength and to transmit longitudinal forces (Nigg and Herzog 2005). The calcaneus, the largest bone in the Hindfoot, sits under and supports the talus forming the skeletal framework of the heel acting as a short lever for muscles of the calf attached to the posterior surface. (Graaff 1998 and Drake *et al* 2005).

2.1.2 Joints of the Foot

The foot's various movements are contributed to by a number of joints (Figure 2.1.2):

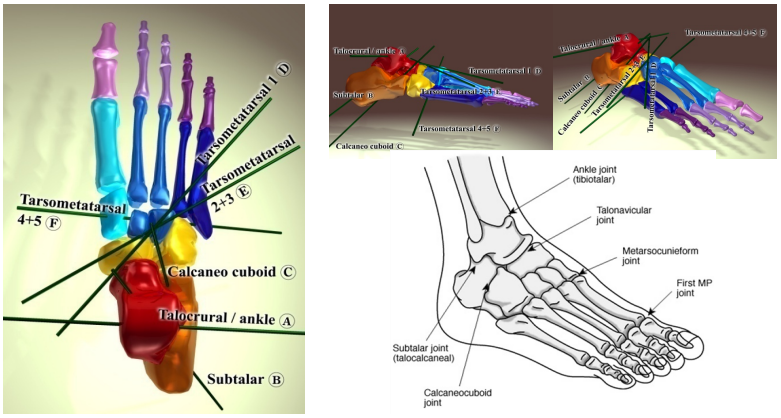

FIGURE 2.1.2 – A summary of the different joint of the foot, reproduced from Cole *et al* (2001).

2.1.2.1 Ankle Joint

The ankle joint is a synovial joint that allows hinge-like dorsiflexion and plantarflexion of the foot. Plantarflexion of the ankle in running has been shown to provide a large amount of shock absorption, as the foot extends away from the body (Gerristen *et al* 1995). For shod running at 3.5-4m/s McClay *et al* (1994) found the ankle to have a plantarflexion range of motion of 18 ±7 degrees and a dorsiflexion range of motion of 19.4 ±7 degrees. The distal ends of the tibia and fibula (the bones of the lower leg) form a socket for the talus, which is much wider anteriorly than posteriorly, therefore the bone fits tighter into its socket when the foot is dorsiflexed, this is where the joint is most stable. It is from this position that, all major thrusting movements are exerted in, walking, running and jumping (Drake *et al* 2005 and Standring *et al* 2005).

Glaister *et al (*2007) investigated ankle function in the transverse plane during turning gait. The elastic behaviour of the first section of the initiation, apex and termination phases were all found to resemble quadratic torsional springs, while the elastic behaviour of the rest of the phases resembled linear torsional springs. It has been noted that the human ankle permits limited motion in the transverse plane, a function absent in the prostheses of many lower-limb amputees, detailed in section 2.4. The use of traditional rigid prosthetics, in robotic testing could, therefore, influence results. The remaining joints that make up the foot and ankle complex are summarised in Table 2.1.1:

Table 2.1.1: A summary of the joints of the foot.

JOINT	LOCATION	FUNCTION	BIOMECHANICS
SUBTALAR	Located between the talus and calcaneus	Allows for gliding and rotation of the bones relative to each other, which are involved in inversion and eversion of the foot (Drake *et al* 2005).	For shod running trials performed at between 3.5-4m/s McClay *et al* (1994) found that inversion of the Hindfoot relative to the leg was 18.7 ±9 degrees and that Hindfoot eversion was 6.6 ±4 degrees.
TALOCALCANEONAVICULAR	The point of articulation between the talus, calcaneus and navicular.	Allows for gliding and rotational movements, which together with similar movements of the subtalar joint	Helps towards inversion and eversion of the foot (Drake *et al* 2005)
CALCANEOCUBOID	This is a joint between the calcaneus and cuboid	Allows sliding and rotating movements involved with foot eversion and inversion. It also contributes in pronation and supination of the foot (Drake *et al* 2005).	The calcaneocuboid joint has been shown to have a functional range of motion of 15 degrees for forefoot inversion and 20 degrees for forefoot eversion (Stacoff *et al 1989*).
TARSOMETATARSAL JOINT	Lies between the metatarsal bones and adjacent Hindfoot bones,	They are plane joints that allow limited sliding movements (Drake *et al* 2005).	This joint has a range of motion of 15 degrees for forefoot inversion and 20 degrees for forefoot eversion (Stacoff *et al 1989*).
METATARSOPHALANGEAL (MPJ)	These are joints between the metatarsals and phalanges	Allows extension and flexion, and limited abduction, adduction, rotation and circumduction (Drake *et al* 2005).	The MPJ has been assumed by (Stefanyshyn and Nigg 1997) to be an ideal hinge point. 'The normal range of motion of extension motion of the 1st MPJ is 65-75 degrees for barefoot walking (Root *et al* 1977). This value may be dependent on the cadence of the push off, which is the rate at which the foot is propelled off the ground (Bojsen-Moller 1979).
INTERPHALANGEAL	Located between the phalanges	Allows flexion and extension	

2.1.3 Arches of the Foot

The arrangement of the foot's bones form two dynamically supported arches relative to the ground; the longitudinal and transverse arches, (Figure 2.1.3 - Cheung *et al* 2006).

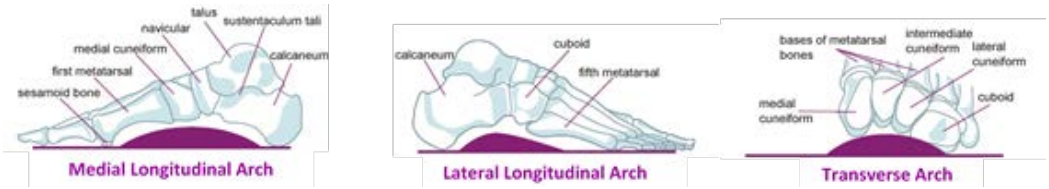

FIGURE 2.1.3 – The three primary arches of the foot, reproduced from Cheung *et al* 2006.

The **longitudinal arch** is formed between the posterior end of the calcaneus and the metatarsal heads; it is highest on the medial side and lowest on the lateral side of the foot. The **transverse arch** of the foot is highest in a coronal plane that cuts through the head of the talus (Drake *et al* 2005). The arches compress as weight is placed on the foot, and 'spring' back as it is lifted, helping to absorb and distribute downward forces from the body (Drake *et al* 2005 and Graaff 1998). The shape of the arch and foot stability is maintained in part because of the anatomical position of the plantar fascia (flat, broad tendons located on the plantar aspect of the foot) and its inherent mechanical properties (Kogler *et al* 1996).

2.1.4 Muscles and Soft Tissue

Muscles that act upon the foot can be classified into one of two groups, **extrinsic** muscles and **intrinsic** muscles. Extrinsic muscles originate in the lower leg and attach to bones within the foot, in the non-weight bearing leg these muscles produce plantarflexion and dorsiflexion; during weight bearing they help to stabilise and raise the heel. Intrinsic muscles are those which originate from within the foot. These muscles help control the tendons and generate fine movement within the toes. Both muscle groups help to support the arches of the foot (Drake *et al* 2005).

The **extensor hoods**, a soft tissue, allow for attachment of the intrinsic muscles, and distribute forces over the toes causing metatarsophalangeal joint flexion and interphalangeal joint extension (Drake *et al* 2005). The **plantar fascia**, a soft tissue band located on the plantar aspect of the foot, is a strong mechanical link formed between the

calcaneus and the toes and is a major stabilising structure (Mitchel *et al* 1981 and Hicks 1954).

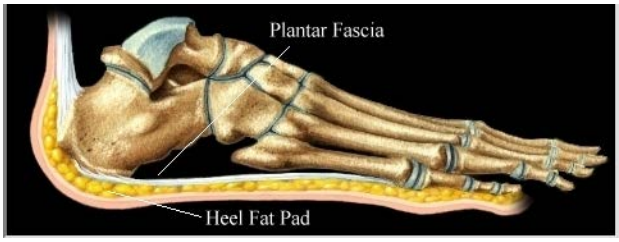

FIGURE 2.1.4 – Soft tissue on the plantar aspect of the foot

The heel pad or calcaneal pad is situated on the underside of the calcaneus (figure 2.1.4). Cavanagh and Lafortune (1980) state that the majority of runners are heel strikers; it is therefore the first point of ground contact for many runners. A number of studies have been conducted in an attempt to characterise the properties of the human heel pad. Weijers *et al* (2003) described the heel pad as a hydro-mechanical shock absorber and that its venous structures can help to contribute to damping. It has also been shown to protect against excessive local stress (Robins *et al* 1989) and reduce plantar pressures (Buschmann *et al* 1993, De Clercq 1994, Godding *et al* 1985, Jahss *et al* 1992, Jorgensen *et al* 1985 and Valiant 1984).

The stiffness of the heel pad is a very important factor to consider, it is the first point of contact with the ground and can heavily influence the ground contact phase. Rome *et al* (2001) investigated the heel pad stiffness in runners with and without plantar heel pain. Results showed runners with plantar heel pain to have lower maximum heel pad stiffness than runners without, 2.86N/mm and 3.22N/mm respectively. Conclusions arising from this work suggested that the heel pad has key functional properties in that it provides shock absorption and reduces the peak force at the point of heel strike.

Challis *et al* (2008) compared the mechanical properties of the heel pad between runners, who repetitively load the heel pad during training, and cyclists, who do not load their heel pads during training. It was found that the stiffness of the heel pad was significantly less for the runners than that of the cyclists. It was concluded that the decreased heel pad stiffness of runners provides more heel pad deformation during walking and running, thus giving a

form of cushioning (De Clercq *et al* 1994). It is clear that the heel pad does have an important role in the gait.

Table 2.1.2: The properties of the heel pads for the two groups (Mean +/- SD); reproduced from Challis *et al* (2008).

	Group	
Property	**Cyclists**	**Runners**
Heel pad thickness (mm) *	14.9 ± 1.5	13.6 ± 1.3
Heel pad thickness (% standing height)	0.84 ± 0.08	0.82 ± 0.08
Deformation (mm) *	4.8 ± 0.53	4.3 ± 0.60
Deformation (% heel pad thickness)	34.0 ± 5.81	32.2 ± 5.16
Energy loss (%)	62.2 ± 6.5	63.8 ± 10.5
Stiffness ($N \cdot mm^{-1}$) *	20.7 ± 4.5	17.5 ± 3.7

Note. Where there was a significant difference between the two groups, these have been marked with * ($p < .05$).

It can be hypothesised that during heel strike when running on a hard surface, the most deformable structures are the human heel pad and the sole of the shoe. De Clercq *et al* (1994) conducted an in-vivo study of the mechanical characteristics of the human heel pad during foot strike in running. Results of their study showed that in barefoot running the peak relative heel pad deformation is 60.5 ±5.5%, in shod running the peak heel pad deformation was much lower at 35.5 ± 2.5%.

In barefoot running the fatty heel tissue can easily expand in the transversal plane, where the deformation is unrestrained. Once it has been compressed the main function of the heel pad is to protect the heel bone against stress. This is not however the case in shod running, where the heel pad has a mechanical interaction with the shoe. If the shoe is well fitting it will mean that sideways displacement of the fat pad will be limited, this will therefore increase the effective stiffness of the heel pad (Cole *et al* 1995 and Jorgensen & Bosjen-Moller 1989).

2.2 FOOT-GROUND INTERACTION DURING GAIT

The main focus of this thesis is the robotic emulation of the shod foot-ground interaction during human gait. Thus, it is necessary to have an understanding of this interaction for a human; the relevant information for the gait kinematics and kinetics are presented in this section.

2.2.1 Stages of the ground contact phase

Perhaps the most common forms of human gait are walking and running and this section considers the ground contact phase of both. The gait cycle begins when one foot contacts the ground and ends when the same foot contacts the ground again. Contact can be initiated with either a heelstrike (where the heel contacts the ground first), mid-footstrike (where the middle of the foot contacts the ground first) or forefoot strike (where the distal region of the foot contacts the ground first) (Novacheck 1998). In walking heelstrike is the most common gait (Cavanagh and LaFortune, 1980), whilst for running, at least at aerobic speeds and for recreational level athletes, heelstrike is the norm (Hasegawa *et al* 2007). Consequently, heelstrike has been the focus of this work. Since there are many similarities between the heelstrike walking and running ground contact phases they are discussed as one below:

2.2.1.1 Preparation for contact

Immediately prior to ground contact the ankle joint is slightly dorsiflexed and the subtalar joint is supinated, this results in foot dorsiflexion and abduction relative to the ground. The velocity of the foot during running is increased compared to walking velocity, due to the downwards and forwards velocity of the foot prior to ground contact (Cole *et al* 2001).

Figure 2.2.1. – An example of the ground preparation phase for shod heelstrike running

2.2.1.2 Initial Contact

As the heel makes contact the initial point of contact is the heel pad, which as previously mentioned, plays a role in the absorption and dissipation of the impact. Aerts *et al* (1996) noted that as the heel strikes the ground, the heel pad is subjected to high ground reaction forces. It is within 20ms of initial contact that the vertical ground reaction force profile exhibits its first peak. This impact peak is as a result of the deceleration of the support leg (Bobbert *et al* 1992), and its magnitude is influenced by the role of other body parts and footwear, *i.e.* running technique has an influence on the impact peak.

2.2.1.3 Midstance

Following initial contact the load transfers from the hindfoot to the forefoot. The tibia rotates forward over the foot, there is also pronation at the subtalar joint. During midstance, the foot is flat on the ground, but by the end of this phase there is no loading under the hindfoot and the heel starts to rise (Henning and Milani 1995). Scott and Winter (1990) states that during midstance, the loading of the lower extremity is at its greatest.

Figure 2.2.2 – An example of the midstance phase

2.2.1.4 Push-off

This stage sees the complete transfer of load onto the forefoot, and the vertical ground reaction force decreases until toe-off. Cole *et al* (2001) came to the conclusion that the rigidity of the foot during push-off influences its ability to act as a lever. Traction becomes important as the foot applies a horizontal propulsive force to the ground.

It's method of attachment to the metatarsal heads means that traction is placed on the plantar fascia as a result of MPJ dorsiflexion and ankle plantar flexion, acting to elevate and stabilise the longitudinal arch. MPJ dorsiflexion also occurs during terminal stance as the body passes over the foot. The overall process of stabilising and elevating the longitudinal arch allows the foot to become a lever system for propulsion. The efficiency of this propulsion is dependent on the radius of the metatarsal heads; this radius is increased for the first MPJ compared to the lateral joints due to the presence of the sesamoid bones. This means that it is possible to generate more tension through dorsiflexion of the great toe (Bojsen-Moller and Lamoreux 1979).

Figure 2.2.4 – An example of the ground push off phase

2.2.2 Walk to run transition

A key difference between walking and running is the double stance and double swing phases. Walking can be defined by having two phases of double limb support, where both feet are in contact with the ground at the same time, one at either end of the ground contact phase. This results in an overlap which means that there is always at least one foot in contact with the ground at all times. The transition from walking into running occurs as the periods of double limb support are replaced by periods of double float, where neither foot is contacting the ground. This means that throughout the entire gait cycle, there is no point where there is more than one foot in contact with the ground and times where neither foot is in contact with the ground (Novacheck 1998).

As velocity increases the walking gait will become running gait. Typically the transition occurs at approximately 2m/s (Kram *et al* 1996). During the walking gait at least 50% of the time is spent in the stance phase, as the gait moves into running and eventually sprinting, this time decreases, with more time being spent in the swing phase decreasing ground contact time. Novacheck (1998) was able to quantify the velocities of different gaits and demonstrate the relationship between an increase in gait velocity and a decrease in ground contact time, as shown in the following table:

Table 2.2.1 – The respective velocity and ground contact times for walking and running (Novacheck, 1998)

Gait	Velocity(m/s)	Approximate Ground Contact Time (s)
Walking	1.2	0.6
Running	3.2	0.2

2.2.3 Ground Reaction Forces

The ground reaction forces are a measure of the three-dimensional forces exerted by the foot on the ground (figure 2.2.5). Typically the vertical ground reaction force profile has two peaks, the first is the impact peak and the second the active peak which occurs during midstance. Nigg (1986) has shown running speed to influence the vertical ground reaction forces. For heel strike running the impact peak has been shown to occur within the foot 15-

20% (approximately 0.04s) of the stance time, and approximately 2 times bodyweight. The active peak occurring between 35-50% of the stance time (approximately 0.05s) (Cavanagh and Lafortune 1980, Munro *et al* 1987). Under walking conditions each of the peaks are more similar in terms of magnitude, both being close to one bodyweight, each occurring at approximately 20% and 80% of stance respectively (Keller *et al* 1996).

Antero-posterior force data represents horizontal forces in the direction of motion. The anterio-posterior GRF components consists of two clear phases, the initial phase immediately following impact represents the braking phase. The second phase corresponds to the push-off in which a propulsive force is applied to the ground. For steady-state walking and running the net impulse of these two phases will equal zero. The magnitude of anterio-posterior GRF component is approximately 0.15BW for walking and 0.3-0.4 BW for running. (Cavanagh & Lafortune 1980).

The medio-lateral force represents horizontal forces perpendicular to the direction of motion (Hunt *et al* 2001). The magnitudes and phases of this force are heavily dependent on the gait style, over pronation for example will result in a larger initial peak. However, both walking and running is much smaller than the vertical and anterio-posterior forces.

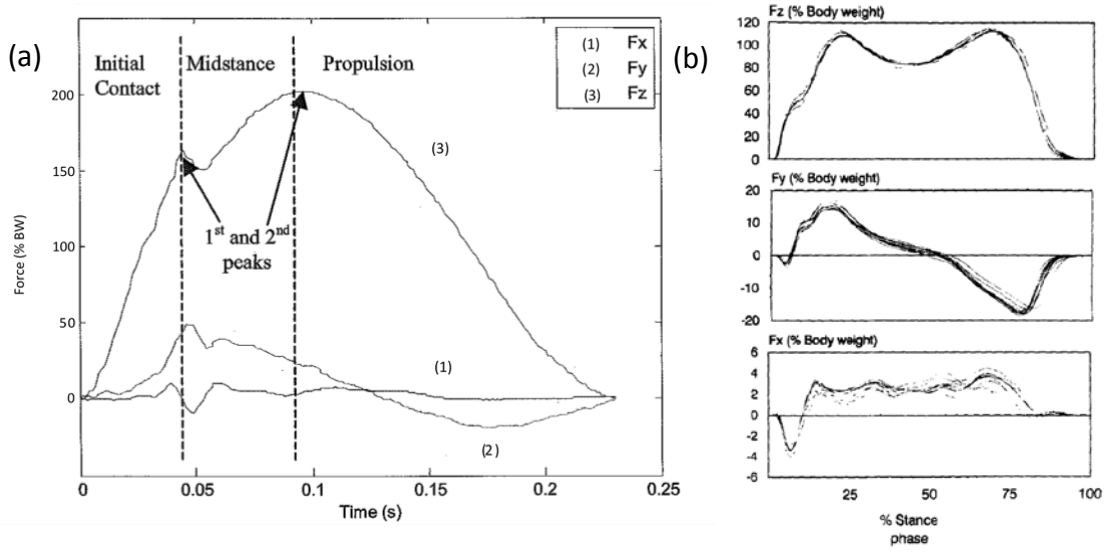

FIGURE 2.2.5 – Figures illustrating the three different force profiles, for **(a)** running and **(b)** walking, Fx = medio-lateral reaction force, Fy = anterio-posterior reaction force, & Fz = vertical reaction force; reproduced from (Mara 2007, Hunt *et al* and Giakas 1996)

2.2.4 Centres of Pressure

Centre of pressure is the point at which the ground reaction forces are applied to the foot. Whilst studying foot and ankle biomechanics during walking, Rodgers (1988) created a figure that linked the phase of the gait, vertical ground reaction force and locations of centre of pressure during walking. This is reproduced by the following figure:

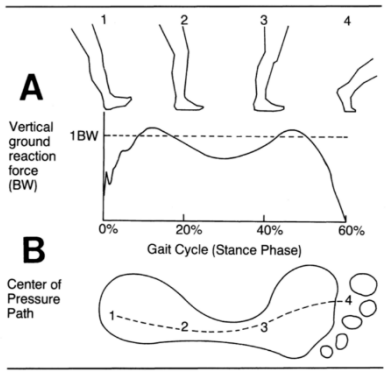

Figure 2.2.6 – An interaction between the foot and the ground during walking. **(1)** Heelstrike, **(2)** foot flat, **(3)** midstance and **(4)** toe-off. Reproduced from Rodgers, 1988.

De Cock *et al* (2008) conducted a study to describe and interpret the CoP trajectory during barefoot running. Initially the peak was found to have a medial bias, indicating pronation. As footstrike continued a lateral shift of CoP, towards the border of the foot, was noted during the forefoot contact phase.

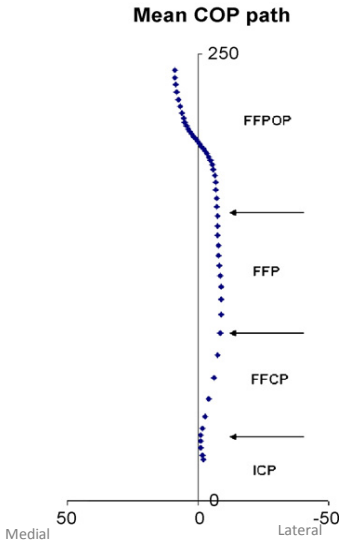

Figure 2.2.7 – The centre of pressure path during barefoot running. Reproduced from De Cock *et al* (2008).

2.2.5 Gait Kinematics

It is important to have a knowledge of the foot and ankle kinematics during each type of gait. The *dynamic biomechanics of the normal foot and ankle during walking and running* was investigated by Rodgers, 1988. A summary of the movements of the lower limb joints was presented, as shown in figure 2.2.8 a reproduction from the work.

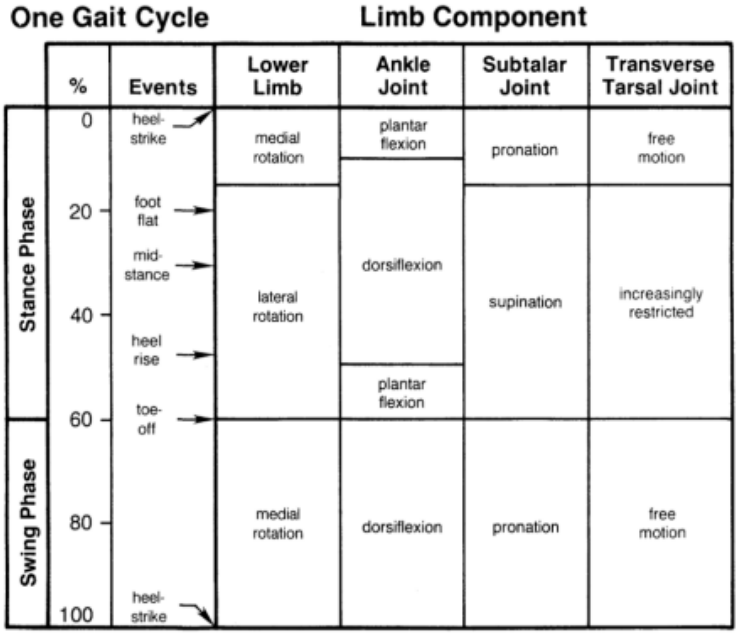

Figure 2.2.8 – A summary of joint motions during the different phases of gait. Reproduced from Rodgers, 1988.

De Wit *et al* 2000 investigated the sagittal and frontal plane kinematics of nine subjects during the stance phase in both barefoot and shod conditions, they assumed that different touchdown geometries are adopted in barefoot compared to shod conditions in an attempt to limit pressure on the heel. Their main kinematic findings are summarised in the following table:

Table 2.2.2 – The frontal and sagittal plane kinematics of 9 subjects, reproduced from De Wit *et al* 2000.

	Running (3.5 m/s)		***Sprinting (4.5 m/s)***	
	Barefoot	*Shod*	*Barefoot*	*Shod*
Vert. ankle deceleration distance (cm)	1.1	1.9	1.1	2.1
Ankle angle at touchdown (deg)	90.4	82.2	91.8	81.7
Sole angle at touchdown (deg)	6.4	18	18	20.8
Heel velocity at touchdown (m/s)	1.23	1.67	1.39	1.86
Horizontal heel velocity at touch down (m/s)	1.11	1.58	1.16	1.64
Vertical heel velocity at touchdown (m/s)	-0.51	-0.52	-0.74	-0.84

Hanson *et al* (2004) studied the movement of the human ankle during walking, with the intention of designing a biofidelic ankle prosthesis. The loading and unloading of the moment versus angle curves showed clockwise hysteresis loops that reduced back to zero during slow walking gait. As gait velocity was increased these loops started to transverse an anti-clockwise path, increasing in area with speed. Given these findings, Hanson *et al* (2004) hypothesised that 'a traditional ankle joint could be replaced with a rotational spring and damper for slow to normal walking speeds'.

2.3 ATHLETIC FOOTWEAR

A key application of robotic emulation of human gait is in the research and development processes of athletic footwear. Therefore, it is important to understand the nature of athletic footwear industry in particular, the design of a shoe and how they are developed, these aspects are covered in this section.

The athletic shoe industry is one of the most lucrative and competitive markets in the world, and the leading companies are prepared to dedicate large amounts of money to the research, development and marketing of athletic footwear - $185.2bn as of 2011 (PRWeb 2013). Typically, there are two main goals when a new type of athletic footwear is designed; either to increase performance and/or to decrease the injury potential (Cole et al 2001), whilst maximising the comfort for the user. It is in achieving these goals where companies are striving to achieve a competitive advantage over their rivals, in offering the customer the best possible product. Specifically the crucial role of athletic footwear was highlighted by Bates et al 1983 - 'the foot shoe complex forms the dynamic base upon which the runner functions. What happens at the foot-surface interface affects the total functional mechanism.'

2.3.1 Footwear Anatomy

The anatomy of a typical running shoe/trainer is given in figure 2.3.1. The outsole is the bottom layer of the shoe and is the primary interface with the ground. Most shoes use carbon rubber with various other compounds for durability and increased traction (Chase 2009 and Mills 2003).

The midsole is comprised of three separate areas that provide cushioning, stability and torsional control for the hindfoot, midfoot and forefoot. The most popular material used in midsole construction is EVA (ethylene-vinyl acetate) with different manufacturers using different formulations. Heel cushioning and absorption units come with various levels of technology and sophistication to dampen the impact and attenuate shock. Forefoot cushioning is similar to that of heel cushioning (Chase 2009).

The sock liner/insole is a supplemental layer of padding closest to the foot implemented to separate the foot from the midsole. Nigg et al (1988) suggested that this layer has varying function depending on the location. The medial hindfoot region is believed to assist in pressure distribution and the lateral hindfoot region is meant to aid in cutting or sidestep movements.

The upper is attached to the midsole and is responsible for restraining the foot; this region is comprised of the heel counter, toe box, lacing system and the tongue. The heel counter is the internal support feature which wraps around the heel, holding it in position during movement. The lacing system helps to keep the upper tight around the foot and helps to hold its form. The tongue is generally a padded area that as well as providing protection help to screen out debris and precipitation. The purpose of the toe box is to cover and protect the toes and should be large enough to accommodate them comfortably (Chase 2009 and Ferrandis et al 1994).

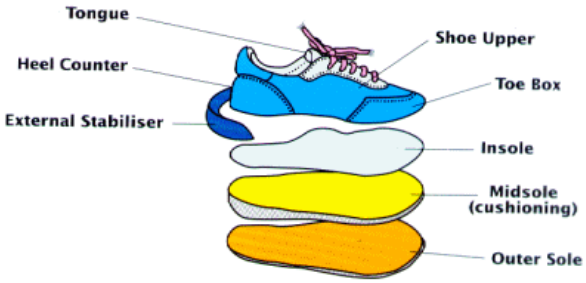

FIGURE 2.3.1 – The anatomy of the running shoe, Chase *et al* (2009)

2.3.2 Footwear Properties.

The main mechanical properties of the shoe that affect its performance are:

Cushioning refers to the ability of a shoe to absorb shock. Cushioning is the part of the shoe where most development occurs (Frederick 1989). As the level of cushioning increases the stiffness of the material tends to decrease and vice-versa.

Stability refers to how easily the shoe can resist the movement of the foot primarily pronation, i.e. features are included to reduce pronation. This for example, could be achieved by increasing the density of the midsole.

Durability is the ability of the shoe to withstand wear, pressure or damage. Athletic shoe degradation helps to sustain the industry, customers seek replacements whilst the manufacturers strive to improve products.

Flexibility (bending stiffness) is the ability that a shoe has to bend.

The **bending stiffness** of an athletic shoe may not have that much of an influence on the shoe ground interaction; Olsen et al (2005) found that the combined stiffness of the foot and the shoe is dominated by that of the foot. However this property shouldn't be ignored as Stefanyshyn and Nigg (1998) suggested that running shoe bending stiffness does influence the shoe-ground interaction.

For a long time, the most popular shoe material was leather, but this was eventually replaced by open-cell foams, the most popular being ethyl vinyl acetate (EVA). This a cost effective lightweight material that was easy to mould, it also has good shock absorbing properties (Johnson 1996). Softer EVA provides more cushioning and harder EVA provides more support for the foot. Research into materials by (Mills 2003) has shown that over time soft EVA will permanently compress and become denser and therefore have reduced cushioning properties. This is similar to the findings of Challis et al (2008), for the human heel pad, i.e. it has reduced in thickness after a lot of running.

Despite the innovations and advancements in the industry, arguments have been made suggesting that the advancements have not been advantageous. Baycroft and Culp (1993) indicate that there was no scientific evidence validating claimed improvement of athletic shoes since the 1970's. (Cole et al 1995) suggest that the shoe may increase the stiffness in the foot by restraining sideways compression. When confined within the shoe, heel pad deformation has been shown to be reduced (Aerts and De Clercq 1993). This may be due to the cushioning of the shoe. However, there are many benefits to athletic footwear, as well as providing protection from the elements; they provide traction, which can improve performance.

2.3.3 Development Process

Mara (2007) shows how the design and development process for footwear can be split into the three subsections of design, prototype and mass production. The design phase begins with an initial concept; the purpose is identified along with potential materials and dimensions. Computer Aided Designs (CAD) are created and some limited mechanical tests are performed in a laboratory setting (Mara 2007).

The prototype phase is the beginning of shoe production, it is where an original type or form is created and can be used as a standard for later stages. The CAD models are used to create moulds for outsole and midsole fabrication, the uppers are cut and stitched from fabrics and the shoe is constructed. Both biomechanical and mechanical tests are performed on the prototype and if certain specifications are not met, changes are made accordingly. The prototype testing may involve individual parts or the whole shoe. The tests performed on the whole shoe can be mechanical (section 2.4) or biomechanical in the laboratory or real world environments (Cavanagh 1980).

The mass production phase employs the most efficient methods with high standards of quality control. A foot model with the desired dimensions made of wood or plastic, called a last, is used for production of the shoe. Lasts, which are straighter, provide more stability, benefiting athletes who have flexible feet (Hilgers et al 2009). There is an obvious disadvantage to this in the fact that the lasts are created for an 'average' foot shape. It may be the case that certain members of the population may not be able to find shoes that are comfortable and that suit them. This may be one of the reasons why many people, especially high standard athletes, are now turning to bespoke shoe customisation with sport specific and individual athlete requirements. A point echoed by (Bates et al 1983) who conducted a study to investigate the effects of athletic footwear on the ground reaction forces during running. Tests were performed on five different subjects wearing five different types of shoe, with shoe type being shown to affect ground reaction forces. The different shoe types varied from those providing better shock absorption to those providing more pronation control. The main conclusion was that there is no "best" shoe, and that each runner may require a different type of shoe due to variations in foot anatomy and function.

2.4 MECHANICAL FOOTWEAR TESTING DEVICES

To support the footwear development process companies utilise a number of research and development techniques; biomechanical, wear and mechanical testing are the most common, while virtual testing (Cavanagh 1985) is also being pioneered by some of the bigger companies such as NIKE and adidas.

The technique of using biomechanical testing is well established and an important step in the design process. The main purpose of biomechanical testing is to subject footwear to real world wear scenarios but these methods are not perfect and there are number of associated drawbacks. The introduction of a human subject to the design process can lead to large amount of variability. Human gait varies across the whole population and comparing it to a predefined set of biomechanical data may prove to be unreliable. The intention of a wear test is to evaluate and understand the properties of the shoe under realistic use conditions. Tests subjects are given the shoes and instructed to use them intensively for a pre-defined period of time, the company will then assess any wear or damage that has occurred to the shoe. The subject may also be asked to complete a questionnaire on their opinion of the shoe and its performance. This test method is not very standardised and can therefore provide a wide range of results. As well as being time consuming, the results can be heavily influenced by a large number of factors including; subject weight, running style and activity levels as well as surface and weather.

As mentioned, the larger athletic footwear companies also employ virtual testing, using finite element analysis methods. Virtual testing can speed up development times by reducing the emphasis on prototypes and allows for a lot more control and consistency of the testing compared to human testing. However, the development of finite element models is a time consuming and challenging process. Furthermore, at present they do not account for any changes in technique a runner may make based on shoe design.

Alongside the techniques outlined above, one of the most common methods is mechanical testing (Odenwald 2006), which has been developed to allow a standardised assessment of footwear. These standards cover multiple aspects of footwear ranging from a materials resistance to tear to the tensile strength of the upper and outsole of a shoe. Some of the most common methods of mechanical testing for footwear involve various compression or flexion tests of the midsole unit. For example the American Standard for Testing Materials (ASTM F1614-99 (2006) 'Standard Test Method for shock Attenuating Properties of Materials Systems for Athletic Footwear' specified that a metal cylinder (45.7 mm diameter; mass 8.5 kg) is dropped vertically from a height of 50 mm onto the heel of the shoe and repeated five times (Newton Running 2013). There are a number of flaws to this type of test method, for example the mechanical nature of the test does not accurately represent the biofidelity of the human gait, and this tends to give poor representation of the shoe response in a sporting action. Such tests can, however, be used to benchmark shoe properties against previous well accepted products.

Increasingly athletic footwear manufacturers are attempting to improve the mechanical tests. Newton running for example approached Knight Mechanical Testing (KMT), who usually specialise in military, aerospace and medical testing; to develop a mechanical test that emulates footstrikes for runners of 60, 70 and 80kg moving at 3 m/s over a minimum of 150 miles. The more realistic conditions (force, cadence and loading angle) has helped to provide an understanding of how the shoe would perform in the real world (Newton Running 2013). As well as attempts to improve the simple mechanical test methods, there have been steps taken to attempt to mechanically emulate the human gait, with varying degrees of success. Advanced robotic emulation of the human running strike would revolutionise the industry and be of considerable importance for the shoe testing and design sector, however it is still in its infancy and many of the techniques are basic and un-refined. The following section outlines the features and capabilities of some robotic test devices that are currently used in industry.

2.4.1 Existing robotic test devices

The **adidas wheel wear machine** (WWM) is used to test the durability of shoes. The motion of this machine attempts to replicate the walking and running gait cycles. Six synthetic legs and feet (made from compliant foam lasts) are arranged in a circular array, each leg has shock absorbers positioned at the ankle and hip. The compliance of the feet helps to make them more biofidelic in mimicking flexion/extension of the MPJ. This configuration is driven in a continuous circular motion by a motor at the centre (figure 2.4.1). If need be, the surface of the floor and environment can be changed.

FIGURE 2.4.1 – The adidas wheel wear machine. Reproduced from Mara (2007)

Mara (2007) found noticeable differences between the gait patterns of a human and the wheel wear machine. The machine provides initial contact with the ground in the hindfoot region, but then becomes less biofidelic as the contact moves from the rear medial region to the forefoot lateral region in a diagonal path. As mentioned in section 2.1.1, this has the drawback of giving a different wear pattern on the shoe as well as not providing the correct pressure distribution. Any measurements recorded by the wheel wear machine should therefore be interpreted carefully.

Analysis of the vertical ground reaction force trace for the WWM running motion show there to be four peaks, as opposed to two for human walking and running, an example of which can be seen in (figure 2.4.2). Analysis of high-speed video of the machine indicated that there are 3 distinct points where the foot is raised slightly and lowered again as the machine moves the foot through heel strike to toe off. The duration of the first peak is

approximately 0.15-0.2 seconds, close to the same time as a human takes to perform one complete foot strike (table 2.2.1), in this time the machine has only been able to perform a heel strike action with no roll on to the more distal aspects of the foot. The overall strike time for the machine is 0.65 seconds, three times longer than a typical heelstrike ground contact period for human running. The machine has however managed to replicate a peak force value that could be expected for a human, of approximately two times bodyweight. The results obtained by Mara (2007) also show that the overall profiles of the ground reactions in the anterio-posterior and medio-lateral directions have very little in common to those obtained in human running.

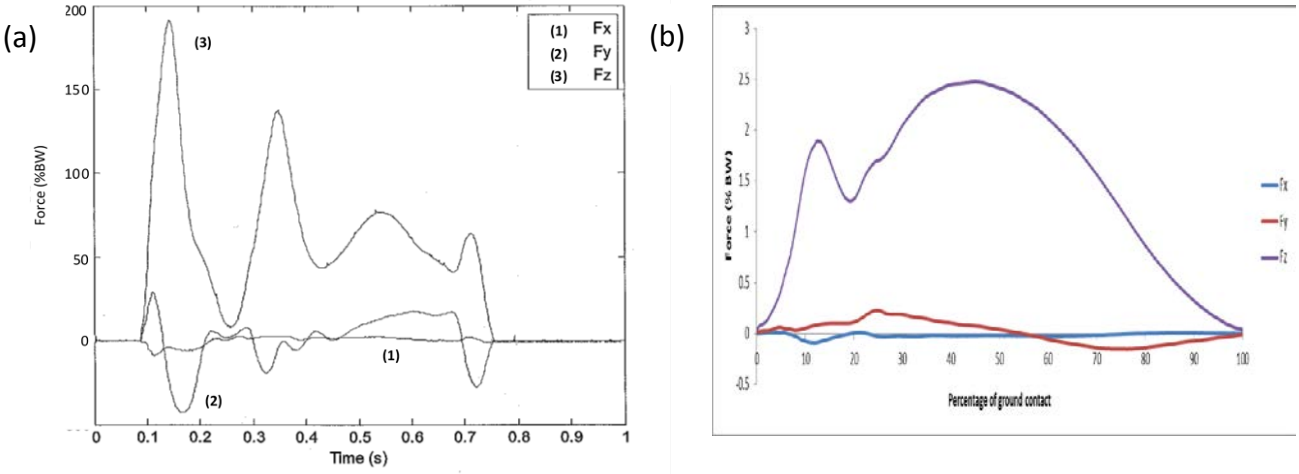

FIGURE 2.4.2 – Typical Ground Reaction Force (a) WWM when running (Mara, 2007) & (b) Human heelstrike running; Fx = medio-lateral reaction force, Fy = anterio-posterior reaction force, & Fz = vertical reaction force.

The **Pedatron** designed by SATRA (SATRA Technology Centre) is a biomechanical abrasion tester intended to provide accelerated wear simulation under realistic conditions. It aims to combine aspects of both human and mechanical wear testing methods, giving the realism of a human test and the speed of a mechanical laboratory test.

The **Pedatron** is made up of two distinct components; sample footwear is mounted on a foot (solid last) attached to a leg which is driven by a ball screw mechanism and a mechanism rotates the floor (to give turning gait) which is synchronised with the leg movement. The force profile achieved by the Pedatron can be altered by adding or subtracting weights to the end of the leg. By altering the velocity of the lead screw the velocity of the robot will also alter, allowing it to 'replicate the action of normal walking through to sprinting'.

FIGURE 2.4.3 – The Pedatron – SATRA, reproduced from SATRA test equipment catalogue.

The Shoe and Allied Trade Research Association (SATRA) claim that the Pedatron can 'impose a true walking action' which is based on motions speeds and pressures obtained in biomechanical studies. However, no published data is available on the kinematics or kinetics of the footstrike. All of the replications are in the form of straight line and turning steps. The shoe is impacting a concrete slab, providing a demanding realistic surface to help simulate wear. Results obtained are similar to those found in the human wear trials; however this stage was reached after 6 hours (12,000 steps) as opposed to the 30-80 days for human running. The machine is currently primarily used to investigate the wear of floor surfaces due to human impact (Hubbard, 2009).

De Raeve *et al* (2014) have used a KUKA 6 degrees of freedom robot (KUKA robotics; United Kingdom) to mimic the kinematics and kinetics of a prosthetic foot during the human walking gait (figure 2.4.3). The results of the work have shown that the robot is able to emulate shank kinematics and produce similar ground reaction forces to those of healthy human subjects. This system now has potential to be adapted to emulate more complex and unusual gait styles.

Figure 2.4.3 The KUKA 6 DoF industrial robot used by De Raeve *et al* (2014), reproduced from De Raeve *et al* (2014)

Starker *et al* (2013) used a ABB IRB 6600 6 DoF industrial robot of the walking gait of a human lower limb amputee (figure 2.4.4), this allowed for the same prosthetic to be used in both robot and human data collection and for a variety of prosthetics to be tested. Position emulation proved to be accurate and force emulation was similar but not identical, with issues applying the force in the correct area. It was possible to emulate the magnitudes of the vertical ground reaction forces, with a good match for the loading rates, the unloading rates for the second peak are lower for the robot compared to the human. The horizontal ground reaction forces proved more difficult to emulate, the magnitudes were too large and they were in single phase (figure 2.4.5).

Figure 2.4.4 The ABB 6 DoF industrial robot used by Starker *et al* (2013), reproduced from Starker *et al* (2013)

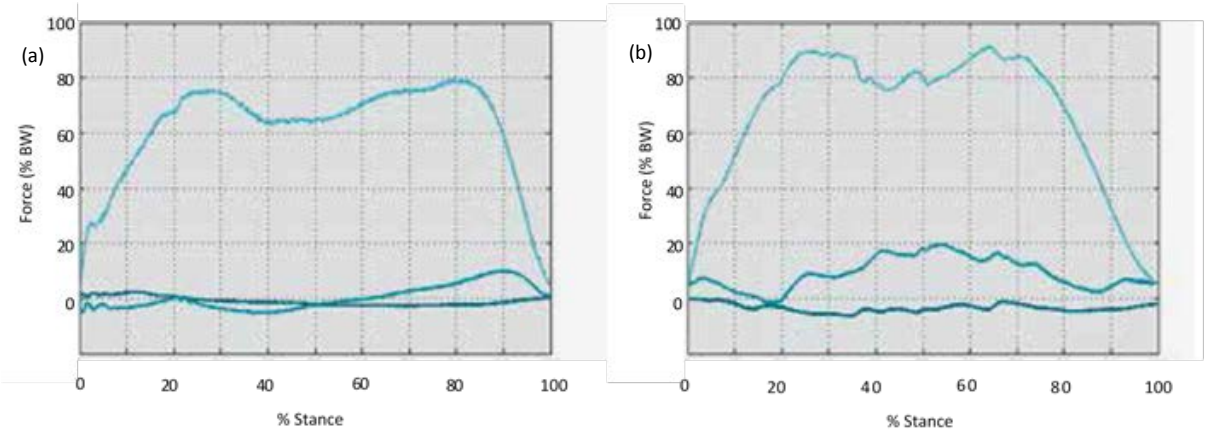

Figure 2.4.5 The ground reaction forces for **(a)** the human subject and **(b)** the ABB robot, reproduced from Starker *et al* (2013)

The **Stewart platform** is a 6 degree of freedom (6DoF) mechanical manipulator device that connects two plates between 6 extendable legs (figure 2.4.6). The functional movement of these legs, are responsible for the movement of one of the plates, the other being fixed (Mara 2007 and Stewart 1995). Monckton and Chrystall (2002) investigated the device and found it to offer control over force and position in 6 degrees of freedom for automated footwear testing, recreating human kinematics of the footstrike. However, the authors were unable to achieve this aim due to a restriction of the motor capabilities of the control system.

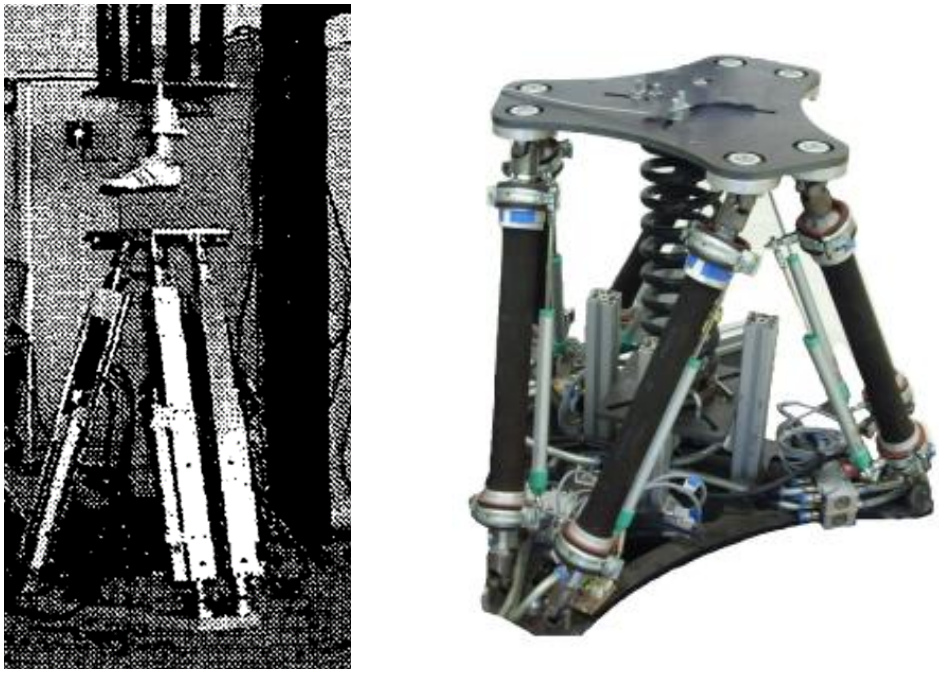

FIGURE 2.4.6 – The Stewart platform (a) - Monckton and Chrystall (2002) & (b) – reproduced from: http://www.robotik.jku.at/joomla16/index.php/forschung/research-projects/stewart-gough-plattform

Starker *et al* (2014) used a hydraulically driven Shore Western (KS2-07) test machine (figure 2.4.7), traditionally used to test prosthetic feet in accordance to ISO22675:2006, to emulate the human running gait using a prosthetic footform. Forces are generated as the footform is pushed down onto a tilt table, which moves through the contact phase, this is a similar concept to the Stewart platform. The results of the study were found to be reproducible. Vertical ground reaction force magnitudes could be matched for a gait that was 60% of the real-time run velocity. There was more of an issue in matching the horizontal ground reaction forces of the human gait.

Figure 2.4.7 The tilt table used by Starker *et al* (2014), reproduced from Starker *et al* (2014)

Ronkainen et al (2008) used a **FANUC R2000iB** robot (FANUC robotics; Mount Fuji, Japan) to quantify robot repeatability and attempt to emulate the kinematics and kinetics of heelstrike and forefoot running using a test device which is not limited to only one or two linear or rotational degrees of freedom. The kinematic motion of the robot was highly repeatable (<2mm mean SD in all marker sets) over 500 cycles for both footstrikes.

Despite being repeatable, some of the emulations were not very close to the human data. Figure 2.4.8 shows the discrepancy between the robot and human for vertical ground reaction force and heel marker trajectories. The magnitudes of the vertical ground reaction force profile are adequate, but the loading rate is not, with the maximum peak occurring at approximately 80% of stance as opposed to 20%. The heel trajectory does not follow the expected profile, appearing to generate a larger footprint. This is perhaps a by-product of robotic smoothing influencing kinematics.

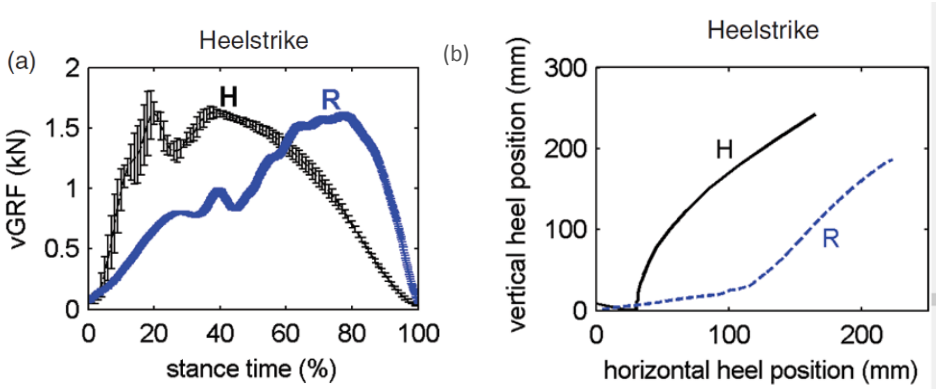

Figure 2.4.8 – Results reproduced from Ronkainen *et al* (2010). **(a)** The vertical ground reaction force for heel strike running for the robot (R) and human (H) and **(b)** The heel marker trajectories for heel strike running for the robot (R) and human (H).

The authors were also able to identify a number of potential improvements that could be made to the system to help achieve the aim of footstrike emulation. One such suggestion was the inclusion of a more realistic end-effector, which is addressed in Chapter 7 of this thesis.

2.4.2 Other robot applications in sport

It is not just in footwear testing that have given rise to challenges in pioneering the use of robots for sports equipment testing. Harper (2006) found that the position of a golfers swing could easily be replicated but golf club shaft deflections were completely different to those found with human subjects.

As well as the running industry, Robots are used all over the world for testing and validation purposes in other sectors the sports industry. For example the United States Bowling Congress (USBC) have developed a state-of-the-art automated ball-throwing robot called EARL (Enhanced Automated Robotic Launcher). The Equipment Specifications and Certifications team at the USBC use EARL to test the dynamics of bowling balls as well as lane conditions. In the design process the engineers at the USBC initially planned on using a six degrees of freedom industrial FANUC robot. However, after further investigation the USBC deemed that the size of the 'off the shelf robot' that they required couldn't generate enough speed for the intended purpose. It is because of this that the USBC decided to move away from using an industrial robot and commissioned a specialist company to make a bespoke robot.

2.5 THE ROBOT FOOTFORM

Any robotic device that aims to emulate human gait requires a specific footform, end-effector or tool. This is the primary interface between the robot and the surface during movement and could be the difference between successful and poor footstrike emulation. Although cadaveric studies have been performed, it is very difficult to use a real human foot in the emulation process, the most common option for the end-effector is a rigid last or a prosthetic foot. There are some immediate disadvantages to using this as noted by Mara (2007); prosthetic feet are rigid and do not necessarily share the same properties as the human foot, this may result in different shoe wear patterns.

There are a number of prosthetic feet available on the market, which are robust enough to withstand the high impact forces and repetitions associated with running and jogging. The main options are outlined below:

2.5.1 Blatchford Elite 2

The 610g *'endolite elite2'* prosthetic is made up of three independent enhanced e-carbon springs (tripod system) encased in a removable rubberised 'foot like' shell. This is intended to provide shock absorption and energy return, allowing the user to perform moderate-high impacts such as running and jogging (Figure 2.5.1).

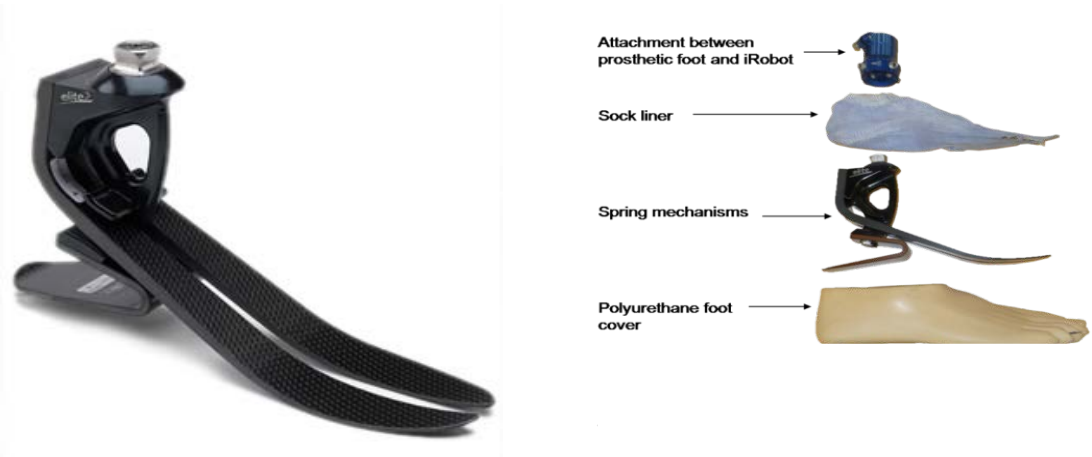

FIGURE 2.5.1 – The Blatchford elite2 and its configuration as a prosthetic device.

The elite2 is designed for enhanced running performance with a dual spring mechanism in a tri-pod orientation that optimises energy response helping to simulate heelstrike and toe push off. Even transfer of shear forces for a smooth roll over and load transfer at late stance which is similar to the human gait.

2.5.2 The Otto Bock Trias

This is a very unique prosthetic, it has a three spring configuration, as opposed to the more common two spring approach of other prosthetics such as the elite2.

FIGURE 2.5.2 – The Otto Bock Trias – www.ottobock.co.uk

Like the elite2 the Trias has springs to represent the forefoot and heel mechanisms, but it also has a third representing the plantar aspect of the foot. All three of the springs are made of a lightweight carbon which are all connected to each other in a triangular configuration. When loading occurs at the heel, the dual heel spring provides shock absorption and cushioning, ankle MPJ plantarflexion is also encouraged through the connection to the base spring. This theory links in with the work of Drake *et al* (2005) and Graaff (1998) who found the plantar aspect of the foot to compress as weight is placed on the foot, and 'spring' back as it is lifted. The prosthetic aids propulsion through the compressed energies stored within the springs also being returned. Tests that Otto Bock have conducted on the prosthesis have shown it to allow biofidelic ground reaction forces, (figure 2.5.3). Mimicking the plantar aspect may also help make the prosthetic more biofidelic, as was suggested by Kogler (1996).

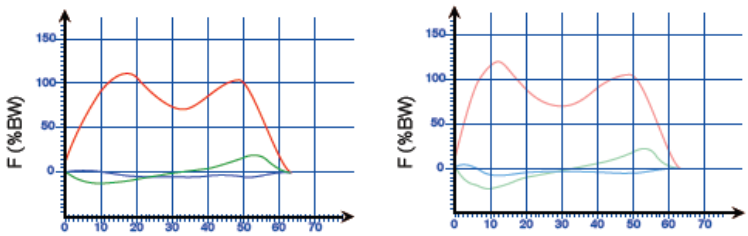

Prosthetic foot Able foot

FIGURE 2.5.3 – Walking vertical GRF for the Otto Bock TRIAS, for the three different force profiles

The main drawback to the Trias is that has been developed for low and moderate activity level and has not been specifically designed for running. It's capability to sustain the loading associated with running gaits are uncertain.

2.5.3 The elite Vector Thrust (VT)

Unlike the elite2 and Trias the eliteVT has an ankle joint, claims to deliver improved levels of power and control. The prosthetic comes with a built in shock attenuation device at the ankle, a machined coil intended to absorb impact loads and torsional shear. The device is also capable of turning the potential and kinetic energy of motion into elastic strain energy in the springs, which is returned efficiently at crucial parts of the gait cycle. Apart from the attenuation device the eliteVT is very similar in construction to the elite2, it has a dual spring heel and forefoot mechanism, and like the elite2 is suitable for high usage and impact loads. Under robot emulation, the role of the attenuation device may be negligible. Particularly if the robot drives the foot through the entire motion then this cannot be influenced by any propulsion that the foot supplies.

FIGURE 2.5.4 – The eliteVT – www. endolite.co.uk

2.5.4 Ossur Ceterus

The Ossur Ceterus (figure 2.27) also has an attenuation device at the ankle joint which is very similar to the eliteVT; it is a three-spring configuration that follows the design of the Trias, with one of the springs located on the plantar aspect.

FIGURE 2.5.5 – The Ossur Ceterus - http://www.oandp.com

2.5.5 Rigid Last

It would also be possible to use a rigid last (figure 2.5.6) as a footform for use with the FANUC robot. This is traditionally used in the manufacture of footwear (section 2.3) and would be the least biofidelic of all of the listed options, as it is one solid mass.

Figure 2.5.6 – A rigid last, traditionally used in footwear manufacturer but could have applications as an end-effector footform.

2.6 SUMMARY

The aim of this chapter was to present a comprehensive review of the current literature relevant to robotic emulation of the human footstrike and thereby help to address research question one of this thesis. One of the most important areas of knowledge is the anatomy of the foot and how the foot interacts with the ground during gait. This has provided empirical, anatomical, kinematic and kinetic information that can support the remainder of this thesis, for example, in the development of a new end-effector for footstrike emulation (Chapter 7).

Having an understanding of the athletic footwear industry, the anatomy of a shoe and how it is manufactured, is important when attempting to create a system that is intended to be used within the industry. This is especially the case when considering tests methods and potential areas of investigation into footwear in subsequent sections. Mechanical testing is currently an important part of the design and test phase of athletic footwear development. There is a clear drive to develop more realistic gait emulation within this, confirming the industrial relevance of this thesis. Ronkainen *et al* (2008) have reported an emulation approach using the 6 DoF FANUC robot that demonstrated potential and is therefore worthwhile pursuing. The system was shown to be highly repeatable and the identified limitations, such as in the end-effector design, have realistic scope for improvement. To understand the mechanical testing landscape provides the background to ensure that developments on the FANUC lead in an industrially relevant direction. When evaluating the success of the emulation produced by the FANUC it will be important to understand where it fits in relation to other available test devices. The wheel wear machine, pedatron, steward platform, KUKA and ABB robots (section 2.4.1) all attempt to emulate the footstrike with differing degrees of success for different aspects of the footstrike. The parameters used to determine the success of these emulations focused heavily on ground reaction forces which have a direct influence on the wear experienced by the footwear. This confirms the need for typical human kinematic and kinetic data relevant to the shoe–ground interaction being emulated. This chapter also provided a summary and comparison of athletic prosthetic feet that are available that could be used alongside the robot end-effector. Again this provides important background information for the development work of this thesis in terms of assessing if an alternative prosthetic represents an improvement to the Blatchford elite 2.

CHAPTER 3

KINEMATICS AND KINETICS OF HUMAN WALKING AND RUNNING

3.1 INTRODUCTION

The primary aim of this thesis is to investigate the potential of using a 6 Degrees-of-Freedom (6-DoF) industrial robot to emulate the human footstrike. In order to programme the robot, accurate human footstrike kinematic and kinetic data needs to be obtained. Further, this information can also be used to validate any outcomes; it is important to know whether or not the robot provides an accurate emulation, and to what degree, if it is to be used for testing.

The human footstrike is a complex three-dimensional (3D) motion that varies with mode and velocity of locomotion. There are a number of kinematic and kinetic parameters (listed below) that describe how the foot moves and what happens during ground contact, these are also necessary to programme and validate the robot in its attempted human gait emulation. It is recognised that during walking and running the dominant movement plane is the sagittal plane. Therefore at this stage only two-dimensional kinematics are considered with the foot assumed to be a single segment:

- Kinematics (robot inputs and outputs)
  - Heel trajectory (sagittal plane)
  - Resultant heel velocity (sagittal plane)
  - Foot angle (relative to the ground in the sagittal plane)
- Kinetics (robot outputs)

- Centre of pressure
- Ground reaction forces (vertical and anterior-posterior)
- Vertical loading rate (first peak)
- Ground contact time

To evaluate the success of the robot emulation, the listed kinematics can be used to programme the robot (Chapter 9) and the above listed kinematics and kinetics can be measured and compared to human data.

At this stage in the process it has been deemed sufficient to collect typical data for one subject to act as a datum. There is no requirement to develop a larger database of gait styles until robotic emulation has been deemed adequate with one and, if necessary, this can be explored in future works. Both walking (1.2 m/s) and running (3.2 m/s) locomotion conditions are investigated, which is in line with the literature (Novacheck 1998), for both conditions the subject was both shod and barefoot. The kinematics for these conditions, can be collected using motion analysis techniques and synchronised with the kinetic outputs from a force platform. When compared to using existing data, found in literature, this process provides an in-depth data set throughout the entire movement that can be quickly and easily converted to a format that can be used as a base programme for the robot or can be referred back to when validating the robot outputs. The process of collecting required data to programme the robot and validate its outputs is addressed in the aims and objectives:

3.1.1 Aims

- To measure the foot kinematics and kinetics for one human subject at two different gait modes (walking and running) under both barefoot and shod conditions.

3.1.2 Objectives

- To collect and analyse the data in order to generate information that can be used to programme the robot and validate its outputs.
- To present the information obtained in a logical manner to allow for a quick referral and interchange with other on-going and parallel investigations.

3.2 METHODOLOGY

The experimental methodology for this chapter is shown in the following sections, documenting subject information, equipment used, data collection and processing methods.

3.2.1 Subject

The human kinematic and kinetic data presented in this chapter was collected from a number of trials carried out by a single male subject; age 25 years, height 175.2cm and mass 68.5kg, with a heel-strike running technique. The subject was an experienced recreational runner, covering 20-25 miles per week. Informed written consent was obtained in accordance with Loughborough University's ethical advisory regulations. All trials that were to be performed shod were done so in a pair of 'worn in' size 9 asics Gel running shoes.

3.2.2 Equipment

VICON

All three-dimensional motion data was digitally recorded using the VICON MX motion capture system (VICON Motion Systems Ltd., Oxford, UK). The system configuration included 9 T-series cameras, controlling hardware, and a computer running the software VICON Nexus 1.7.

The system is made up of a combination of VICON T-20 and T-40, each fitted with LED strobe units that are capable of illuminating the work space, through powerful strobes that spread the light evenly (figure 3.2.1). Retro-reflective markers that are attached to the subject, reflect the LED light back to the camera. Once the light has been collected by the camera, two-dimensional greyscale information is used to locate the markers 2D centre and radii.

Figure 3.2.1: An example of a VICON T-series camera

The passive VICON markers are made up of spheres, 14mm in diameter that are covered in retro-reflective tape and mounted on small discs, which are adhered to the subject using double-sided tape.

The nine T-series cameras were positioned around the test space focused on the central section of the 20m runway and were set to record at 250Hz, figure 3.2.2.

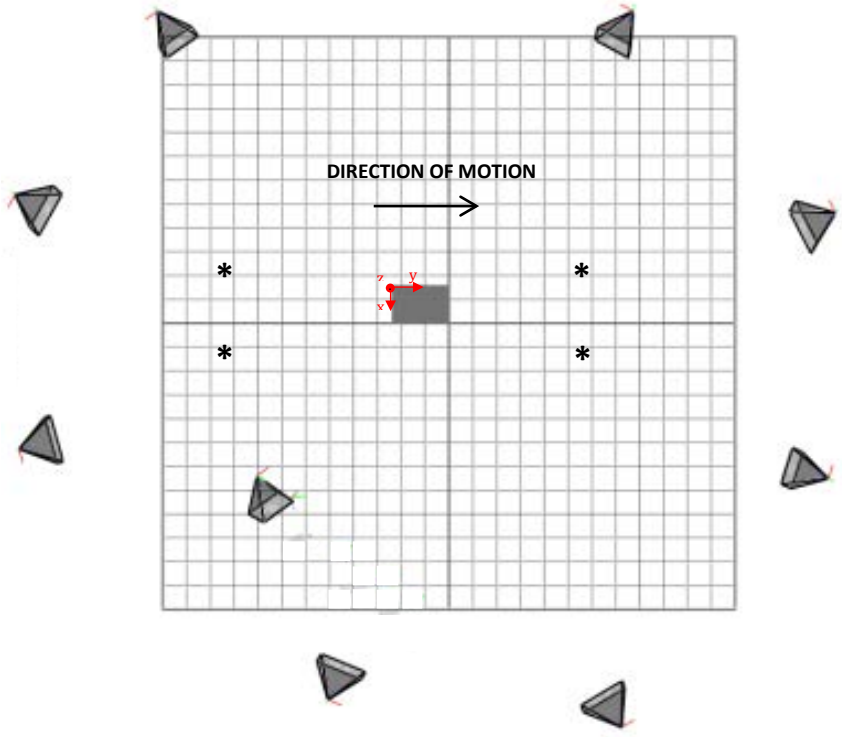

Figure 3.2.2: A schematic of the test set up used in the data collection process, showing the force plate and location of the VICON cameras. The timing gates are positioned at the locations marked (*).

The central section of the runway also contained a force plate (Kistler, Switzerland; 9281CA) that was embedded into the ground and set to record at 2000Hz. A tripod mounted highspeed camera (Photron Limited Europe, UK; Fastcam SA-1 675K-MK1) was used to record footage of the trials at 500Hz (figure 3.2.3). The camera was set up perpendicular to the direction of motion in line with the force plate, and filmed the ground contact phase of each footstrike in the sagittal plane (figure 3.2.2).

Figure 3.2.3: An example of a Photron Fastcam High speed camera

Smart Speed light gates (Fusion Sport, Pty Ltd. Cardiff, UK) (Figure 3.2.4) were set up in the central section of the runway at a distance of 4m apart, it was ensured that their range encompassed the force plate and therefore the main capture volume (figure 3.2.2). The purpose of the light gates was to ensure the subject was performing the trials at the desired velocity (running - 4±0.1 and walking – 1.5±0.1m/s). Any trials outside of this range were discarded.

Figure 3.2.4: The Fusion sport smart speed light gates

Calibration of the VICON system consists of two stages – dynamic calibration followed by setting the origin of the workspace. The dynamic calibration requires the movement of a calibration wand through the capture volume, to allow the software to calculate the position and orientation of each of the cameras and define the capture volume. The calibration wand used was made up of a 500mm bar attached perpendicularly to a 300mm bar, each with two 14mm diameter markers along their lengths and a fifth marker positioned at the joint (figure 3.2.5).

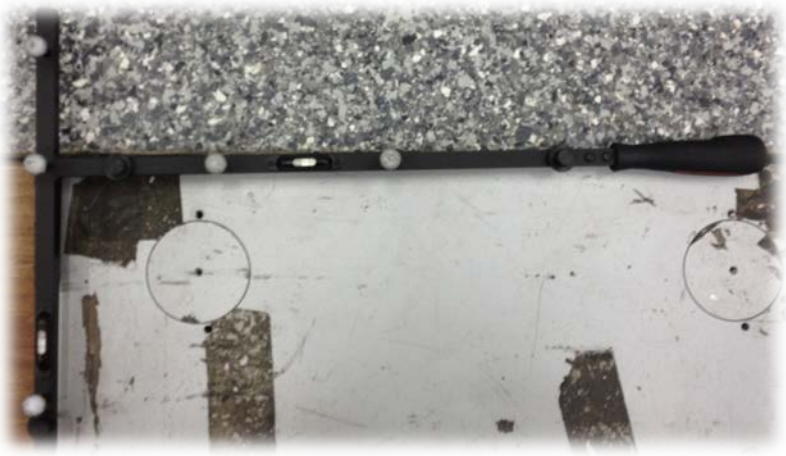

Figure 3.2.5: The wand used for static and dynamic calibration of the capture space within VICON

The same wand is used for the static calibration process, the system measures the position of the markers which are in a fixed location, to generate a global coordinate system. The wand was positioned in the corner of the force plate, thus creating the global origin (0, 0, 0). Following both types of calibration the camera positions were reviewed on the software to see if real world camera positions agree with those in Nexus.

3.2.3 Data Collection

The test subject was instructed to undertake a self-selected warm up and was allowed to practice the desired walking and running motions in the test runway area. Eleven 14-millimetre markers were attached using double sided tape to each of the subject's right shank and foot. The anatomical landmarks (outlined below), are all important and ensure that all likely kinematics are collected by providing three dimensional kinematic data of the shank, ankle rearfoot and forefoot during human footstrike. This data can in turn can be used to programme the robot and validate its outputs. The locations were first identified using a marker pen for easy and consistent re-attachment should the markers fall off:

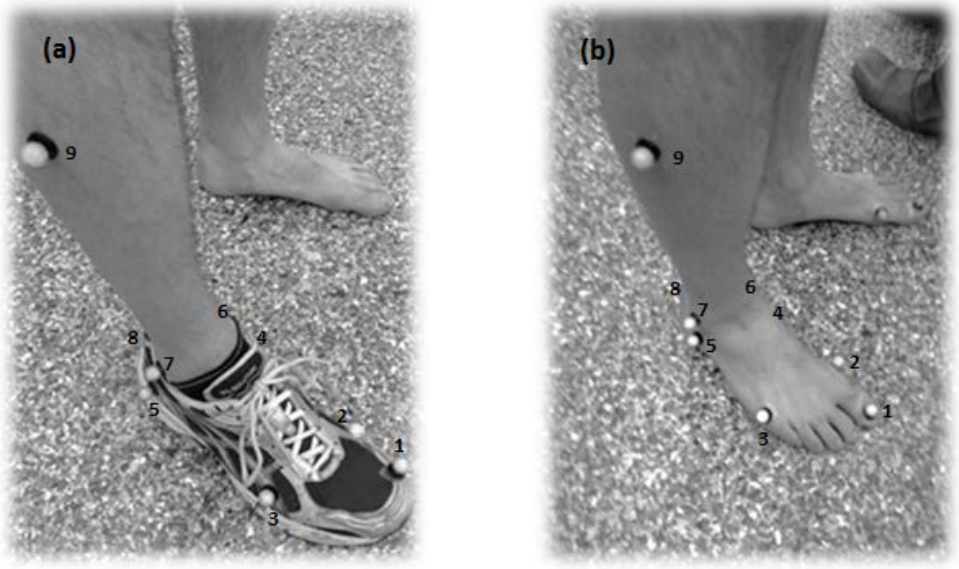

Figure 3.2.6. The anatomical positions of the VICON markers (not all are visible) for (a) shod & (b) barefoot conditions. The locations were identified through palpitation and manual manipulation of the subject. The marker locations are as follows: 1. hallux 2. Medial metatarsal 3. Lateral metatarsal 4. Medial calcaneus 5. Lateral calcaneus 6. Medial malleolus 7. Lateral malleolus 8. Heel 9. Lateral aspect of the mid-shank 10. Medial femoral condyle (not shown) 11. Lateral femoral condyle (not shown)

The data collected in this investigation was for barefoot and shod trials for both walking and running, the walking trials were conducted at 1.5±0.1m/s and the running trials were at a velocity of 4± 0.1m/s. A successful trial was one in which the subjects right foot impacted the force plate fully during footstrike and with the velocity of the subject's motion was within the desired range. It was also ensured that none of the VICON markers fell off during the trial, if this was the case the markers were re-attached and the trial was repeated. Five successful trials were captured for each of barefoot and shod walking and running respectively, i.e. twenty successful trials in total.

3.2.4 Data Processing

Each trial was reconstructed within Nexus creating the markers and their trajectories in 3D. Once identified, each marker was labelled, in accordance with the anatomical landmark list (section 3.2.3) using a pre-defined template file.

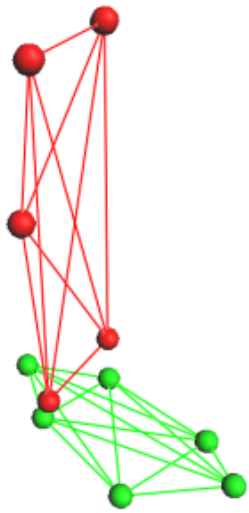

Figure 3.2.7 A visual representation of the foot reconstructed within the VICON software. The markers correspond to those identified in Figure 3.2.6.

There were some instances of marker occlusion leading to gaps in marker trajectories that needed to be filled. Small gaps, of less than five frames, were automatically filled based on kinematic information either side of the gap using functions built into Nexus, whereas, for larger gaps the software had to be instructed to do this, using a spline interpolation of the data before and after the point of interest. Care was taken when using this technique, as trajectories may not be representative of the actual test data. The next stage was to manually crop each file to only include the desired motion; from toe-off of the right foot contact prior to that on the force plate to heel-strike of the right foot contact following that on the force platform. The ground contact phase was identified using the vertical ground reaction force data, with a threshold of 10N identifying the period of contact.

Once all of the trial data had been fully labelled and saved, each trial was exported as a file which included the 3D marker trajectories as well as the 3D ground reaction and centre of pressure data. The exported data was filtered using a zero lag fourth order Butterworth

filter with a 15Hz cut off frequency, as part of the data processing within Nexus. While the ground reaction force data was unfiltered.

Each file was opened in Microsoft Excel, where it was either graphically analysed straight away or used in further calculations, all of which generated values on the following parameters, identified in the introduction to this chapter:

- Heel marker position (two dimensional in the sagittal plane)
- Heel marker velocity (two dimensional resultant velocity in the sagittal plane)
- Angles and Orientations of the plantar aspect of the foot (relative to the ground using the markers at the heel, lateral MPJ and Hallux) at impact and takeoff.
- Timings (the point of ground contact, +10N, was used as a reference point)
- Ground reaction forces (vertical and anterior-posterior)
- Vertical loading rate (first peak)
- Centre of pressures (transverse plane)

The High-speed video for each trial was cropped so that only the force platform footstrike was captured; these video files were then saved and exported for further visual analysis and, if need be, digitisation for further analysis of the above parameters. The results gained from the timing gates were used to quantify locomotion velocity and to ensure that the subject was performing the trial within the desired velocity window.

Most of the presented results are for one out of the five trials recorded for each condition. The most typical trial for each condition was selected based on evaluation of all the results.

Table 3.2.1 The selected trials for data presentation for each of the locomotion conditions.

	Trial number used
Barefoot Walk	3
Barefoot Jog	1
Shod Walk	5
Shod Jog	2

3.3 RESULTS

3.3.1 Foot Angle

The angle of the foot between the heel marker and Hallux marker and the ground in degrees, at impact and takeoff is shown in figure 3.3.1 and table 3.3.1.

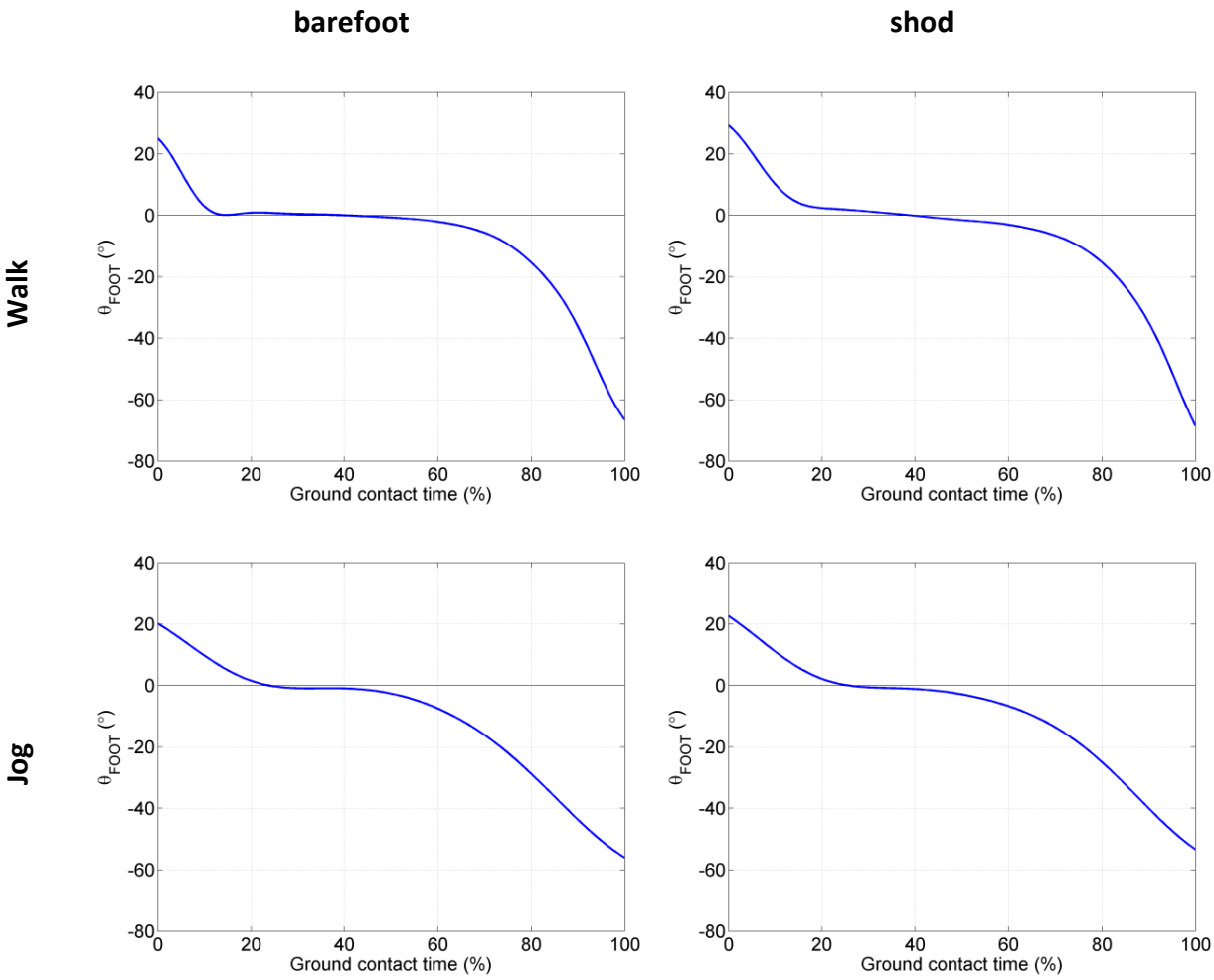

Figure 3.3.1 The angle of the foot throughout ground contact for walking and running under both barefoot and shod conditions. A positive angle at impact indicates a heelstrike.

Table 3.3.1: The angle of the foot at impact and takeoff for walking and running under both barefoot and shod conditions. A positive angle at impact indicates a heelstrike.

	Angle of foot at impact (degrees)	Angle of foot at takeoff (degrees)
Barefoot Walk	25.1	-67.7
Barefoot Jog	20.2	-57.8
Shod Walk	29.3	-70.2
Shod Jog	22.7	-55.2

3.3.2 Positions

Figures 3.3.2 and 3.3.3 provide visual information of the footstrikes (in the sagittal plane) at key instances as obtained from the high speed video data. These indicate that for each condition the initial ground contact is with the heel of the foot/shoe.

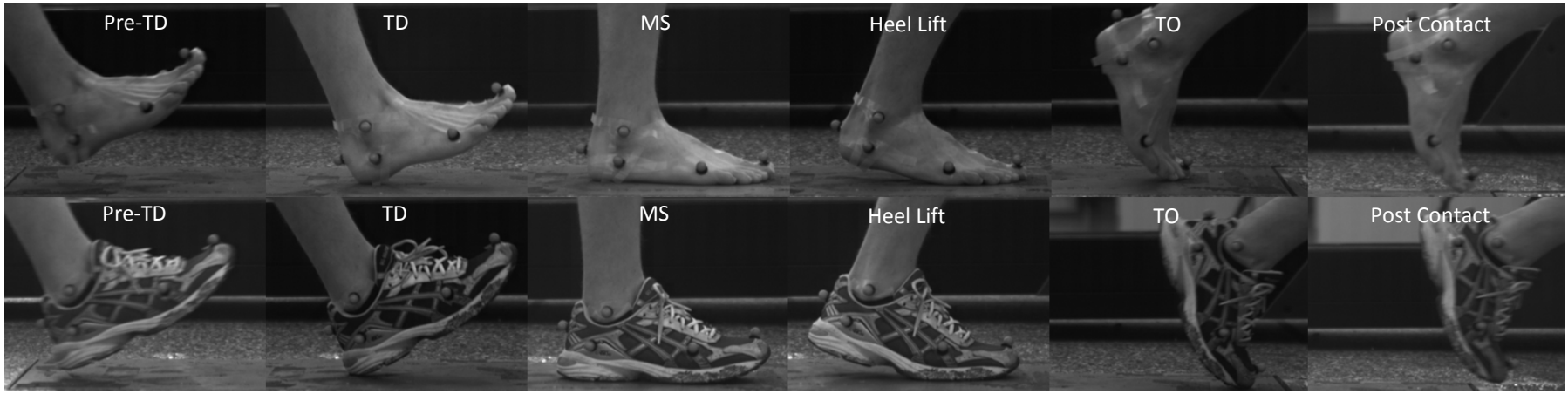

Figure 3.3.2: The ground contact phase for both barefoot and shod walking. Starting prior to impact (pre-TD), moving through contact (TD) into the mid-stance (MS) and heel lift. The heel continues to rise to toe-off (TO) before the foot leaves the ground as part of the post contact phase.

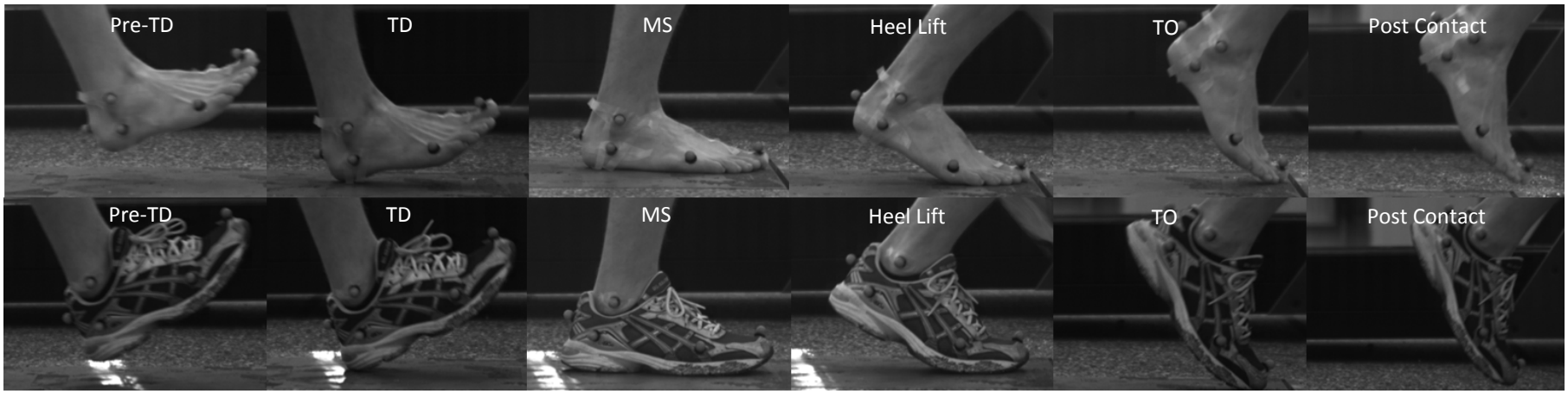

Figure 3.3.3: The ground contact phase for both barefoot and shod running**.** Starting prior to impact (pre-TD), moving through contact (TD) into the mid-stance (MS) and heel lift. The heel continues to rise to toe-off (TO) before the foot leaves the ground as part of the post contact phase.

3.3.3 Heel Velocity

The velocity of the heel marker plotted against the percentage of ground contact time from just before ground contact to after toe off is shown in figures 3.3.4 and 3.3.5. As expected, the peak values are higher for the running gaits compared to walking.

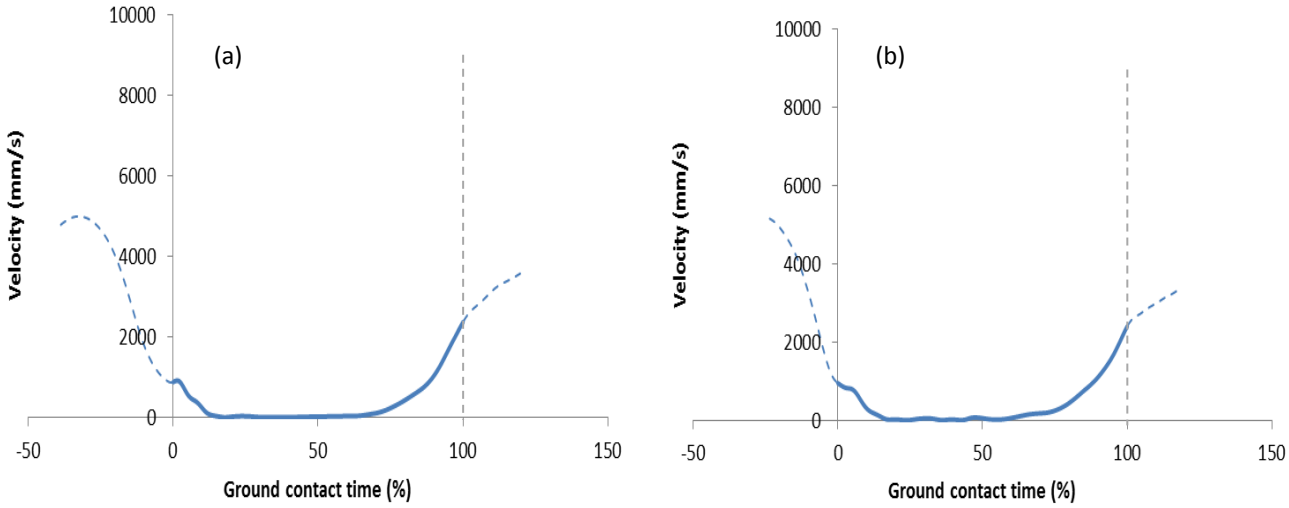

Figure 3.3.4: The velocity of the heel marker versus percentage of ground contact for walking under (a) barefoot and (b) shod conditions. The solid line represents the ground contact phase.

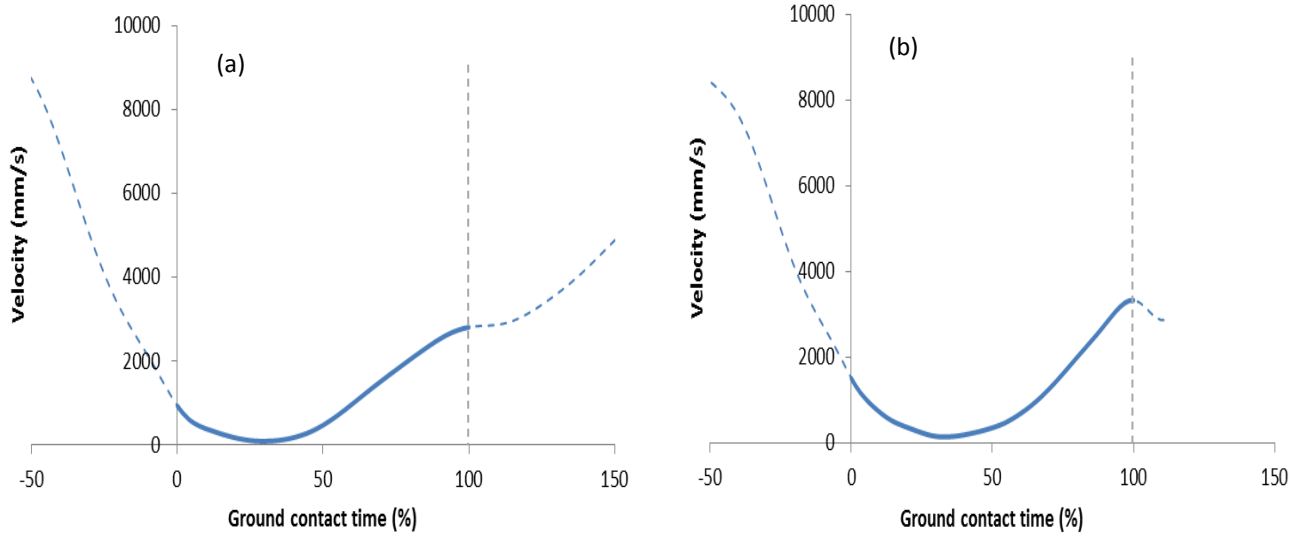

Figure 3.3.5: The velocity of the heel marker versus percentage of ground contact for jogging under (a) barefoot and (b) shod conditions. The solid line represents the ground contact phase.

3.3.4 Ground Contact Times

The ground contact times for each of the locomotion conditions are given in table 3.3.2.

Table 3.3.2: The ground contact time for walking and running under both barefoot and shod conditions for all trials.

Trial	BF Walk (s)	BF Jog (s)	Shod Walk (s)	Shod Jog (s)
1	0.589	0.218	0.602	0.248
2	0.582	0.226	0.626	0.254
3	0.605	0.219	0.641	0.238
4	0.613	0.234	0.623	0.246
5	0.602	0.235	0.631	0.232
Average	0.598	0.226	0.624	0.244
Standard Deviation	0.011	0.007	0.013	0.008

3.3.5 Ground Reaction Forces

The vertical, medio-lateral and anterior-posterior ground reaction forces for each of the four conditions as a plot against the percentage of ground contact time are given in figure 3.3.6. The respective loading rates for the first peak of the vertical ground reaction forces are shown in table 3.3.3.

Table 3.3.3: Vertical ground reaction force loading rates to the first main peak (taken as the slope of the line fitted to data for 20% and 80% of the peak force value).

	Vertical loading rate (kN/s)	Vertical loading rate (BW/s)
Barefoot Walk	11.7 ± 1.4	17.5 ± 1.4
Barefoot Jog	101 ± 29	151 ± 43
Shod Walk	12.0 ± 1.5	17.8 ± 2.3
Shod Jog	64.4 ± 4.3	96.0 ± 6.5

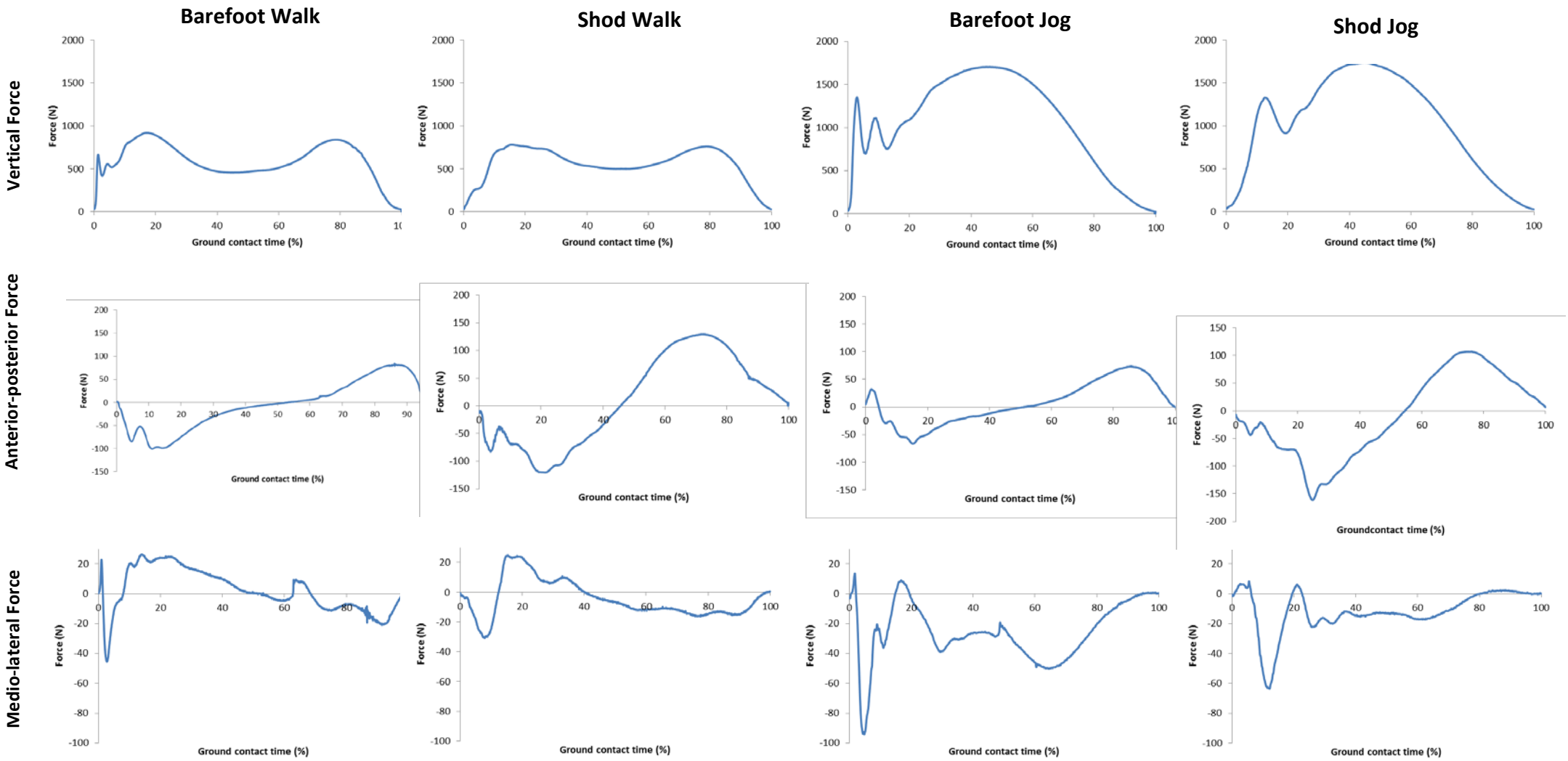

Figure 3.3.6 The ground reaction force data versus ground contact time percentage for walking and jogging under barefoot and shod conditions.

3.3.6 Centre of Pressure

The centres of pressure (CoP) maps for the four locomotion conditions are given below. These are based on where the impacts occur on the force plate (figure 3.2.6) relative to the initial point of ground contact (0, 0), a force threshold of 15N was used.

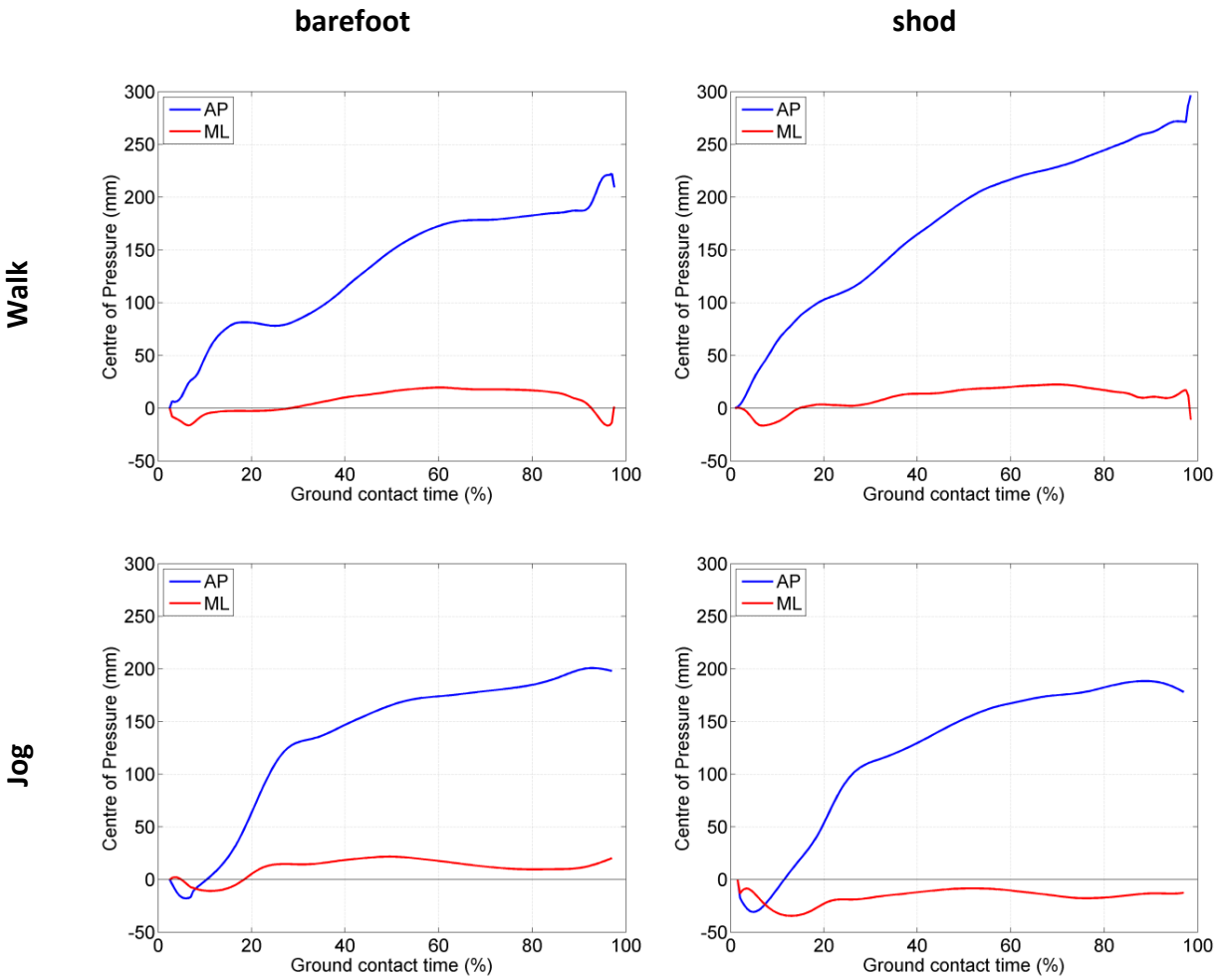

Figure 3.3.7: The centre of pressure in the anterior-posterior and medial-lateral directions for walking and running under both barefoot and shod conditions. Both are presented relative to the position at impact.

3.4 DISCUSSION

This chapter has documented the methods and results for collecting human kinematic and kinetic data used to programme and validate the motion of the robot. The reason for only using one test subject was because at this early development stage in the robot's approach to footstrike emulation only a single 'typical' data set is required to perform the methods by which this can be achieved. In future stages it would be beneficial to collect human kinematic and kinetic data for more subjects, increasing the test database and emulation potential of the robot. The collected data has two main roles within this thesis: The first being used as an input for programming the robot; and the second is as a validation aid for the outputs of the robot.

3.4.1 Robot Inputs

Some of the collected kinematic and kinetic data are required for programming the robot allowing it to perform the desired motions; i.e. heel positions, heel velocities and foot orientation relative to the ground. As outlined in Chapter 4 the three-dimensional positional and rotational co-ordinates are used along with velocity information to plot the individual points of any programme. The VICON data that was collected provides an accurate set of 3D positional data for all four locomotion conditions, from which velocity can be derived. The software allows for the on screen markers to be linked to create whole body segments, in this instance the foot was created which is useful for analysis – for example in calculating its angle in relation to the ground.Table 3.3.1 shows that for all four conditions, the initial ground contact is with the heel of the foot/shoe, thus making the subject a heelstriker. The foot appears to approach the ground contact at a shallower angle when barefoot for both walking and running ~ 11-12° (Table 3.3.1 and figure 3.3.3), this is consistent with the findings of De Wit *et al* (2000).

The heel marker velocity information that has been captured is useful in showing the values needed for the emulation (figures 3.3.4 and 3.3.5). In each case during ground contact, the velocity drops to a level close to zero before increasing again. This is where the heel marker moves into contact with the ground, remains stationary through midstance and moves up

again into toe-off. For walking gaits this trough is larger (approximately 50% of ground contact). The troughs are much smaller for the running gaits, suggesting that the heel marker is at its lowest velocity for a shorter fraction of ground contact.

The highest velocity that can be programmed into the robot is 2000mm/s and there are sections where the velocity of the human foot rises above this value – in these instances the robot can be programmed to the maximal value. This may not be ideal in achieving accurate human footstrike emulation using the robot, however, the area of greatest interest is during ground contact where the velocities mainly fall within the range of the robot. It may be possible to improve the robot velocity by implementing a new end-effector design or by altering the approach phase.

3.4.2 Robot Outputs

The kinetic data (ground contact time, ground reaction forces and centres of pressure) that were collected have a role in the validation of the robot emulation. There are a number of measurable outputs that can be taken from the robot system; marker locations based on image digitisation as well as ground contact time, ground reaction forces and centre of pressure information from the Kistler Force Plate. All of this data can then be compared to the same information collected from the human trial.

As well as being used to programme the robot, the heel position, velocities and foot angle data obtained from VICON can also be used as a validation tool for robot output. The motion capture that was recorded for the robot can be compared against the original human data, used to programme it, to determine the degree of success of the emulation from a kinematic perspective.

For the walking trials the ground contact times were 0.605 ±0.011 seconds and 0.631 ±0.013 seconds for barefoot and shod respectively (Table 3.3.2). For the running trials, the ground contacts were 0.226 ±0.007 seconds and 0.254 ±0.008 seconds for barefoot and shod respectively, values which correspond to the findings of Hunt *et al.,* 2001. For both gait modes, barefoot conditions tend to result in a slightly shorter ground contact time. For walking, the vertical force is shown to have two peaks of approximately 900N, which is

expected given the weight of the subject (Keller *et al.,* 1996). These form the impact and pushoff peaks and the trough represents the midstance phase. This is not the case for the same trials under shod conditions, which appear to only have one impact peak. Both are consistent with the findings of Nigg, 1987. The magnitude of the impact appears less under shod conditions, which is probably due to cushioning, and may also be easier to emulate. Another area that needs to be emulated is the anterior-posterior force. The trial data is as expected, with the negative phase representing braking (first half of stance) followed by the positive phase representing propulsion.

All of the magnitudes displayed are easily achieved on the robot, but this may involve a trade off with other parameters. One of the main emulation challenges has proved to be generating accurate force peaks within the desired time frame obtaining an accurate profile shape. Previous work, (Ronkainen *et al* 2010), with the robot has shown a number of emulation challenges with difficulty in achieving ground contact times, to match those of a running gait. Emulating the walking gait, at least initially, may prove to be easier as the ground contact times are larger and closer to values that have already been achieved. Given the correct robot configuration improving the ground contact times is still feasible.

For a mechanical wear test, it is desirable to be able to emulate the correct force magnitudes acting on the correct part of the shoe. The centre of pressure maps are very important for showing how the foot interacts with the ground and where the forces act upon the shoe, figures 3.3.7 and 3.3.6. The results would suggest that under shod conditions the forces move predominantly in a posterior to anterior direction, from impact on the heel through to toe-off on the toe. In the early stages of footstrike emulation, it seems reasonable to neglect movement in the medio-lateral direction.

3.5 CONCLUSIONS

The primary aim of this chapter was to measure the kinematics and kinetics for one human subject under four locomotion conditions. This information is critical to addressing research question one (page 4) and is also used in further preliminary work before this research question four can be addressed (Chapters 5, 6, 7 and 8).

The investigation has ensured that the required human kinematic and kinetic data for the subject has been collected and results presented in a way that allows for quick referral for the use of future investigations on the robot. Perhaps most importantly, the collected data can be used both as an input when programming the robot and as a validation for its outputs.

Some of the human data may prove difficult to emulate on the robot in its current state, clever programming techniques and end-effector considerations may help to overcome some of the issues.

CHAPTER 4

THE FANUC R2000*i*-B INDUSTRIAL ROBOT

4.1 INTRODUCTION

In 2008, Loughborough University's Sports Technology Institute purchased a 6 degrees-of-freedom (6DoF) industrial robot from FANUC (FANUC robotics; Mount Fuji, Japan). The R2000*i*-B robot would traditionally be situated within a factory setting completing simple repetitive tasks such as palletising, welding or painting. The overarching aim behind the purchase of the robot was to investigate whether or not an off the shelf industrial robot can be used in the sports equipment industry as a means to mechanically test the equipment under more biofidelic (human like) conditions than existing test devices. The use of robots in the sports equipment industry is not uncommon, however the majority of these robots are bespoke and have a single application, despite being excellent for the intended use, there is a distinct lack of diversity. It is also common for there to be a lack in independent support for such robots in terms of set-up, maintenance and general use, all teething and operational problems would have to be dealt with in house. In theory, the use of a commercially available robot allows for the system and protocol to be adopted elsewhere; this would only require the transfer of any intellectual property concerning robot programming.

This chapter aims to give a general introduction to the robot. It outlines the key specifications briefly explaining the different methods that can be used to programme it and summarises the previous footstrike emulation that has been undertaken on the robot within the Institute prior to this thesis. The main objective is to provide the reader with sufficient background knowledge on the robot to allow the remaining chapters to be understood.

4.2 ROBOT SPECIFICATION

4.2.1 Specification

FANUC are one of the World's leading industrial automation suppliers, the R2000*i*-B robot (Figure 4.2.1) was designed to be located within an automated industrial setting; therefore the robot is very robust and is able to work in an industrial environment for prolonged hours without stopping.

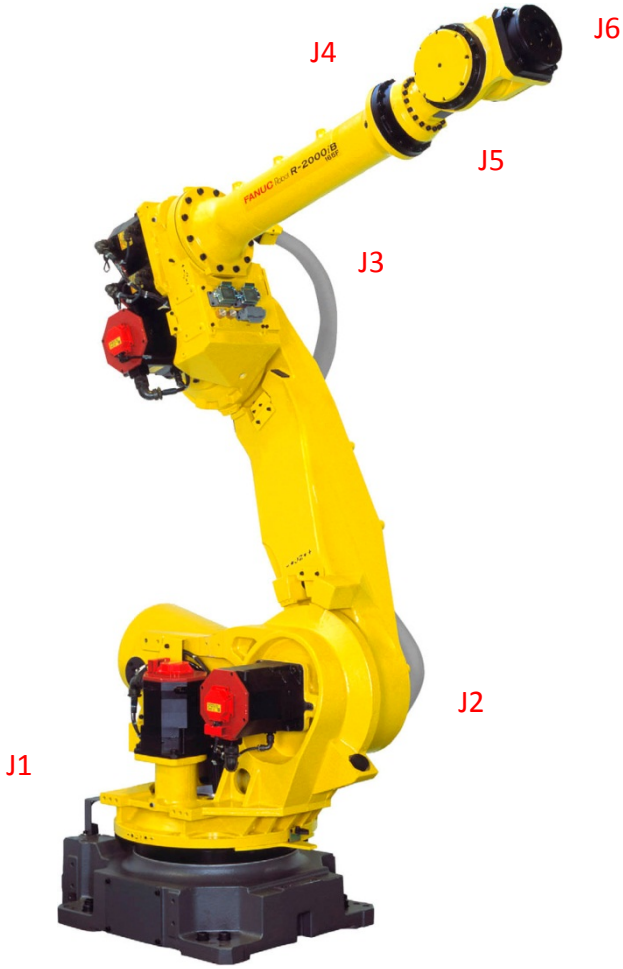

Figure 4.2.1 – The FANUC R2000*i*-B 6 Degrees-of Freedom industrial robot. Also shown is the location of each robot joint (J1-J6), moving from the proximal joint 1 (the attachment to the floor) to the most distal joint 6.

The specification sheet for the robot is given in table 4.2.1. Each joint has different capabilities in terms of payload (how much weight it can hold), range of motion and velocity. Notably, the end-effector (wrist) payload is 165 kg, maximum velocity is 2000mm/s and repeatability is ±0.2mm; i.e. it can be classified as heavy duty, moderate speed (in human context) and highly repeatable.

FANUC are not the only manufacturer of industrial robots that have the potential to be applied to the concepts outlined in this thesis. Another two major industrial robot are ABB robotics and Kuka. Both companies produce a robot that is capable of achieving similar speeds to the FANUC, but there is nothing that stands out as more appropriate for this application, i.e. a faster robot with a larger payload. A summary of each company's robot closest to the FANUC is also shown in table 4.2.1.

Table 4.2.1 – The specification sheet for the FANUC robot along with the specifications of two similar robots from ABB and KUKA respectively. The robot joints (J1-J6) are shown in figure 4.2.1.

	FANUC R-2000*i*B	ABB IRB6640	KUKA 150 R2700 extra
Repeatability (mm)	**0.2**	0.07	0.06
Reach (mm)	**2650**	3200	2700
Payload (kg)	**165**	235	150
Joint RoM			
J1	**360**	340	185
J2	**135**	150	145
J3	**362**	250	275
J4	**720**	600	360
J5	**250**	200	125
J6	**720**	600	350
Max. joint velocity (degs/sec)			
J1	**105**	110	123
J2	**105**	90	115
J3	**105**	90	120
J4	**130**	190	292
J5	**130**	140	258
J6	**210**	235	284
Maximum end-effector velocity (mm/s)	**2000**		
Cost (£)	**£36,000**	£35,000	-

Of the aforementioned robots, the FANUC is the best at providing a large range of motion (RoM). The potential reach and dimensions of the different segments of the robot may

influence any future tests and their location with respect to the robot, Figure 4.2.2 shows a schematic outlining these parameters.

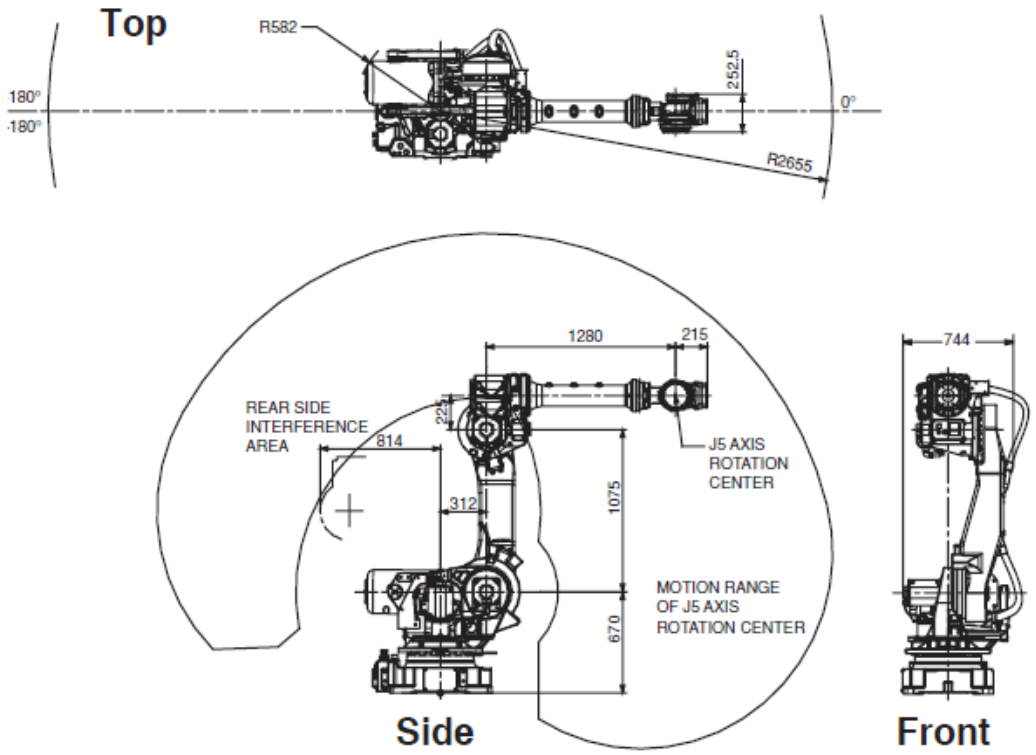

Figure 4.2.2 –The dimensions and potential Range-of-Motion (RoM) of the robot.

4.2.2 The Robot End-Effector

The end-effector or tool of the robot is one of the main factors behind what makes the robot so versatile and is a crucial aspect of the robot system regardless of environment; the end-effector function can vary from painting and welding to grabbers and manipulators. In-house alterations allow for easy manipulation of the mounting and orientation of an end-effector. In footstrike emulation, the end-effector will need to include a footform, but its properties and method of attachment are variable and are discussed in future chapters.

4.2.3 Safety Features and robot cell

The FANUC robot is a dangerous piece of equipment and as such special steps have been taken to ensure user safety. A polycarbonate guarding forms a physical cell in which the robot is located. This offers protection and full visibility for the user located outside of the cell. Access to the cell is permitted through a single door which has fortress lock that

partners the robot control key in a key exchange, i.e. the robot cannot be operated with the door unlocked.

As an additional safety feature, a series of light curtains (Figure 4.2.3) are fitted inside the cell (SICK sensor intelligence, Minneapolis, MIN). These have 180° coverage and have been programmed to encapsulate the inside of the cell. If anything were to break the curtain of light, the robot would automatically shut down. As a final safety feature, upon installation, the robot was set-up with a defined area in which it could operate. Therefore no part of the robot will move to or operate outside of the area defined by the cell.

Figure 4.2.3 – SICK laser proximity sensor, used to emit a protective light curtain around the inside of the robot cell

4.3 PROGRAMMING THE ROBOT

4.3.1 Instructing Robot Movement

The robot control system is capable of storing numerous programmes within its internal memory. Each one of these programmes corresponds to a particular motion that the robot can carry out. On the whole, each line of code in these programmes represents one point in space along the intended motion path. Part of the programing process requires a number of manually entered inputs for each line:

- The three dimensional positional co-ordinates for each point.
- The rotation (yaw, pitch and roll) relative to the global co-ordinate system.
- The velocity of the robot for that particular moment.
- The level of robotic smoothing applied for that particular moment.
    - *The level of robotic smoothing specifies how the robot moves between and through each of the programmed points. There are two types of motion termination that can be selected, 'FINE' and 'CNT' (continuous).*
    - *With 'FINE' termination selected, the robot visits each point (with the accuracy limitation of 0.5mm; FANUC) and momentarily stops at each point before moving on to the next point.*
    - *With 'CNT' selected, the robot moves from the start to the end of the movement in a smooth manner but does not necessarily pass through the intended points.*

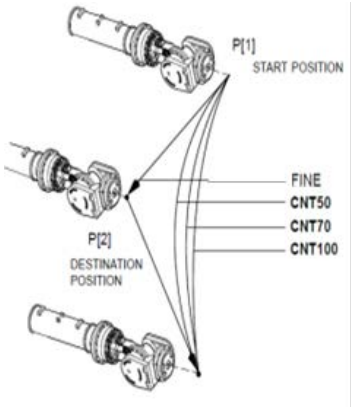

Figure.4.3.1 - An example of how robotic smoothing level may affect the robot motion, reproduced from the FANUC programming manual.

When programming the robot it is also possible to specify other features that aren't necessarily part of the robot's motion path. The collision detect feature, for example, allows for a proper interaction with an external rigid surface. If this feature were turned on, footstrike emulation would not be possible – an increased work load on the motors would alert the robot to contact thus shutting it down.

The above mentioned features can be inputted into the robot control system in a variety of ways:

1. Manually entering the information using the teach pendant attached to the control unit (figure 4.3.2). This is the most common approach that allows for quick and easy creation and editing of programmes. It requires the user to be stationed with the robot throughout. Efficiency in robot use is compromised as the robot has to be offline whilst being programmed, this however is not an issue in a University environment.
2. Inputting the relevant programming parameters using the accompanying computer software RoboGuide (Chapter 6). Here, the information is entered into a virtual robot environment, which also allows for the robot motion to be verified and checked before applying it to the real world robot. This has the advantage of reducing downtime of the robot and allows to see the effects of changes without having to apply them to the robot.
3. A third approach is to use Microsoft Visual Basic. Similarly to RoboGuide the motion parameters can be inputted into the computer software before being downloaded to the robot. Unlike RoboGuide, however, it is not possible to see a virtual demonstration of the robot path. As before, this can reduce robot downtime but may not be beneficial if the nature of the use requires regular programme alteration.

Only methods 1 and 2 have been used within this thesis.

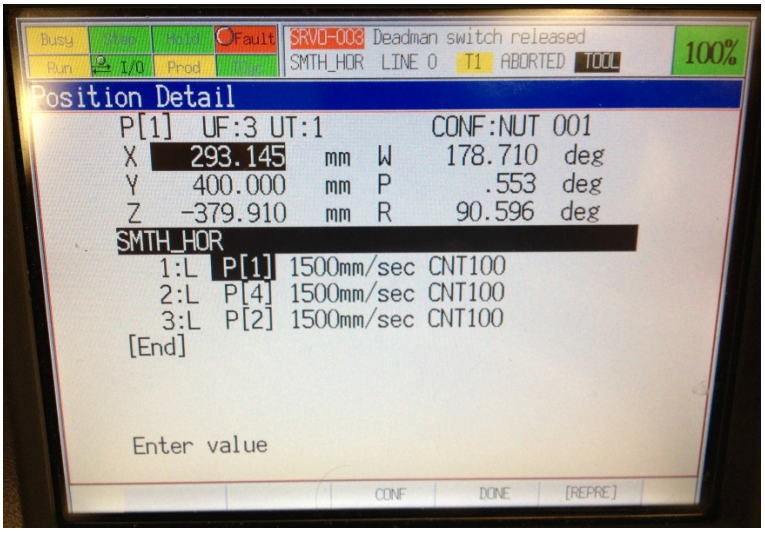

Figure 4.3.2 – A screenshot from the teach pendant showing the required input parameters.

4.3.2 Tool Centre Points and Coordinate Frames

The final task in creating a programme is manually specifying a global co-ordinate frame in which the robot movements take place. A global reference frame is established thus identifying the positive direction of each movement (x, y and z). This reference frame can be positioned and orientated anywhere within the robot environment. The origin of this reference frame is the tool centre point (TCP), which is a fixed point in relation to the end-effector. For example, if the heel of a footform is programmed to be the TCP all kinematic inputs will be for that point with any rotations centring on that point.

4.4 PREVIOUS FOOTSTRIKE EMULATION

Since acquiring the robot, a number of pilot studies have been conducted; the primary aim of these has been to assess the viability of using it for the simulation of complex sporting movements. Ronkainen et al (2010) used the robot to emulate the kinetics and kinematics of two running gaits, heel strike and forefoot strike running respectively. The robot successfully produced highly repeatable kinetics and kinematics over 500 cycles. The kinematics and ground reaction forces for the shod prosthetic foot showed more variability, but still less than that observed in the athlete trials. Three main issues arose from the interaction of the footform with the ground in this testing, which have subsequently laid the foundations for the work documented in this thesis:

1. **Positional Control -** The effect of robotic smoothing makes it difficult to predict what motion path the robot will take. It becomes even more difficult if multiple co-ordinate points or higher velocities (both important aspects of emulating footstrike) are used.
2. **Ground Contact -** The time in which the footform is in contact with the ground as well as the area covered by the contact phase is too large. This is directly affected by the potential velocity that the footform is able to attain as it moves through contact.
3. **Propulsive Force Application –** It has not been possible to generate propulsive ground reaction forces. The anterio-posterior forces are braking throughout the contact phase.

4.5 SUMMARY

The aim of this Chapter was to introduce the FANUC robot to the reader. It explains how the robot can be programmed and what information is required to do so. The robot specifications are presented alongside the specifications of industrial robots from other manufacturers which are also suitable for the task of footstrike emulation. It also introduces previous emulation attempts conducted at Loughborough University using the FANUC, as well as their limitations. This is important as it helps to establish the capabilities and intricacies of the robot, which directly addresses research question two.

CHAPTER 5

INITIAL CHARACTERISATION OF THE ROBOT MOVEMENT

5.1 INTRODUCTION

The robot has a number of programmable and embedded features within its control system which influence its output motion (section 4.3); this is the case for simple linear motions as well as more complex motions. The robot user has little control over its embedded features, but investigations can be conducted on the effect of the programmable features. The following programmable input parameters are key in determining the output motion of the robot:

- 3D position co-ordinates; their frequency and their relationship to each other
- Programmed velocity
- Level of robotic smoothing
- Acceleration (This is always set to maximum, so is not investigated in this chapter)
- Tool orientation

The level of robotic smoothing specifies how the robot moves between and through each of the programmed points. There are two types of motion termination that can be selected, 'FINE' and 'CNT' (continuous). With 'FINE' termination selected, the robot visits each point (with the accuracy limitation of 0.5mm; FANUC) and momentarily stops at each point before moving on to the next point. With 'CNT' termination selected, the robot moves from the

start to the end of the movement in a smooth manner but does not necessarily pass through the intermediate points. The continuous value can vary from between 0 (the equivalent of 'FINE') and 100, which determines how close the robot will come to the intended point. The higher the degree of 'CNT' the smoother the path taken, but the more the robot may deviate from the programmed path (Figure 5.1.1). The frequency of co-ordinate points and their location relative to each other may also affect the influence of robotic smoothing on the output motion of the robot. The programmed velocity (and therefore acceleration) may also have an influence on the output of the robot, for example there may be differences in how quickly the robot can register its position within space.

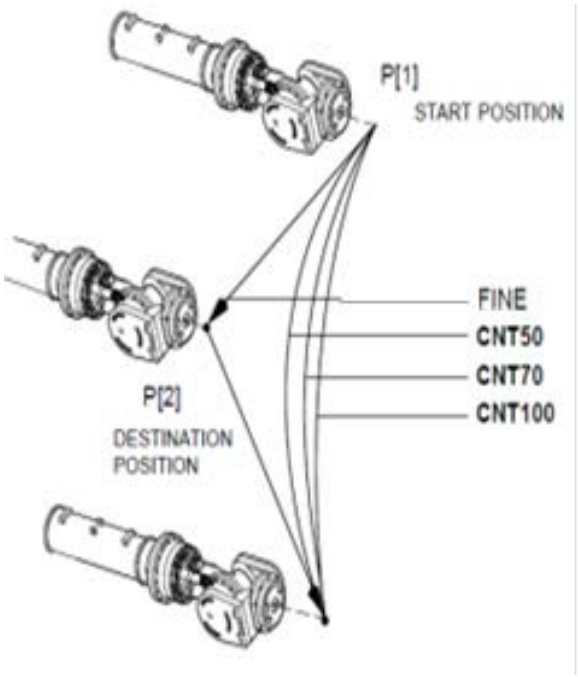

Figure 5.1.1. An example of how robotic smoothing level may affect the robot motion (Reproduced from FANUC programming manual).

Although it is known that the identified parameters affect the kinematics of the robot, this has yet to be quantified, the following aims and objectives are intended to address this issue:

5.1.1 Aims

- To investigate the effects of varying the level of robotic smoothing, velocity and the number of programmed co-ordinate points on a program instructed to move in straight line paths (horizontal and vertical) and a 90° corner path.

5.1.2 Objectives

- To program the robot to move in linear (vertical and horizontal) motions. Then combine to create a 90° corner motion.
    - First of all, simplified movements were investigated to help provide an initial understanding of the features. As they are combined to make a more complex movement, a deeper understanding will be gained.
    - The movements are in two dimensions and are to be located directly above the force platform (Chapter 8), i.e. the area where the interaction with the ground will occur, which is the area of greatest interest.
- To determine the effect of various levels of robotic smoothing, velocity and number of co-ordinate points on the movement trajectory, specifically end-effector position, movement time and velocity.

5.2 METHODOLOGY

The following section outlines the steps taken to create the robot programmes with the differing variables (smoothing level, velocity and number of co-ordinate points), and how the movements were recorded to allow for comparisons and analysis of the three kinematic parameters (positions, timings and velocities).

5.2.1 Equipment and set up

The primary piece of equipment for this study is the FANUC R-2000*i*B industrial robot, as introduced in Chapter 3. The robot was fitted with an end-effector in the form of a spike, with the tip covered in retro-reflective tape. This was deemed a good and consistent reference point for tracking and was easily identified against the dark background. The robot was orientated so that the faceplate of the 6th robot joint (the point of end-effector attachment) was parallel to the floor within the robot enclosure and therefore perpendicular to the spike (Figure 5.2.1). It was decided that the work envelope for all of the tests was to be directly above the centre of the force platform, the eventual area where foot strikes take place.

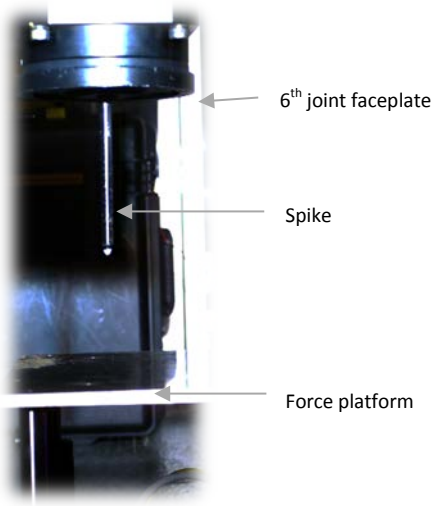

Figure 5.2.1 The end-effector spike used to provide a consistent reference point on the robot.

A high speed camera (Photron Limited Europe, UK; Fastcam SA-1 675K-MK1) was used to capture the various robot movements at 1000Hz, with a shutter speed of 1/1000 frames per second and a resolution of 1024 x 1024 pixels (Figure 4.2.3). The high recording frequency required lighting, positioned directly behind the camera, to enhance the image quality. To reduce perspective errors the camera was set up on a tripod and positioned as far away from the region of interest as possible whilst within the robot cell, i.e. 1950mm from the centre of the raised force plate. The camera was positioned perpendicular to this region (Figure 5.2.2), with the turn-points and corner point of the motion profiles positioned in the centre of the shot.

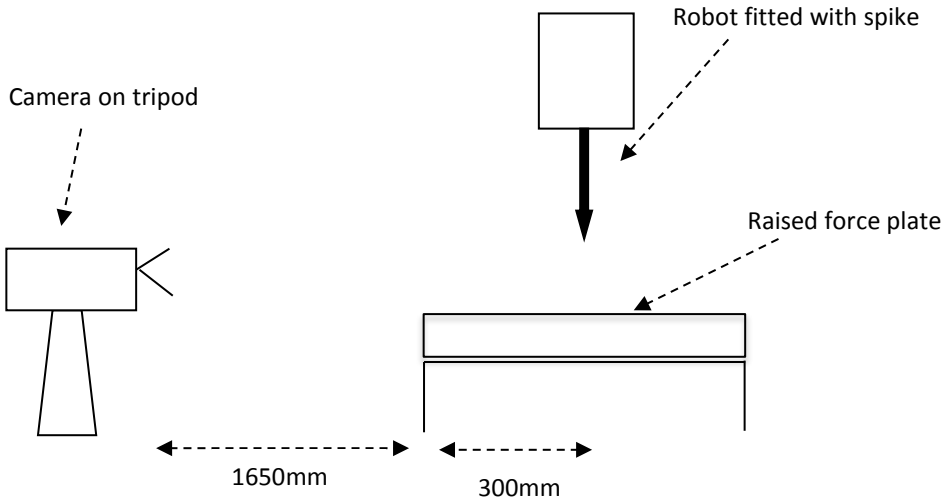

Figure 5.2.2 - A schematic outlining the test area and equipment positions. The test area is located above the centre of the raised force platform with robot movements taking place perpendicular to the camera view.

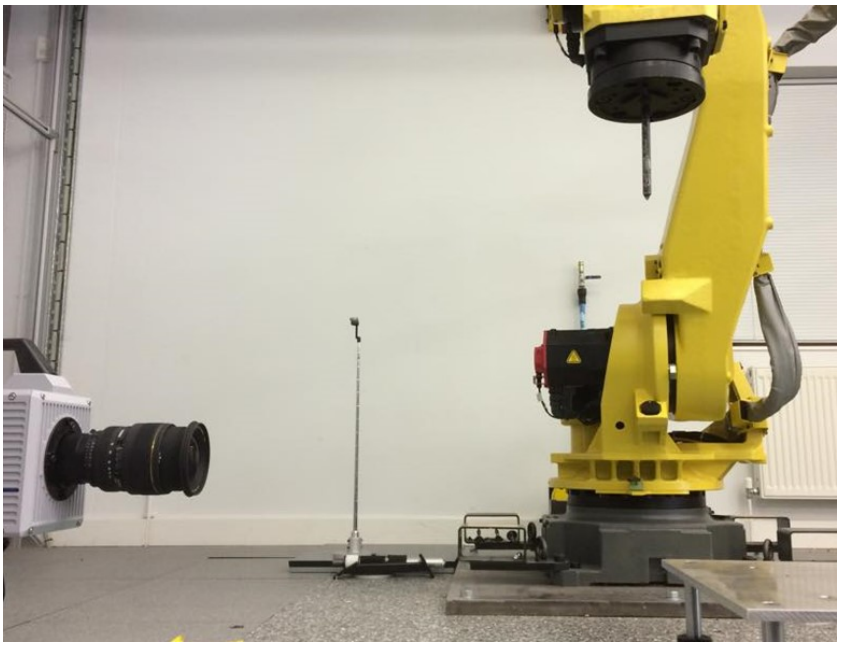

Figure 5.2.3 – A real World representation of the schematic shown in figure 5.2.3.

5.2.2 Robot Programmes and Trials

To fully cover the potential robot range of motion, similar tests were carried out in different planes. The end-effector was instructed to move in a linear motion, to a specified turn-point and back, both in the vertical and horizontal planes. Camera positioning resulted in the horizontal plane being perpendicular to the long axis of the force plate. For these movements the robot was programmed with various velocities and with different levels of robotic smoothing applied. For each linear motion (vertical and horizontal) the turn point was set 400mm away from the start point. When added extra co-ordinate points were included these were positioned at 360mm and 320mm from the start location.

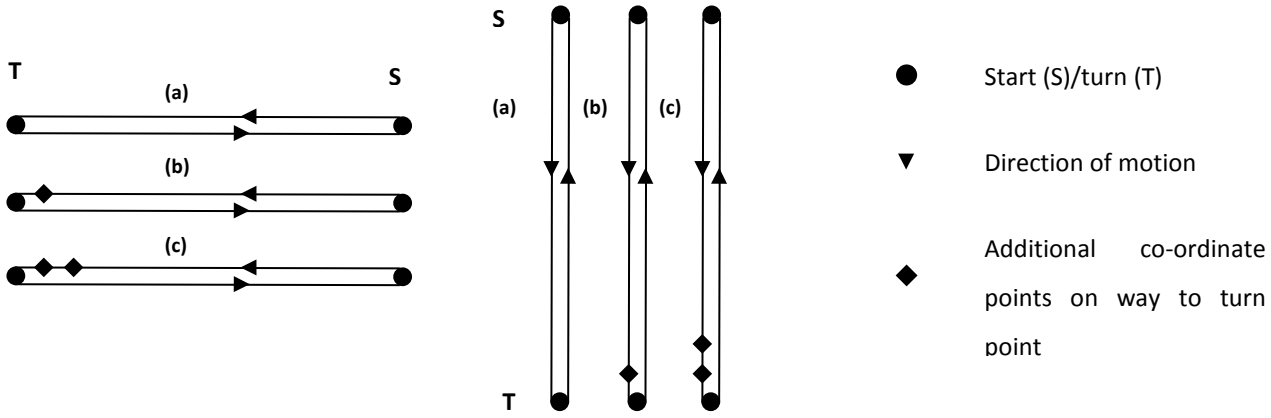

Figure 5.2.4 - The configuration of the simple linear (horizontal and vertical) motion paths; showing **(a)** no additional points, **(b)** one additional point and **(c)** two additional points.

Following on from the simple linear motions a corner motion was created using the same vertical and horizontal components. The robot was instructed to move through the vertical motion to the 90° corner point before undertaking the horizontal motion and returning back to the start point along the same path (Figure 5.2.5). As before, additional co-ordinate points were added in increments of 40mm. These were added either side of the corner point and used in both outward and return movements.

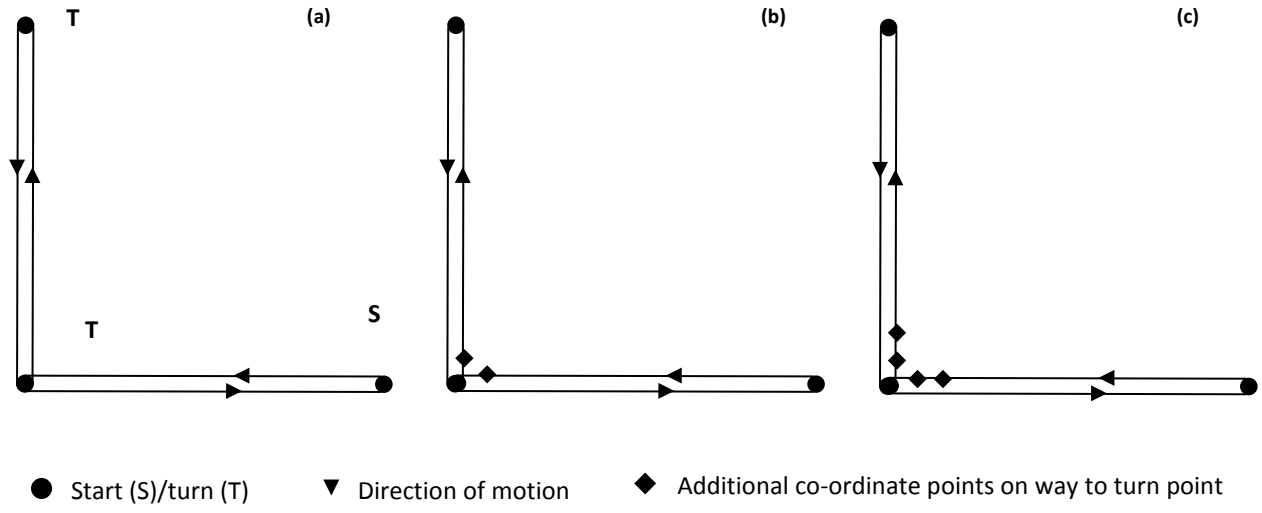

Figure 5.2.5 - The configuration of the 90° corner motion paths; showing **(a)** no additional points, **(b)** one additional point and **(c)** two additional points.

Trials were performed in every combination of the following variables (leading to a total of 81 trials):

- Movement direction
  - Horizontal
  - Vertical
  - Corner
- Smoothing level
  - CNT100
  - CNT50
  - FINE
- Velocity
  - 1500mm/s
  - 1000mm/s
  - 500mm/s
- Number of co-ordinate points between start and turn/corner point
  - No additional points
  - 360mm from start point
  - 320mm and 320mm from start point (2 additional points)

5.2.3 Data Collection and Processing

The robot was instructed to perform each of the trials in turn, which were recorded by the high-speed camera. Each of the videos were cropped so that they only included robot motion, before being saved and exported ready for digitising (Image-Pro Analyzer 7.0; Media Cybernetics, MD - USA). The software has a tool which allows for automatic tracking of a given section of the video, the pixel at the tip of the spike can be tracked, simply by clicking on it for specific frames. Various kinematic data (x and y co-ordinates, distance from start position and distance from previous position) is outputted for each point. It was deemed that tracking every tenth (i.e. 100Hz) frame of each video was sufficient; this was based on a small pilot study that showed that using higher digitising frequency did not affect the results. A measurement tool built into the software was used to measure a known distance, in the plane of motion, for calibration purposes, resulting in a conversion ratio of 195.375pixels:150mm. Once all of the desired frames had been tracked, the co-ordinate data was exported to Microsoft Excel for analysis.

5.2.4 Data Analysis

The following kinematic parameters for each of the trials was isolated and graphically presented in Microsoft Excel (section 5.3):

- Position
  - The two-dimensional position of the end-effector throughout the movement.
- Movement time
  - The time taken to complete the movement and the time to the turn point.
- Velocities
  - The peak velocity attained by the end-effector and the average velocity during the movement.

Manual digitisation of video files does run the risk of human error affecting the results; an error analysis was conducted, to quantify the error. A sample video of the robot moving in one of the liner motions was chosen and digitised five separate times. The standard deviation in finishing position and movement times were identified as the digitising error and were applied to the presented results outlined above (section 5.3).

5.3 RESULTS

5.3.1 Vertical and Horizontal Movements

Displacements

The vertical and horizontal linear motion displacements from the start to the programmed turn point (400mm away), for the robot with varying smoothing levels, velocities and co-ordinate points applied are shown in figures 5.3.1 and 5.3.2. The general trend was for the level of displacement to drop as the level of robotic smoothing or velocity increased or fewer additional co-ordinate points were used; tending to reach only two-thirds of the programmed value. The programmed displacement of 400mm was reached only where no smoothing was applied. Similar observations apply to the horizontal motion, which also reached full displacement with no smoothing and no additional co-ordinates applied.

Timings

The total movement time and time taken to reach the turn point for the vertical and horizontal linear movements on the robot with varying smoothing levels, velocity and number of additional co-ordinate points are shown in figures 5.3.3 and 5.3.4. Generally, as the level of applied smoothing was increased, movement time decreased. There is also a trend for the robot to take longer for the first half of the movement (start to turn point) than the second (turn point back to the start). The addition of extra co-ordinate points increased all of the recorded movement times.

Velocities

The peak velocity attained and average velocity for the vertical and horizontal linear motions are shown in figures 5.3.1 and 5.3.2. As expected, increasing the programmed velocity led to an increase in outputted peak and average velocity respectively. There are a few instances where the peak velocity exceeded the programmed value, but it is noticeable that the majority of the values are less than the input.

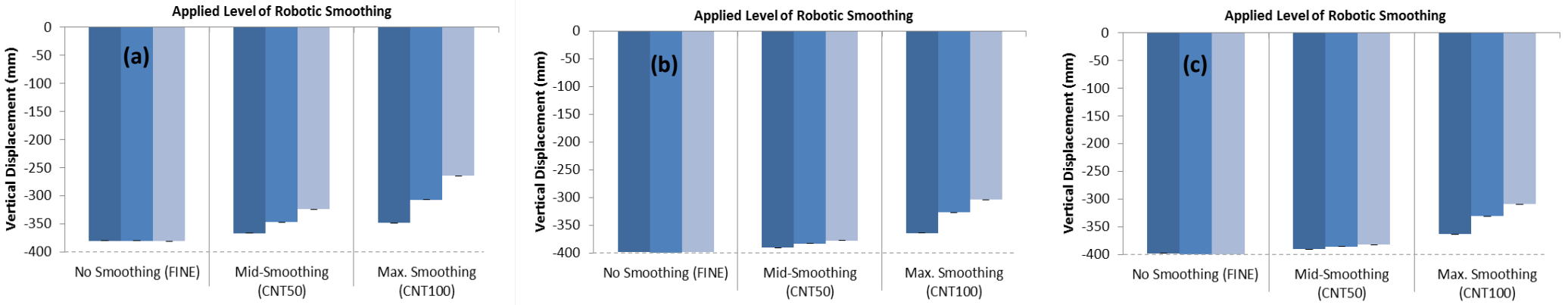

Figure 5.3.1 Downwards vertical displacement from the start point (programmed displacement was 400 mm, shown by the dashed line) to the turn point for the robot with different levels of robotic smoothing applied at different velocities; with **(a)** no additional co-ordinate points **(b)** one additional co-ordinate point and **(c)** two additional co-ordinate points programmed.

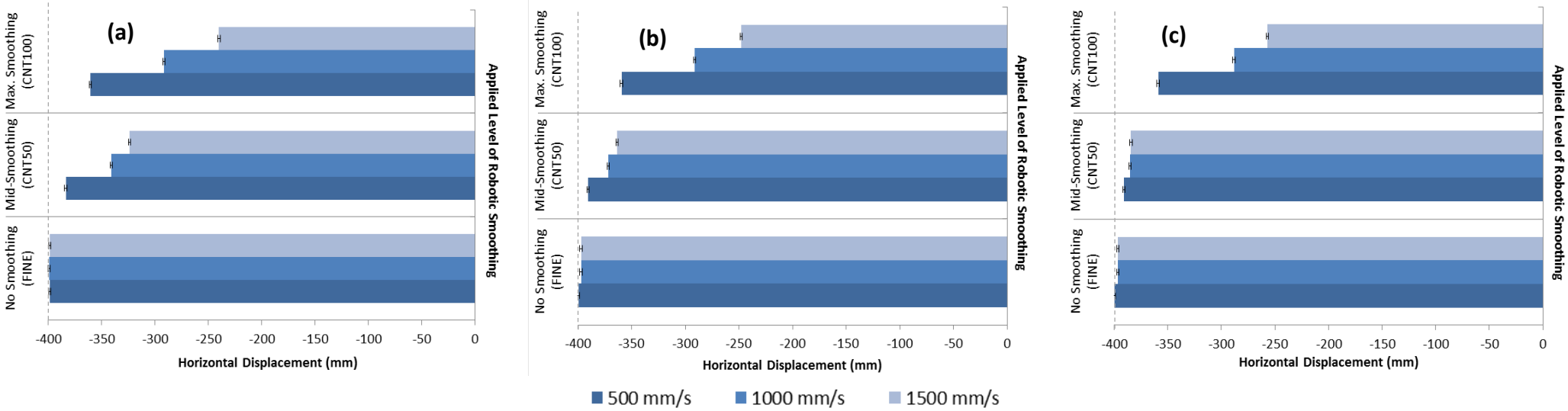

Figure 5.3.2 Horizontal displacement from the start point (programmed displacement was 400 mm, shown by the dashed line) to the turn point for the robot with different levels of robotic smoothing applied at different velocities; with **(a)** no additional co-ordinate points **(b)** one additional co-ordinate point and **(c)** two additional co-ordinate points programmed.

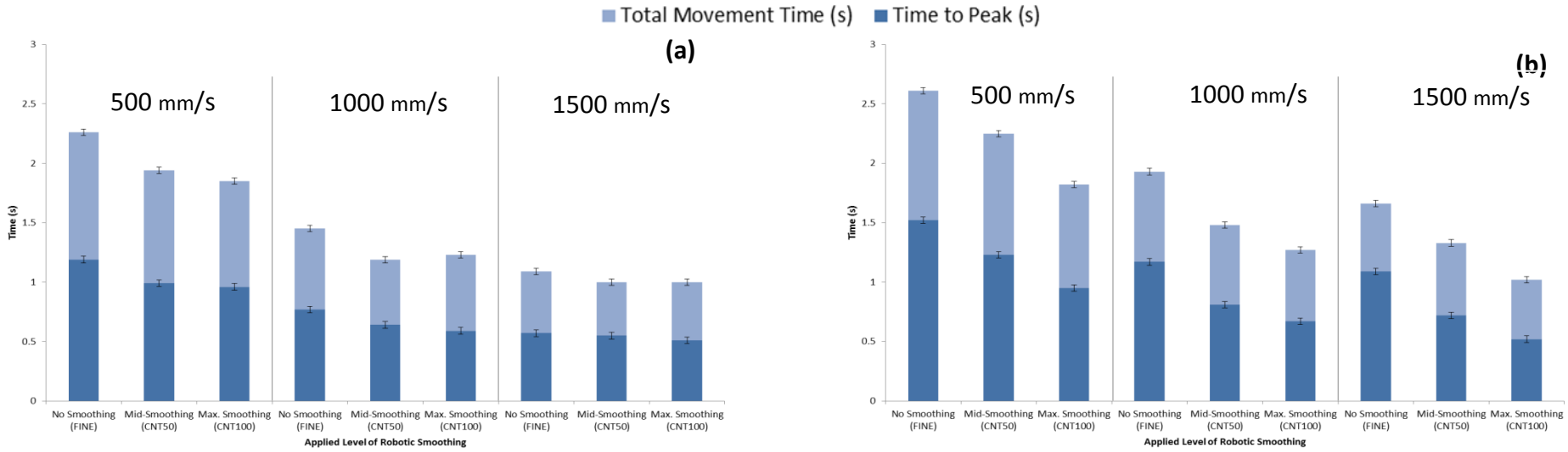

Figure 5.3.3 Total motion times and the time taken to reach the turn point for the robot moving in the simple vertical motion with different levels of robotic smoothing and velocity applied with **(a)** no additional co-ordinate pointes programmed and **(b)** two additional co-ordinate points programmed.

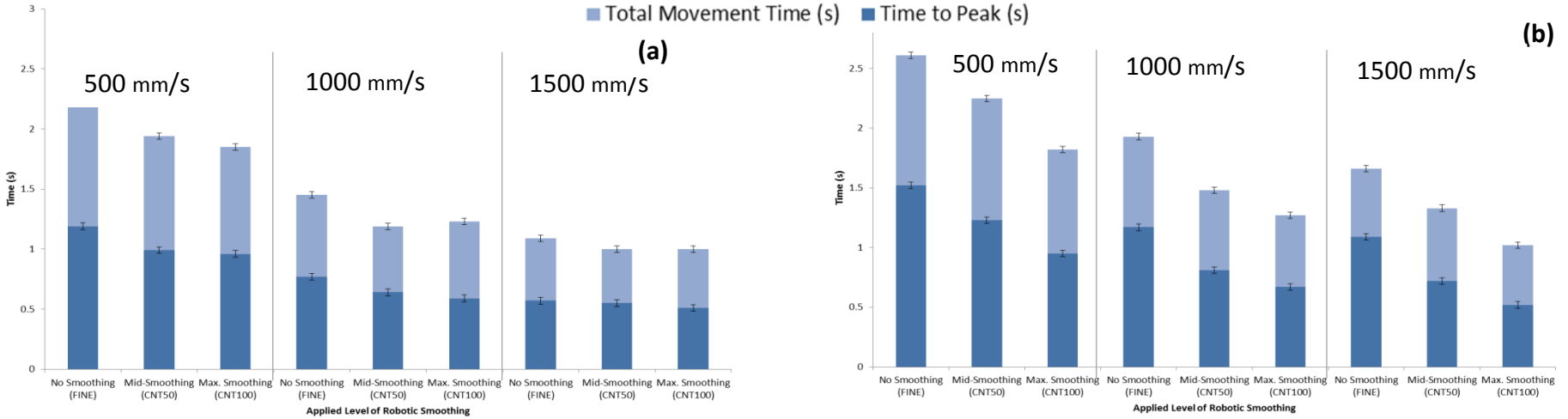

Figure 5.3.4 Total motion times and the time taken to reach the turn point for the robot moving in the simple horizontal motion with different levels of robotic smoothing and velocity applied with **(a)** no additional co-ordinate pointes programmed and **(b)** two additional co-ordinate points programmed.

Programmed Velocity	Peak Velocity (mm/s) 500 mm/s	1000 mm/s	1500 mm/s
0 Additional Co-ordinate Points			
No Smoothing (FINE)	614	998	1382
Mid-Smoothing (CNT 50)	461	998	1152
Max. Smoothing (CNT 100)	461	921	921
1 Additional Co-ordinate Points			
No Smoothing (FINE)	537	921	1305
Mid-Smoothing (CNT 50)	537	921	1152
Max. Smoothing (CNT 100)	537	921	998
2 Additional Co-ordinate Points			
No Smoothing (FINE)	537	921	1228
Mid-Smoothing (CNT 50)	537	845	1228
Max. Smoothing (CNT 100)	537	921	1075

Programmed Velocity	Average Velocity (mm/s) 500 mm/s	1000 mm/s	1500 mm/s
0 Additional Co-ordinate Points			
No Smoothing (FINE)	302	457	638
Mid-Smoothing (CNT 50)	342	513	554
Max. Smoothing (CNT 100)	348	488	481
1 Additional Co-ordinate Points			
No Smoothing (FINE)	320	382	457
Mid-Smoothing (CNT 50)	336	526	535
Max. Smoothing (CNT 100)	351	504	518
2 Additional Co-ordinate Points			
No Smoothing (FINE)	245	324	347
Mid-Smoothing (CNT 50)	293	446	503
Max. Smoothing (CNT 100)	356	464	559

Figure 5.3.1 The outputted velocities against the programmed velocities under all conditions for the vertical linear motion showing **(a)** the peak velocity attained and **(b)** the average velocity.

Programmed Velocity	Peak Velocity (mm/s) 500 mm/s	1000 mm/s	1500 mm/s
0 Additional Co-ordinate Points			
No Smoothing (FINE)	739	1067	1149
Mid-Smoothing (CNT 50)	575	1149	1231
Max. Smoothing (CNT 100)	575	903	821
1 Additional Co-ordinate Points			
No Smoothing (FINE)	903	1149	1067
Mid-Smoothing (CNT 50)	657	1067	1149
Max. Smoothing (CNT 100)	575	821	903
2 Additional Co-ordinate Points			
No Smoothing (FINE)	903	1067	1067
Mid-Smoothing (CNT 50)	657	1149	1231
Max. Smoothing (CNT 100)	575	821	821

Programmed Velocity	Average Velocity (mm/s) 500 mm/s	1000 mm/s	1500 mm/s
0 Additional Co-ordinate Points			
No Smoothing (FINE)	371	560	553
Mid-Smoothing (CNT 50)	391	576	581
Max. Smoothing (CNT 100)	380	471	456
1 Additional Co-ordinate Points			
No Smoothing (FINE)	368	552	583
Mid-Smoothing (CNT 50)	382	590	669
Max. Smoothing (CNT 100)	375	463	483
2 Additional Co-ordinate Points			
No Smoothing (FINE)	368	572	583
Mid-Smoothing (CNT 50)	379	582	639
Max. Smoothing (CNT 100)	383	484	451

Figure 5.3.2 The outputted velocities against the programmed velocities under all conditions for the horizontal linear motion showing **(a)** the peak velocity attained and **(b)** the average velocity.

5.3.2 Corner Movements

Positions

The two-dimensional end-effector trajectory for the robot with the differing levels of smoothing, velocity and number of additional co-ordinate points applied (figure 5.3.5). For all of the profiles, where no smoothing was applied, the trajectories follow the inputted co-ordinates (dotted line) fully (400mm x 400mm). An increase in smoothing level or applied velocity saw the end-effector trajectory move further away from the programmed corner and turn points. The inclusion of additional co-ordinate points pulled the trajectory back closer to the corner point.

Timings

The total movement here and time taken to reach the turn point for the corner movement profiles with varying smoothing levels, velocity and number of additional co-ordinate points, are shown in figure 5.3.6. As with the simple linear motions, a reduction in smoothing level led to an increased motion time. There appears to be much more of a balance in the timings of each half of the movement. The addition of extra co-ordinate points increased all of the recorded times.

Velocities

The peak velocity attained and average velocity for the corner motions are shown in Figure 3.5.7. As expected, increasing the programmed velocity led to an increase in outputted peak and average velocity.

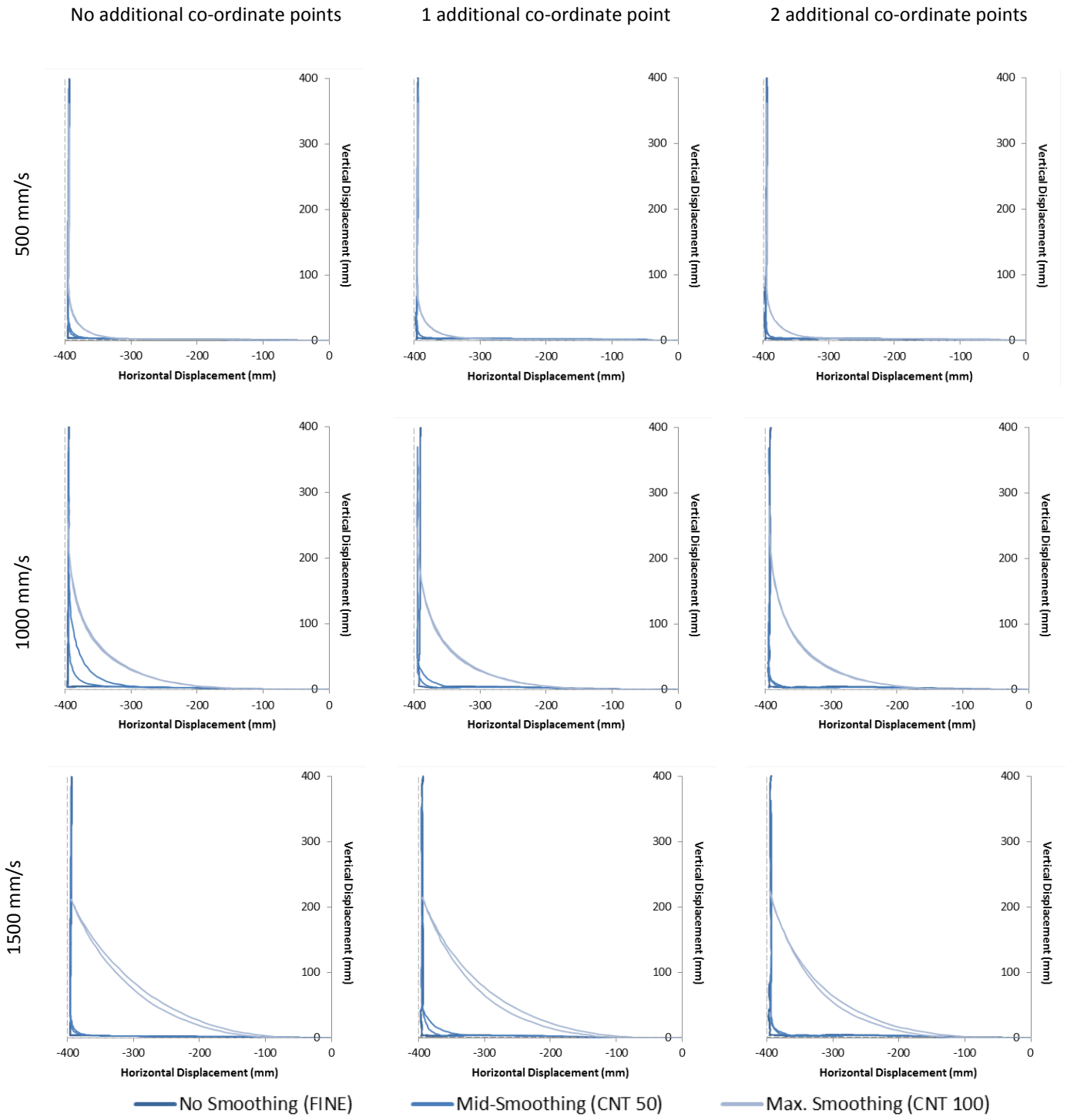

Figure 5.3.5 The corner movement trajectories for the robot with different levels of robotic smoothing applied and with different numbers of additional co-ordinate points (+ 0, +1 and + 2) at different velocities (500 mm/s, 1000 mm/s and 1500 mm/s). The movements start at the origin (0, 0) and the inputted trajectory is shown by the dotted line.

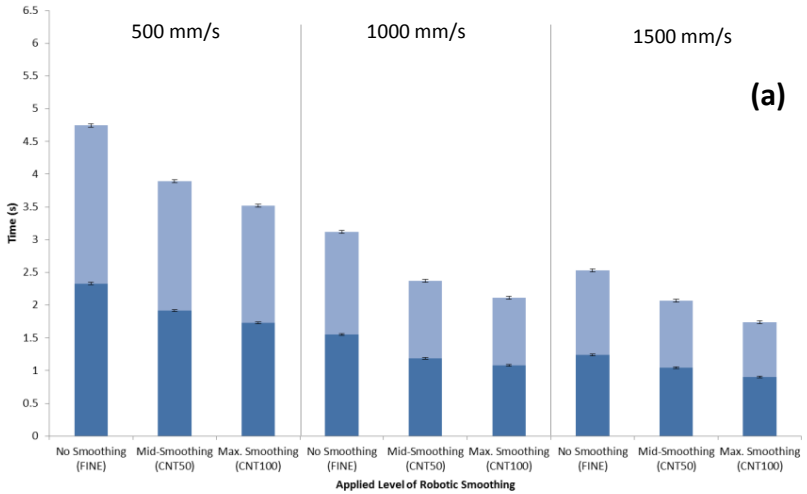

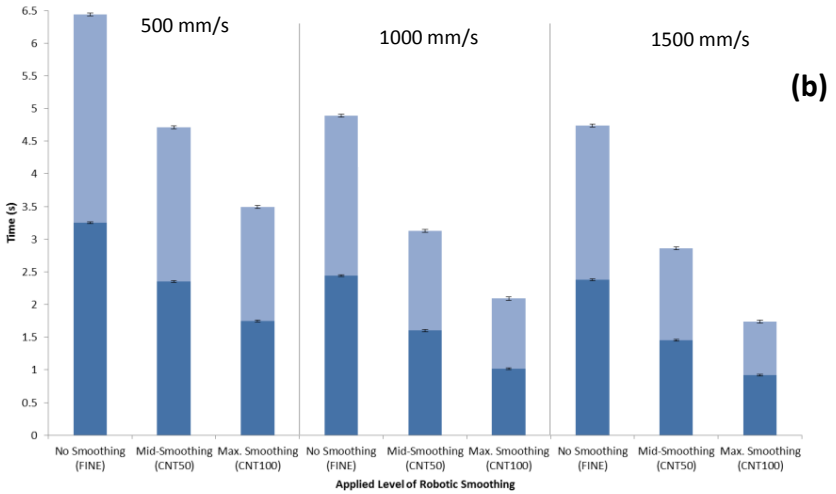

Figure 5.3.6 Total motion times and the time taken to reach the turn point for the robot moving in the corner motion with different levels of robotic smoothing and velocity applied with **(a)** no additional co-ordinate pointes programmed and **(b)** two additional co-ordinate points programmed.

	Peak Velocity (mm/s)		
Programmed Velocity	**500 mm/s**	**1000 mm/s**	**1500 mm/s**
0 Additional Co-ordinate Points			
No Smoothing (FINE)	563	1038	1432
Mid-Smoothing (CNT 50)	557	1047	1117
Max. Smoothing (CNT 100)	563	879	1019
1 Additional Co-ordinate Points			
No Smoothing (FINE)	637	557	1432
Mid-Smoothing (CNT 50)	637	958	1114
Max. Smoothing (CNT 100)	642	879	1019
2 Additional Co-ordinate Points			
No Smoothing (FINE)	637	1038	1353
Mid-Smoothing (CNT 50)	563	958	1034
Max. Smoothing (CNT 100)	563	958	1007

	Average Velocity (mm/s)		
Programmed Velocity	**500 mm/s**	**1000 mm/s**	**1500 mm/s**
0 Additional Co-ordinate Points			
No Smoothing (FINE)	336	511	633
Mid-Smoothing (CNT 50)	396	616	673
Max. Smoothing (CNT 100)	414	565	559
1 Additional Co-ordinate Points			
No Smoothing (FINE)	288	227	447
Mid-Smoothing (CNT 50)	363	539	576
Max. Smoothing (CNT 100)	408	549	591
2 Additional Co-ordinate Points			
No Smoothing (FINE)	249	328	339
Mid-Smoothing (CNT 50)	329	481	521
Max. Smoothing (CNT 100)	416	564	587

Figure 5.3.7 The outputted velocities against the programmed velocities under all conditions for the corner motion showing **(a)** the peak velocity attained and **(b)** the average velocity.

5.4 DISCUSSION

This chapter aimed to investigate and compare the effects of varying the level of robotic smoothing, velocity and the number of programmed co-ordinate points on robot end-effector trajectory for programs instructed to move in straight linear paths (horizontal and vertical) and a 90° corner path. The effects of the variables were quantified by analysing and comparing the outputted robot kinematics (trajectories, timings and velocities).

5.4.1 Vertical and Horizontal Movements

One of the primary findings for the linear motions was that as the programmed velocity and/or level of robotic smoothing is increased, the overall vertical displacement decreased (figures 5.3.1 and 5.3.2), i.e. the robot turned closer to the start point. This could be attributed to the possible theory that as the rate at which the robot is trying to reach the next co-ordinate point is increased, priority is given to that and it doesn't actually move to the current point.

The use of the 'FINE' termination (no smoothing), regardless of velocity, caused the robot to move the fully programmed displacement of 400mm; except for the vertical motions with 0 additional co-ordinate points (~380mm). However, this anomaly is not present for all of the other motions and it may be the case that the vertical motions cause the robot to behave differently to the horizontal motions. It is also shown that the addition of extra co-ordinate points have an influence on the location of the turn point; where used they encourage the robot to move closer to the programmed point in all situations. The addition of a second co-ordinate point has less of an influence compared to that of the first, possibly because the location is encompassed by the 'draw' of the first. It is clear that the addition of extra points has an effect on being able to improve the control over robot position whilst using some level of smoothing, as shown with the vertical programme with mid-smoothing and additional points, which has a larger displacement than the FINE program without addition. However, there may be a compromise on the time taken to complete the motion.

As expected, a decrease in velocity or level of smoothing results in an increased time taken to reach the maximum displacement, because the distance is greater and target movement velocity is lower. This is magnified with the addition of extra co-ordinate points and lower smoothing levels, where the robot had the largest trajectory and is delayed by the virtual stop at each point.

The average velocity increased as the level of robotic smoothing increased and as expected increasing the programmed velocity led to an increase in outputted peak and average velocity respectively. The average velocities were much lower than the inputted values, never exceeding 100mm/s. This suggests that fast motions over a small area may be difficult to achieve on the robot. Even when programmed within this range (500mm/s), the output still doesn't match the input. It may be required to over-estimate the velocity needed when programming the robot in future. However, these values are only an average, and as shown by the peak values the robot is capable of faster velocities, in some cases faster than the input value indicating possible difficulties in achieving accurate motion control. Perhaps the input value will give more of an indication of the peak velocity to be obtained as opposed to the average velocity between co-ordinate points. It is surprising to see that the peak velocities tended to be higher where less or no robotic smoothing was applied. It is known that in the trials the end-effector would have momentarily stopped at each point, the greater displacement area with more space to accelerate into and the velocity discrepancy to make up mean that an exaggerated peak is possible before levelling off.

For the maximum smoothing level, the peak velocity doesn't vary when additional points are used. This may be because it has the same turn point located before the additional points, and regardless of programmed velocity, there isn't enough space for adequate acceleration. There is no noticeable effect on the average velocity of the FINE programme between one and two additional points. As the robot moves to each point discretely, there is not enough space to attain a higher peak velocity, which also indicates that the peak velocity is reached before the location of the 2nd additional point, meaning a period of deceleration.

It is also interesting to note that both the peak and average horizontal velocities are higher; except where maximum smoothing is used or where the programmed velocity is 1500mm/s. This indicates that as well as being influenced by the input variables, the output kinematics can be affected by the plane of movement.

5.4.2 Corner Movements

As with the linear motions, the increase in smoothing level or velocity cause the corner profiles to not follow the inputted path as closely; be it by not moving to the turn point or 'cutting' the corner point (figure 5.3.5). The inclusion of additional co-ordinate points pulled the trajectory back closer to the corner point. This reinforces the opportunity of using additional points as a method of further control to the position of the robot where some levels of smoothing is used. However, there may be a trade off in movement time and velocity (figures 5.3.6 and 5.3.7).

5.4.3 Implications for the emulations of sporting movements

Emulation of human gait on the robot is a more complex motion than those presented in this chapter. The results for the simple movements indicate that obtaining fine control over position with adequate timing and velocity for human gait may be challenging. The outcomes of this chapter have laid a foundation for the direction of subsequent work. It may be the case that alternative methods of driving the end-effector through the required motions will be required.

5.5 CONCLUSIONS

In this chapter the effect of the level of robotic smoothing, velocity and the number of programmed co-ordinate points on robot kinematics (positions, timings and velocities) for programmes instructed to move (a) in straight linear paths (horizontal and vertical) and (b) in a 90° corner path were investigated. This information is critical to addressing research question two for this thesis (page 4) as well as providing key relevant background knowledge for research question three.

The output kinematics were influenced by all three variables; indicating that the features within the control system and the way in which the robot is programmed affect the resultant motion, the main conclusions drawn from the investigation are shown below:

- Vertical and horizontal displacement becomes more smoothed as velocity increases, as smoothing increases or as fewer points are used. For the corner profiles, the use of no robotic smoothing caused the robot to follow the inputted trajectory. An increase in smoothing level or applied velocity sees the robot move further away from the corner and turn points. The inclusion of additional co-ordinate points pulled the trajectory back closer to the corner point.
- Generally, as the level of applied smoothing was increased, movement time decreased. For the linear motions, the trend was for the robot to take longer for the first half of the movement (moving to the turn point) than the second (returning to the start). This was not mirrored for the corner movements which had more balanced timings. The addition of extra co-ordinate points increased all movement times.
- Velocity increased as smoothing level increased and where fewer co-ordinate points were used. Increasing the programmed velocity led to an increase in outputted peak and average velocities.
- As these features have been shown to occur in linear motions. It has therefore concluded that they will also affect a more complex motion, i.e. human gait.

CHAPTER 6

EVALUATION OF ROBOGUIDE TO SIMULATE THE FOOTSTRIKE IN A VIRTUAL ENVIRONMENT

6.1 INTRODUCTION

One of the accompanying tools provided with the FANUC™ robot, is the computer software RoboGuide, which simulates the robot in a virtual environment. The robot's environment, layout and motions can be simulated giving the advantage of not having to alter real world parameters until potential benefits are assessed. Results from a more traditional industrial setting have shown that fast-track programming using RoboGuide can help to reduce robot downtime by creating, editing and implementing other programmes whilst the robot is performing other tasks thus making the manufacturing process more efficient (Jin and Yang, 2009 and Liu *et al,* 2011).

Within RoboGuide the virtual robot is programmed by the same means as the real world robot (section 4.3). If the virtual robot 'impacts' an object the interaction is not modelled, the robot simply passes through the object, therefore a direct comparison between the robot and RoboGuide should be carried out with no ground interaction i.e. 'mid-air'. Despite this, the collision detect feature, built into the software, alerts the user (during and post movement) to the contact. The resulting kinematics can still be evaluated using a number of analysis features; trajectories can be monitored and measured, the built in timers can be used for further analysis alongside the ability of recording movements to a video file. As such, this software also has the potential to support research into the development of human emulations on the FANUC™ robot.

It was shown in Chapter 5, that the robot has a number of programmable and embedded features within its control system that affect its resultant motion. Trajectories and movement times are affected by smoothing level, velocity and number of co-ordinate points used. It remains unknown whether these same features have been built into RoboGuide, and whether or not they affect the robot in the same way. A previous study has compared a 90º rotation on the robot and RoboGuide and found the finishing position to be the same in both cases (Jamaluddin *et al* 2006); however, no study has attempted to compare the complete trajectories of RoboGuide versus the robot based on the same input programme.

For applications in emulating the ground contact phase of human locomotion a detailed comparison of RoboGuide versus the robot kinematics is necessary in order to quantify the level of agreement. This will help to assess the degree to which RoboGuide can be used to support the development of the emulation of the ground contact phase, and complex sporting motions on the FANUC^{TM} robot. This support may range from simple robot cell design to full kinematic programming and output validation.

6.1.1 Aims

The main aim of this Chapter is as follows:

- To compare the kinematics (trajectories and movement timings) of RoboGuide versus the robot using initially a number of simple one and two-dimensional movements, followed by the more complex movement of human heelstrike running.

6.1.2 Objectives

The following objectives will be used to achieve the stated aim:

- To generate the required motions in RoboGuide in the same way as those on the real world robot.
- To compare the RoboGuide two-dimensional movements with the results obtained in Chapter 5.
- To compare the more complex footstrike motions from RoboGuide, with the robot and human footstrikes.

6.2 METHODOLOGY

The work undertaken in this Chapter was split up into two sets of trials as outlined below and described in figure 6.2.3:

1. Simple vertical, horizontal and 90° corner movements, in both the real and virtual environment, the robot was fitted with an end-effector in the form of a spike, used as a distinct reference point to track. The physical robot data for this set comes from Chapter 5, which can be referred to for further information on protocols and set-up.

2. Sagittal plane heelstrike running based on the human kinematic data described in Chapter 3. The robot was fitted with a shod Blatchford prosthetic foot end-effector, and a CAD representation of this end-effector was used in the RoboGuide trials.

In each case, the resulting movement on the robot and RoboGuide were measured and comparisons made between the programmed movement and the actual movement.

6.2.1 Creating the Virtual Robot Environment

The FANUC robot cell environment was recreated within RoboGuide (figure 6.2.1) by importing CAD files of robot attachments and cell furniture (figure 6.2.2). As interactions with the external environment are not modelled within RoboGuide, accurate representations are not always necessary. The force platform has the same dimensions as physical force platform and was positioned within the robot cell at the same location. The metal spike used for the linear movements was also accurately replicated, and attached to the virtual robot in the same position and orientation. The prosthetic foot attachment to the robot was accurately detailed in CAD; however, due to the complex shape the Blatchford prosthetic foot (section 3.5.1) section was not accurately detailed in the CAD model, rather the general outline was obtained with key dimensions and positions like the centre of rotation maintained.

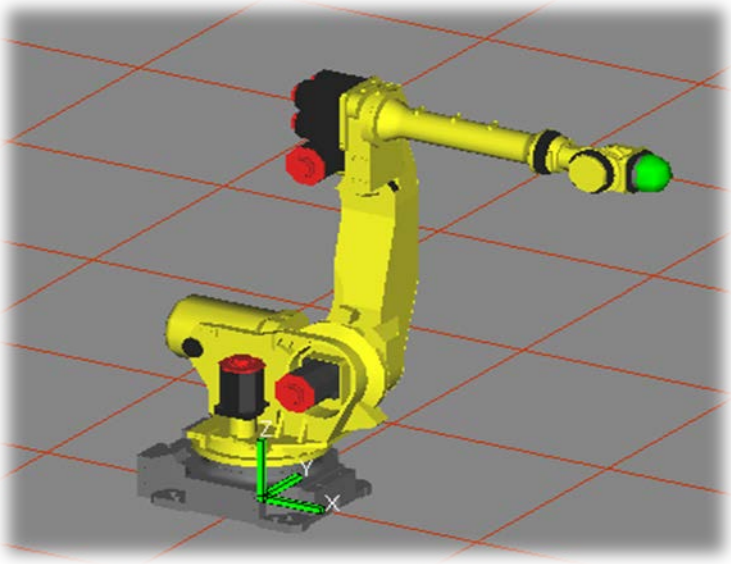

Figure 6.2.1 The FANUC robot cell environment was recreated within RoboGuide

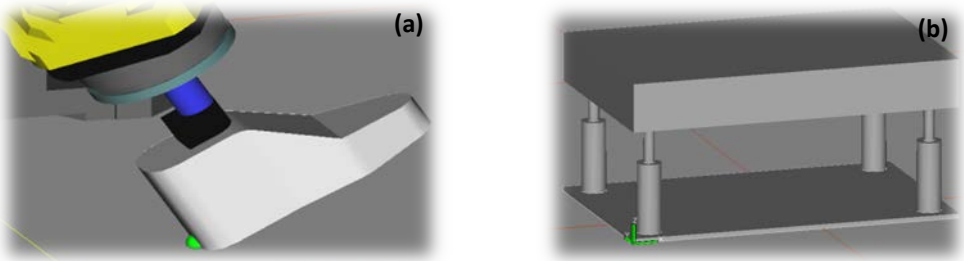

Figure 6.2.2: (a) The imported CAD model of the Blatchford end-effector; (b) The imported CAD model of the Kistler Force Platform

6.2.2 Data Collection

Set (1) was made up of simple vertical and horizontal linear movements; a programmed displacement of 400mm from the start point to the destination point (turn point) and back. These were then combined to make the corner profile, involving a programmed horizontal displacement of 400mm to a corner point and a further 400mm vertical to the destination point (turn point) and back. The investigation looked at the effects of robotic smoothing (maximum, medium and none), movement velocity (500 mm/s, 100 mm/s and 1500 mm/s) and number of additional co-ordinate points used to define the movement (end points, end points + 1 and end points + 2; each at 10% intervals i.e. 40mm) on movement trajectory and timing. Trials were performed for every combination of the above variables on the robot (Chapter 5) and RoboGuide, a total of 81 trials on each. The physical robot movement was recorded using high-speed video cameras recording at 1000Hz (SA 1.1; Photron Fastcam-Buckinghamshire, UK); and the virtual robot movements in RoboGuide were outputted by the software to a video file (125Hz).

Set (2) compared the footstrike in the sagittal for the human, physical robot and virtual robot, in terms of movement trajectory and timings. Human heelstrike shod running data was taken from the database generated in Chapter 3 to programme the robot and RoboGuide as described in Chapter 4. The human sagittal plane position and velocity of the heel marker as well as the foot orientation from 2 seconds before impact to 0.5 seconds after impact were used to create the respective programmes. The maximum level of robotic smoothing was used in an attempt to reduce the amount of jerk in the movements. For both the robot and RoboGuide the motions were recorded in a similar fashion to set (1). As RoboGuide is unable to simulate the ground contact interaction (it just moves through the footform through the obstacle) it was decided that the best comparison would be with both the robot and RoboGuide set to run in ‘mid-air’. This was achieved by vertically offsetting a programme which had been instructed to run over the force platform as in the human running trial.

Set	Input Movement	Robot	RoboGuide	Variables
(1)	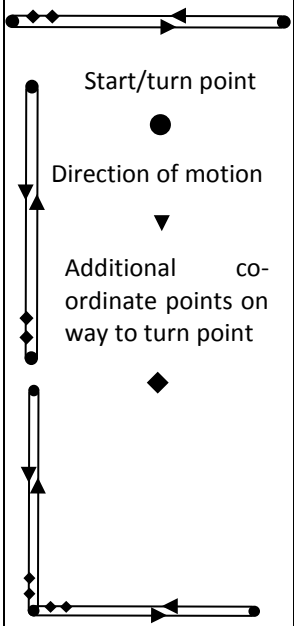	 	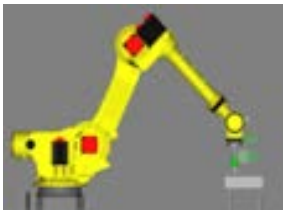 	Effect of: ❖ Level of robotic smoothing ❖ Input velocity. ❖ Number of additional co-ordinate points (Programmed at 10%intervils ~ 40mm) ❖ Movement trajectory & timings.
(2)				Comparisons of: ❖ Ground contact time. ❖ Heel marker trajectory.

Figure 6.2.3: A summary of the two sets of trials completed on both the robot and RoboGuide, showing input movements, robot and RoboGuide positions and the investigated parameters.

6.2.3 Data Processing

The kinematic data for the linear and corner trajectories within (set (1)) was obtained by digitising the respective videos, using Image Pro Plus (Media Cybernetics, Inc. USA). Thus generating two-dimensional co-ordinate data for the tip of the spike, for both the robot and RoboGuide.

For set (2), the outputted RoboGuide videos were digitised in the same way as in set (1), with the trajectories of the heel of the shoe being documented. This data was compared to the heel trajectories of the real world robot and a human. Force platform data was analysed to determine ground contact time (based on a minimum force threshold of 10N). For RoboGuide this was established using the built in collision detect feature, where an alarm is active whenever there is an external contact to the robot and or end-effector i.e. the ground contact phase.

6.3 RESULTS

6.3.1 Set 1 – Simple Linear Movements

Vertical and horizontal movements

The displacement results for the horizontal and vertical linear movements on the robot and RoboGuide are shown in figure 6.3.1 and 6.3.2. The general trend for both the robot and RoboGuide was for the displacement to decrease as the level of robotic smoothing or velocity were increased or fewer additional co-ordinate points were used. The displacement range was from 400mm (as programmed) for no smoothing, 500mm/s and two additional points; to only ~250mm for maximum smoothing, 1500mm/s and zero additional points.

The RoboGuide displacements tended to be slightly greater than those of the robot, up to 30 mm. For the robot, the programmed displacement of 400 mm was only reached when no smoothing was used with lower velocities and additional co-ordinate points. For RoboGuide, the programmed displacement of 400mm was only ever reached whenever no smoothing was used for the horizontal motion.

The times for the total movement to reach the turn point for the vertical and horizontal linear movements on the robot and RoboGuide are shown in figure 6.3.3. Generally, as level of smoothing was decreased, movement time increased. The robot tended to take longer moving from the start point to the turn point compared to returning to the start point, whereas the opposite was observed on RoboGuide particularly at higher smoothing levels.

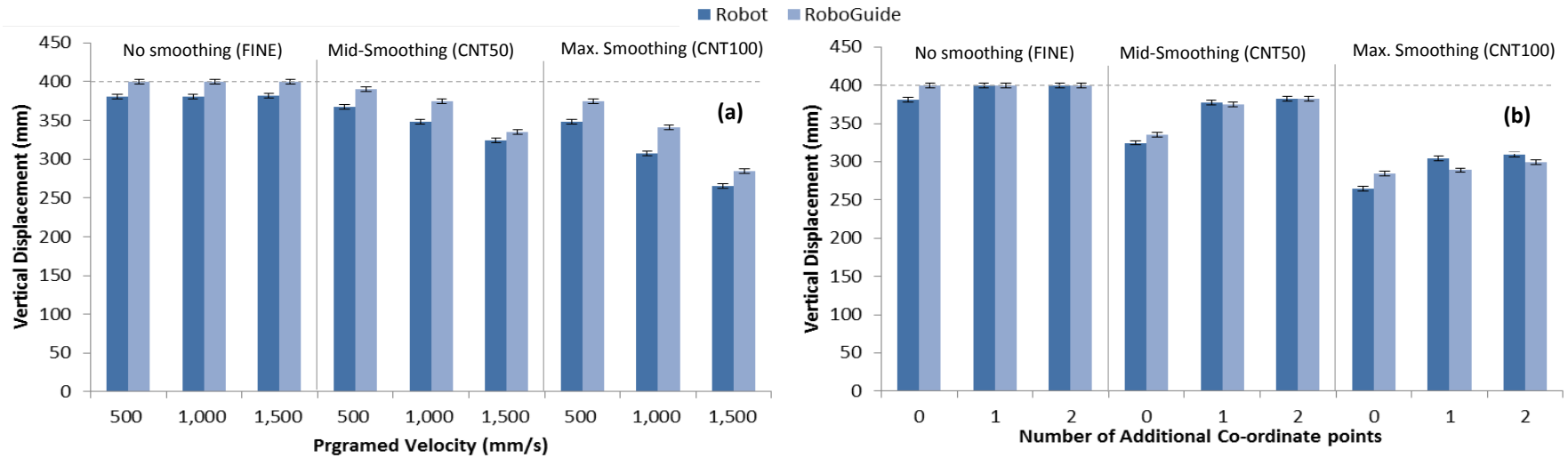

Figure 6.3.1: Vertical displacement from start point to turn point (programmed displacement was 400 mm, shown by the dashed line) for the robot and RoboGuide with **(a)** different levels of robotic smoothing and velocity (using no additional co-ordinate points) and **(b)** different numbers of additional co-ordinate points and levels of robotic smoothing (using a velocity of 1500 mm/s).

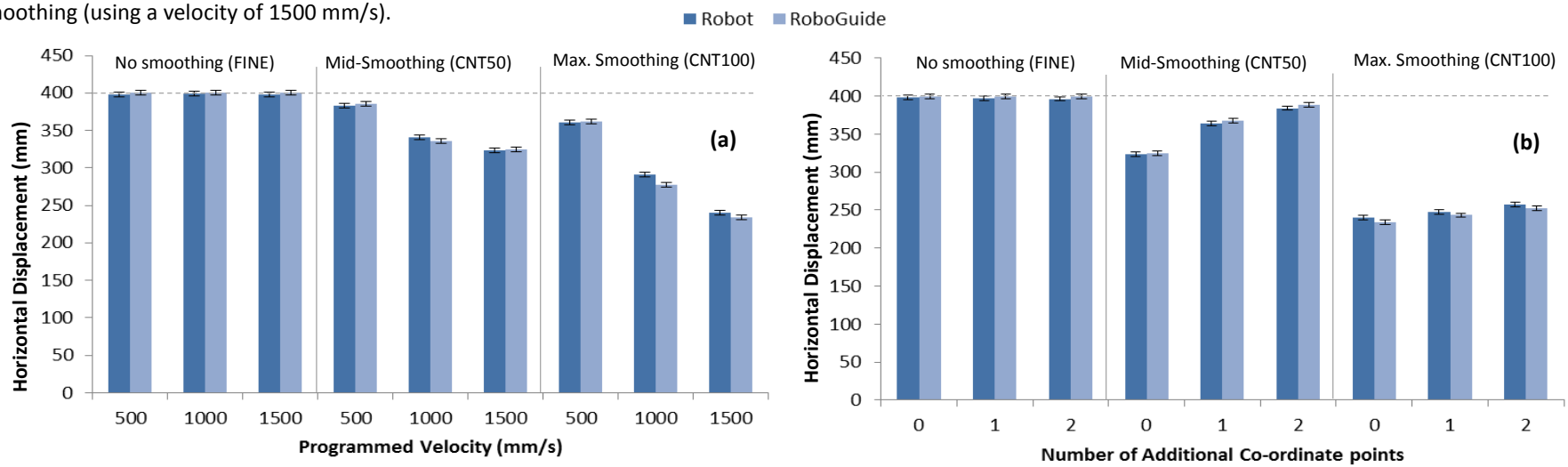

Figure 6.3.2: Horizontal displacement from start point to turn point (programmed displacement was 400 mm, shown by the dashed line) for the robot and RoboGuide with **(a)** different levels of robotic smoothing and velocity (using no additional co-ordinate points) and **(b)** different numbers of additional co-ordinate points and levels of robotic smoothing (using a velocity of 1500 mm/s).

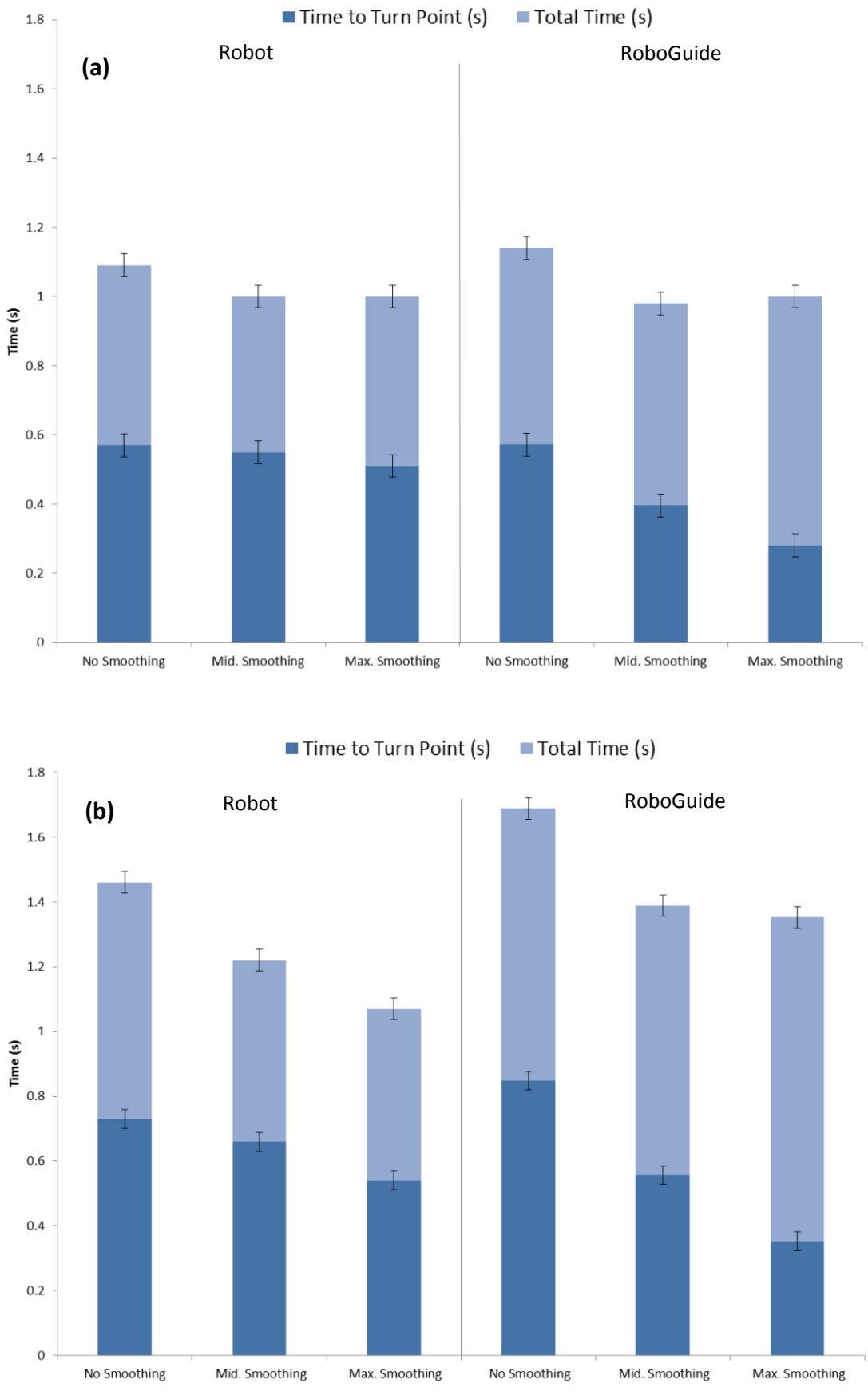

Figure 6.3.3 Total motion times and the times taken to reach the turn point for the robot and RoboGuide at 1500mm/s with various levels of smoothing applied for **(a)** vertical and **(b)** horizontal linear movements.

Corner Movement

Typical trajectories of the robot and RoboGuide for the corner movement are shown in figure 6.3.4. As smoothing level and velocity were increased, both the robot and RoboGuide trajectories moved further from the corner point and from the programmed vertical turn point. When additional co-ordinate points were used the trajectories were pulled back closer to the programmed movements. For no smoothing and 500 mm/s both the robot and RoboGuide moved very close to the corner point and vertical turn point regardless of the number of additional co-ordinate points. Comparing the robot and RoboGuide, there were differences of up to 8mm between trajectories for the turn point and similarly for the corner arc.

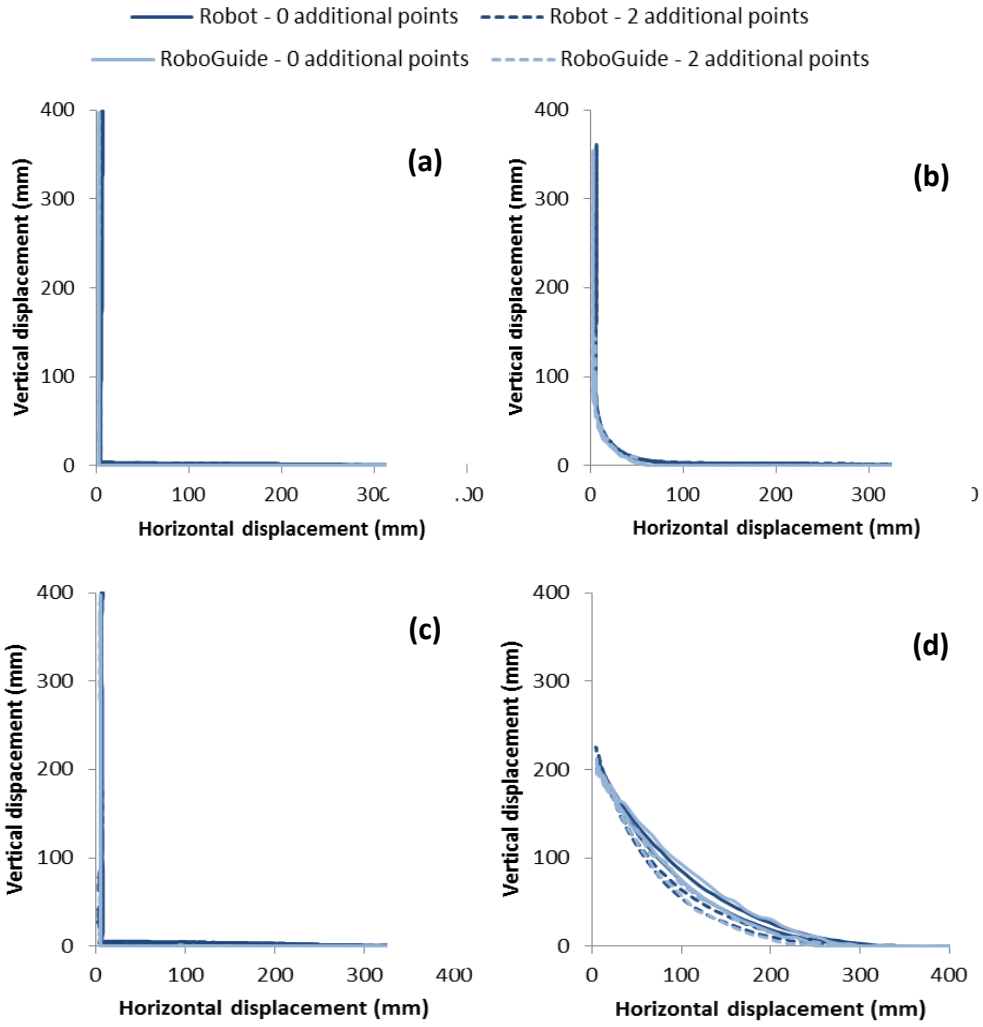

Figure 6.3.4 The corner movement trajectories for the robot and RoboGuide with different numbers of additional co-ordinate points (+ 0 and + 2) at the extremities of applied level of smoothing and velocity respectively. **(a)** No smoothing at 500 mm/s, **(b)** Maximum smoothing at 500mm/s, **(c)** No smoothing at 1500 mm/s and **(d)** Maximum smoothing at 1500mm/s.

The time for the total movement and to reach the turn point for the corner movement profiles for the robot and RoboGuide are shown in figure 6.3.5. As with the simple linear motions, a decrease in level of smoothing led to an increase in movement time. There is much less of a discrepancy in the times of the out and back sections of the movement when compared to the simple linear movements. As before, RoboGuide tended to take longer to return to the start point compared to the outward movement to the turn point.

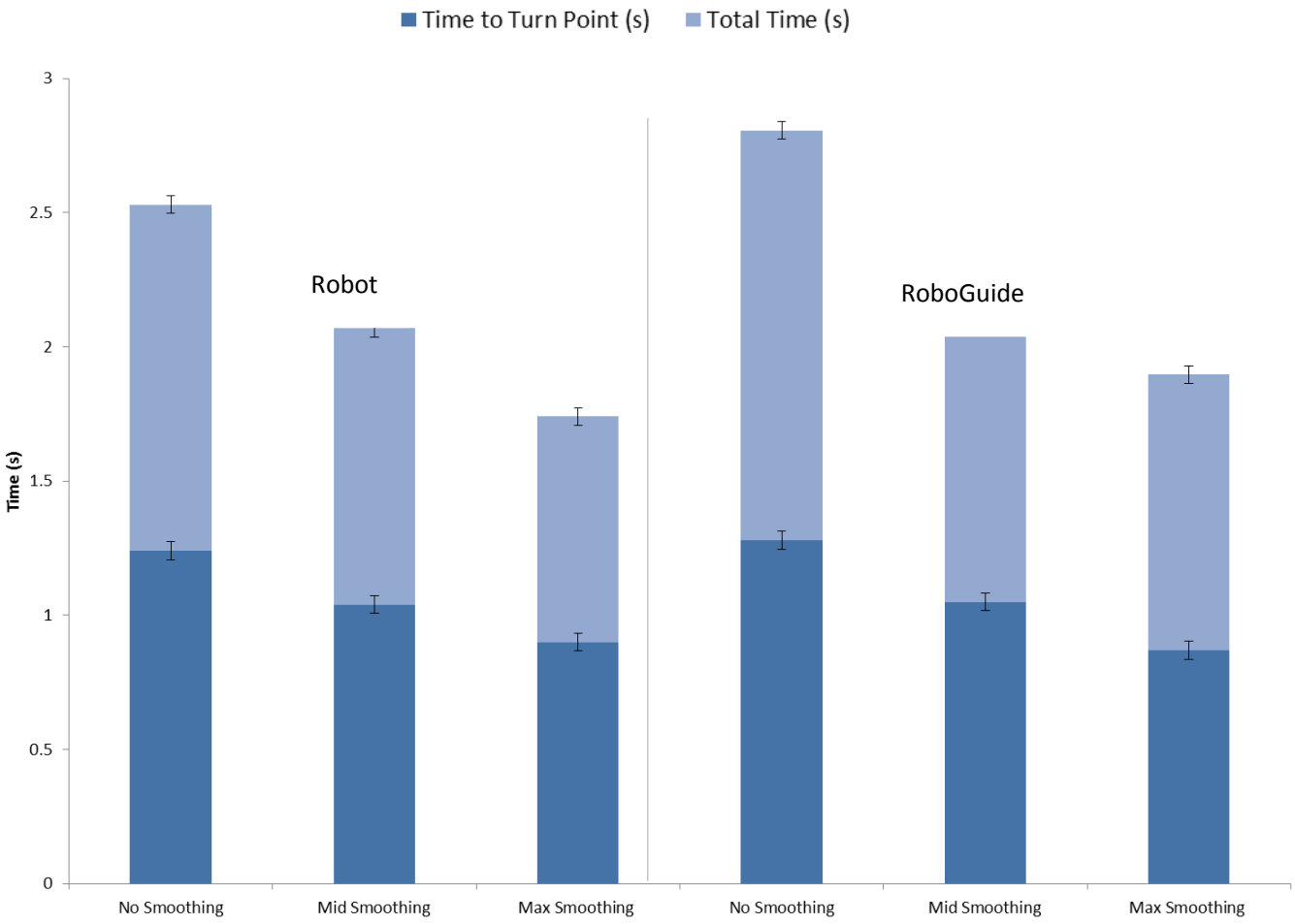

Figure 6.3.5 Time for the total movement and to reach the turn point for the robot and RoboGuide at a velocity of 1500mm/s with various levels of smoothing applied to the corner movement.

6.3.2 Set 2 –Human Heelstrike Running

The heel marker trajectories for the heelstrike running trials are shown in figure 6.3.6, where the robot and RoboGuide trajectories are for the mid-air trials. The RoboGuide trajectory was far closer to the human trajectory compared to the robot, deviating typically by < 10 mm. In comparison, the robot had a shallower approach and take-off, and the trajectory differed markedly from the human data during mid-stance, i.e. foot flat on the ground with minimal heel marker movement. The ground contact time for human running was 0.209 s, and much higher for both the robot (0.656 s) and RoboGuide (0.584 s – determined using the built in collision detect feature before raining to mid-air). Figure 6.3.7 gives results of the human, robot and RoboGuide at key instances during ground contact.

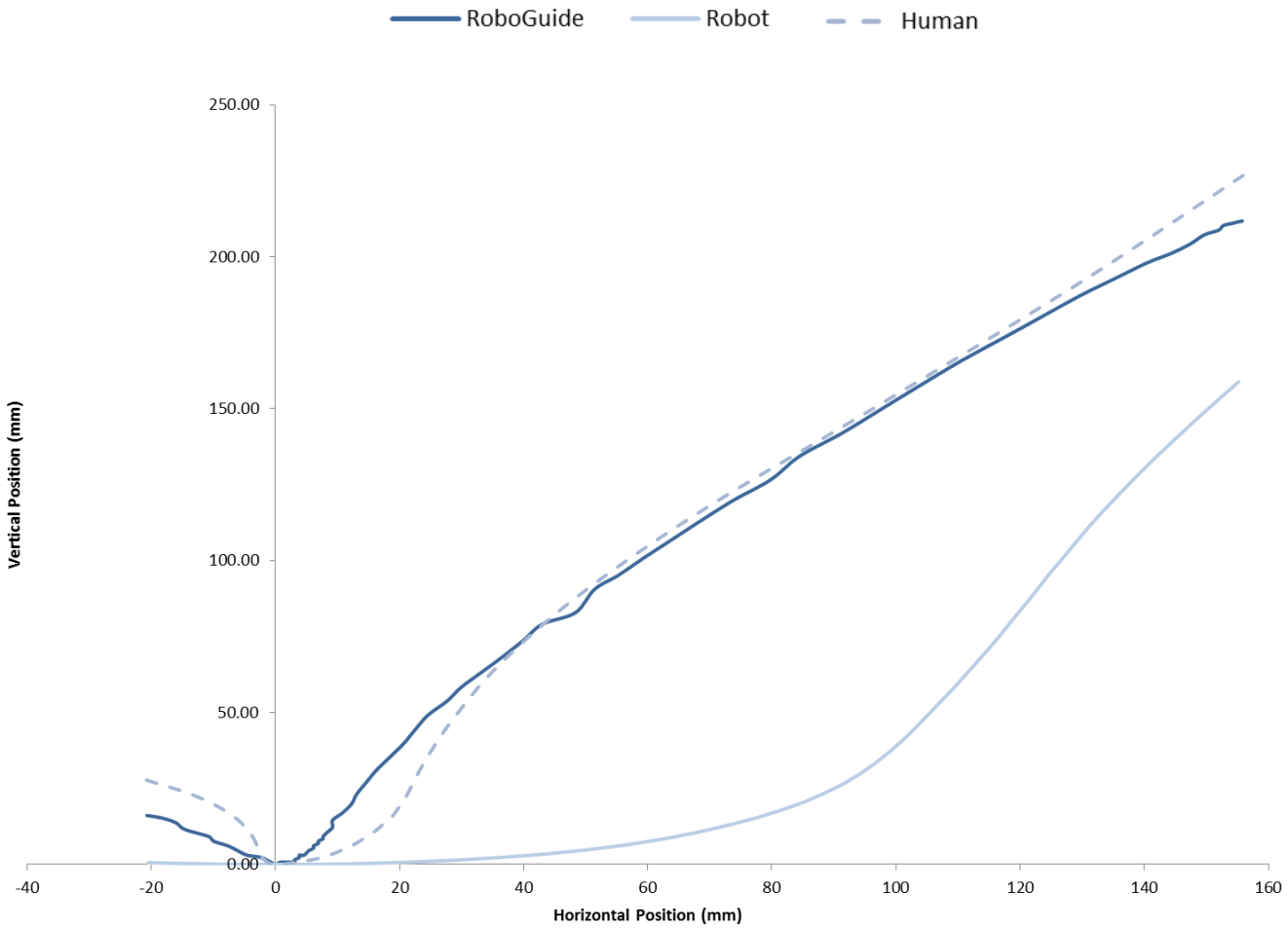

Figure 6.3.6: Heel trajectory data for heelstrike human running, the robot and RoboGuide throughout the ground contact phase, which starts at 0 mm in the vertical and horizontal plane, trials start 20 mm horizontally prior to initial contact, ending 150 mm after contact in the sagittal plane.

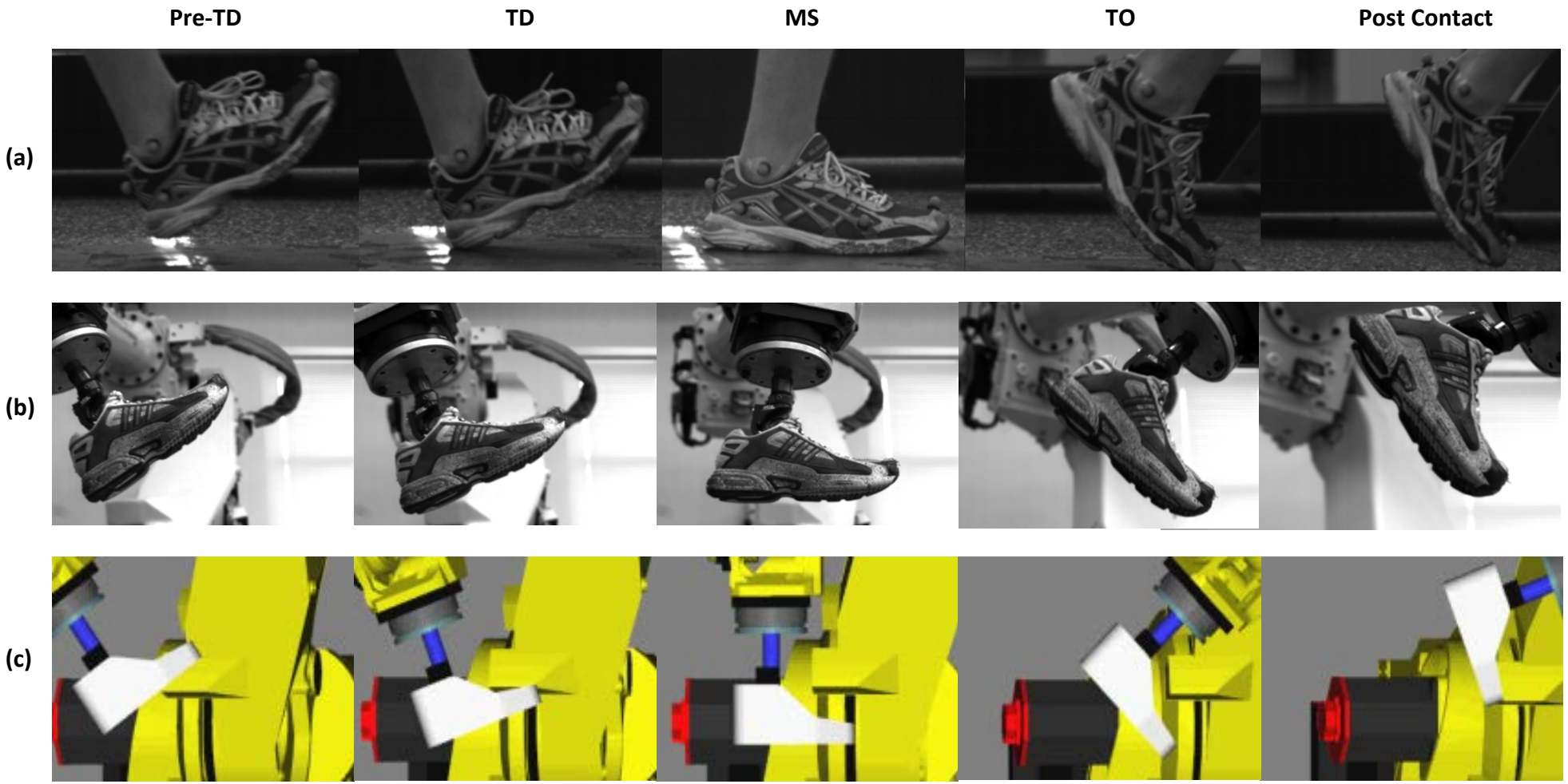

Figure 6.3.7 A comparison of running gaits for **(a)** a human, **(b)** the robot and **(c)** RoboGuide; both the robot and RoboGuide are programmed to run through 'mid-air'. Starting prior to impact (pre-TD), moving through contact (TD) into the mid-stance (MS). The heel continues to rise to toe-off (TO) before the foot leaves the ground as part of the post contact phase.

6.4 DISCUSSION

This study aimed to compare the kinematics of RoboGuide against those of the physical robot firstly for simple (linear) and then complex (human heelstrike running) movements. The results suggest that for a given input trajectory, the resultant kinematics of RoboGuide and the robot exhibit small differences for simple horizontal and vertical motions which become much greater for the more complex heelstrike running movement. These findings were observed across a range of movement velocities, levels of robotic smoothing and number of co-ordinate points defining the trajectory, with increased levels of smoothing tending to produce greater differences between the two. Furthermore, neither RoboGuide nor the robot trajectory matched the programmed trajectory unless there was no robotic smoothing, which also resulted in a jerky movement suggesting that the velocities would be poorly matched.

As expected the total movement time and the time taken to reach the turn point decreased as more smoothing was used, probably because the displacements were decreased. The general trend was for the movement in RoboGuide to take longer than that on the robot, especially to the turn point. This supports the observation that RoboGuide does not accurately simulate the built in features of the robot in terms of movement deceleration and acceleration. Thus the differences in trajectories and timings obtained relate to differences in the control features that dictate how each moves given input kinematics.

Although there were clear differences in the movement trajectories between RoboGuide and the robot, the trends were similar. For both, displacements decreased as velocity increased, as smoothing increased or as fewer co-ordinate points were used. Also a difference in movement time was noted where smoothing levels were increased or where fewer co-ordinate points are used.

The differences in the trajectories between the robot and RoboGuide appeared significantly larger for the heelstrike ground contact than for the linear and corner movements, (despite

similar ground contact times). The biggest difference occurred at midstance where the heel marker velocity was at its lowest (close to 0 mm/s). RoboGuide gave a reasonable approximation to the human heel marker trajectory; however, the movement timing was poor for both the robot and RoboGuide taking almost three times longer in ground contact time compared to the human footstrike. Visual inspection of the key instances during the ground contact (figure 6.3.6) indicates that all three profiles were similar; however, as discussed, the timings were very different suggesting the velocities or accelerations differed. It was also apparent that the robot has a large 'slide' upon ground contact – resulting in an increased footprint. Since RoboGuide could not model the shoe-ground contact phase both the robot and RoboGuide were programmed to run in mid-air, so there were no external confounding factors contributing to the differences between the robot and RoboGuide.

It is surprising that the differences in the results were so large. Further investigations may be beneficial in understanding the reasons behind these differences. One potential reason for the differences could be measurement error; however, a basic error analysis on both measurement methods (video digitisation for the robot and using the built in measure tool for RoboGuide) indicated positional errors of < 3 mm, which is far smaller than the observed differences during the programmed movements.

RoboGuide does not accurately simulate the robot and it appears that it is not programmed to move in the same way; suggesting that it has limitations in supporting human locomotion emulation on the robot. However, the similarities in trends suggests that RoboGuide may still be a useful tool to support applications related to the physical robot. For example, in optimising the force platform location within the robot cell to minimise movement time, multiple locations can be tested much faster using RoboGuide than the physical robot. Or as a visualisation tool for creating and simulating workspace environments and end-effectors prior to their physical development and as an offline programming tool, as demonstrated by Liu LX. Yang X. *et al.* (2011). Significant work remains in order to be able achieve the wider aim of the research of emulating the human gait using the physical robot.

6.5 CONCLUSIONS

This Chapter compared the kinematics of the robot against those of the accompanying computer software RoboGuide, for simple linear motions and the more complex motion of the human heelstrike running. One of the main conclusions that can be drawn was that RoboGuide closely simulates the robot movement for simple two-dimensional movements; however, it less closely simulates the robot for more complex movements such as a human heelstrike running. It is known that the robot has a number of features built into its control system that affect its resultant movement (Chapter 5). It appears that the RoboGuide software has features within its control system that affect the resultant movement; however, these differ to those of the physical robot.

The wider aim of this thesis is to investigate the use of the robot to emulate the human footstrike during running and walking. The differences in kinematics and timing between the robot and Robo-Guide for a given input suggest that RoboGuide has only limited use in supporting this aim. Although RoboGuide may not be useful to support very accurate emulations, it has potential to support for example, optimising the robot cell design and in offline programming of the robot. As such, it may represent a useful tool for addressing research question two (page 4) of this thesis.

CHAPTER 7

DESIGN AND CHARACTERISATION OF A NEW END-EFFECTOR

7.1 INTRODUCTION

The nature of using a commercially available robot that has a variety of potential uses means that in this particular application there is no specific tool or end-effector that can be used to aid footstrike emulation. As such there is need for a bespoke end-effector which will support a biofidelic footstrike. In this context the end-effector refers to what must be attached to the robot to allow the footstrike emulation, i.e. the footform and attachment mechanism. The original end-effector was made by Loughborough University to attach a Blatchford prosthetic foot (figure 7.1.1). This has been used in previous studies (Ronkainen *et al* 2010) as reported in Chapter 2; the results of which indicated that in this set-up, there are a number of issues in human footstrike emulation some of which can be related to the end effector design:

- Ground contact time is too long (0.6 seconds for attempted running emulation).
- Vertical ground reaction force has no impact peak and loading rates are too low.
- The horizontal ground reaction force is in a single phase, with braking throughout stance.
- The ground contact area or 'footprint' is too large.

The first three of these factors can be related to the end-effector which will affect how the robot is required to move in order to perform the footstrike, potentially influencing the speed of movement as well as the rigidity of the footform affecting the applied forces.

Figure 7.1.1 – The original end-effector used in previous footstrike emulations using the FANUC.

The aim of this chapter is to design, develop and test a new robot end-effector that can better support the emulation of human gait, specifically the ground contact phase, compared to the existing end-effector design.

The methodical approach to achieving this aim was as follows:

- Characterise the original end-effector design through visual and technical analysis, robot testing and characterisation of the footform. This work will include an investigation of (a) the end-effector position and orientation in relation to the robot faceplate and (b) the ability of it to be able to generate pseudo static loading.
- Identify an area for improvement and develop a design specification.
- Generate a range of concept ideas with a view of improving it so that the robot has the best chance of producing a better ground contact emulation. These can then be tested against the design specification and converge to a final design proposal.

7.2 ORIGINAL END-EFFECTOR CHARACTERISATION

The process of developing and designing a new end-effector requires the benchmarking and characterisation of the original. It is important to understand how the original performed compared to the real human footstrike, which in turn can lead to the identification of areas for improvement. This section outlines the findings from visual and technical analysis of the original end-effector in tests conducted with the as well as biofidelic characterisation.

The visual comparison was an investigation into the robot joints range of motion; the robot doesn't output its movement but this is explored further in Chapter 8 to evaluate the observations presented in the following section. The technical comparison was based on the kinetics of the ground contact phase – ground contact times and vertical ground reaction forces.

7.2.1 Visual and technical analysis

The original end-effector consisted of a 12mm thick circular mounting plate (160mm diameter), that can be bolted to the faceplate (6^{th} joint) of the robot; a bicycle seat post clamp fixed to the centre of the plate extends inferiorly, providing a method of attachment for the footform. In this case the footform is a shod prosthetic (UK size 9) manufactured and donated to Loughborough University by Blatchford Orthotics for testing in conjunction with the FANUC R-2000iA; the *'endolite elite2'* prosthetic is described in more detail in section 3.5.1. When attached to the mounting plate, the plantar aspect of the footform is parallel to the face of the 6^{th} joint of the robot, located 250mm from the mounting position.

This orientation means that the majority of the robot joints move during footstrike, with the more distal joints of the robot having to move 'up and over' the area of ground contact. All of the ground reaction forces were created by the robot driving the footform through the ground contact phase, despite there being a definitive force peak value over a definitive time period there was, unfortunately, no propulsive force being generated.

7.2.2 Ground contact emulation using the original end-effector

An investigation was conducted where Human kinematic data (Chapter 3) was used to programme the robot, mounted with the original end-effector, thus producing a footstrike emulation. Along with the findings of Ronkainen *et al* (2010), who also used the original end-effector, it is clear that the ground reaction force profiles and ground contact times do not match those of the human subject (Chapter 3). Despite being able to achieve the desired force magnitudes (approximately 1.5 kN) the vertical ground reaction force only generated one peak as opposed to two and displays a much lower loading rate; taking almost 90% of total stance time to reach the maximum force as opposed to approximately 20%. The ground contact times are also over twice that of the human value.

7.2.3 Biofidelic footform characterisation

By comparing the Blatchford prosthetic to human data, it is possible to assess its worth for both previous and future footstrike emulation attempts. One of the best comparisons is the stiffness of the prosthetic and a human foot under similar loading conditions, which were quantified through mechanical compression tests using an Instron (5569 series; Bucks, UK) mechanical testing machine; a dual column system in which a ballscrew drives the crosshead to apply a load. The prosthetic was tested under three conditions (shod, un-shod and the carbon fibre blades only), the orientation was such that the plantar aspect was parallel to the flat impact surface (a 200mm x 300mm solid steel plate) with the movement restricted to one linear motion perpendicular to the plantar aspect (Figure 7.2.1). The load was driven through the ankle joint, which simulated the footform being in midstance. The prosthetic was loaded and unloaded at a rate of 80 kN/min to a value of 850N (peak force attained during the human walking gait; Chapter 3); for a total of 20 cycles.

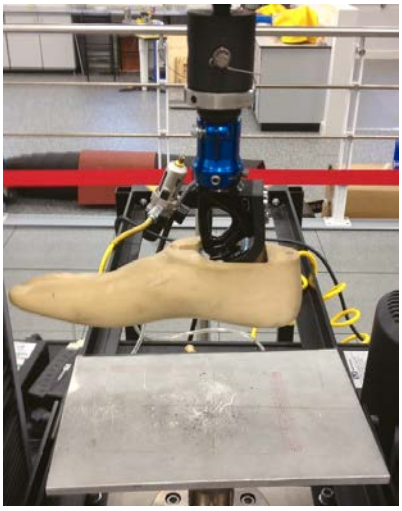

Figure 7.2.1 – An example of the original end-effector mounted onto the Instron mechanical test machine for characterisation.

Table 7.2.1 - The compression information for each state (shod, barefoot and blade) of the Blatchford prosthetic footform for the 1st and 20th cycles of 20 cycles.

	Shod		*Barefoot*		*Blade*	
	Cycle 1	*Cycle 20*	*Cycle 1*	*Cycle 20*	*Cycle 1*	*Cycle 20*
Total Time (s)	3.5	3.5	1.7	1.6	1.7	1.7
Loading Time (s)	2.0	2.0	1.1	1.1	1.0	1.0
Unloading Time (s)	1.5	1.4	0.5	0.5	0.7	0.7
Max. Load (N)	-857.1	-845.0	-822.9	-831.9	-861.8	-871.9
Max. Extension (mm)	-16.7	-16.7	-9.2	-9.2	-8.2	-8.2
Average Stiffness (N/mm)	51.3	50.5	89.1	90.1	104.9	106.0

The results from the mechanical testing are presented in figure 7.2.2 and table 7.2.1. The results indicate that the prosthetic is most biofidelic under shod conditions, where the stiffness is at the top end of the documented human range for the desired loading rate. These results can be compared to human data for runners and cyclists (section 3.1.4); Rome *et al* (2001) documented a stiffness of between 2.86N/mm and 3.22N/mm for runners and Challis *et al* (2008) found a stiffness of ~20.7N/mm for cyclists and ~17.5 N/mm for runners.

The loading rates used in the mechanical testing were somewhat lower than those used in the human testing. This was down to the capabilities of the Instron machine which was working at full speed. It has been decided that in terms of stiffness response, the footform can be used within the final end-effector system. The blade and barefoot condition seem to be very consistent throughout, this indicates that the variance and hysteresis exhibited by the shod prosthetic is down to the shoe in question.

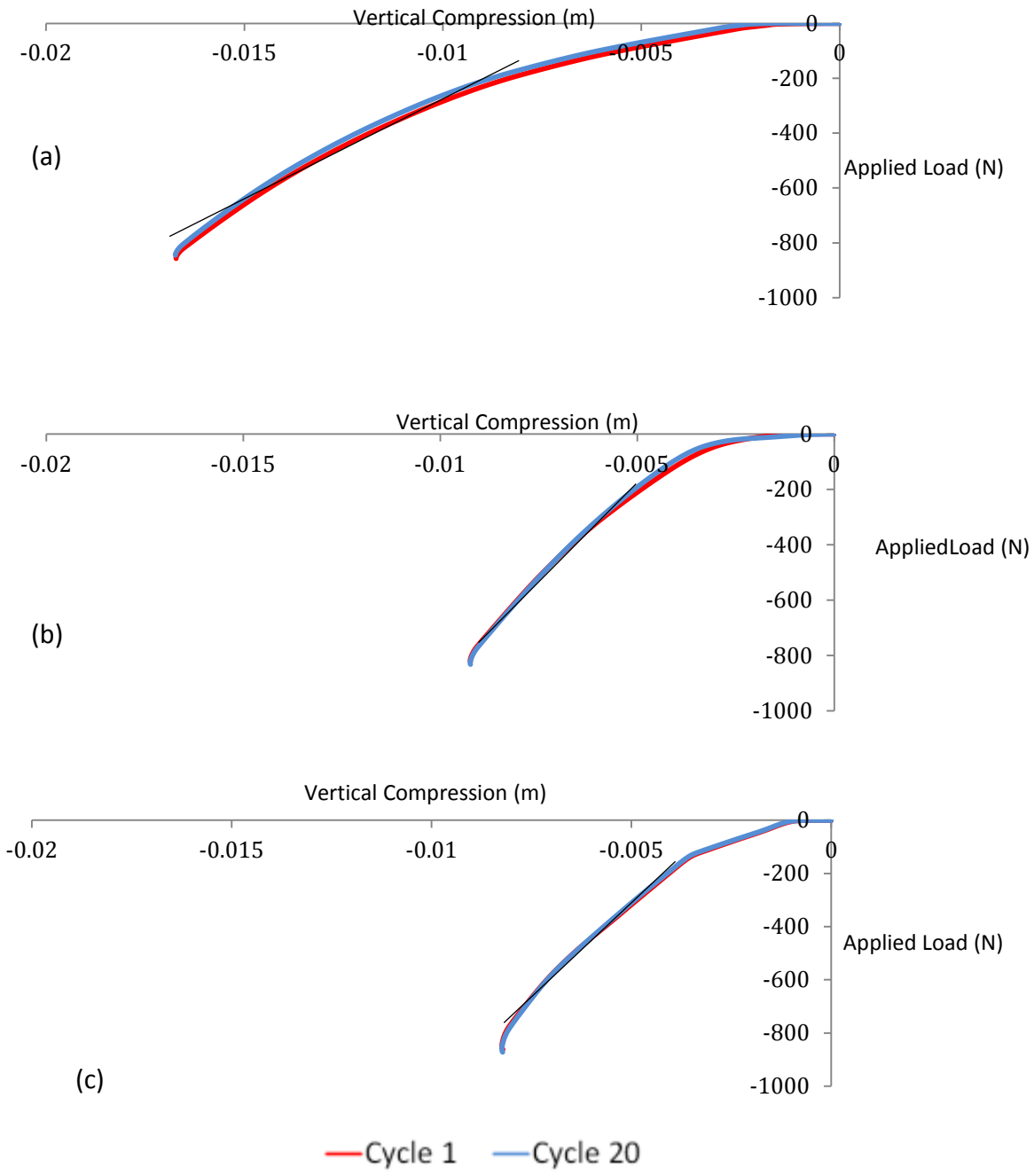

Figure 7.2.2. . The compression information for each state of the Blatchford prosthetic; shod (a), barefoot (b) and blade(c) for the 1st and 20th cycles of 20 cycles. Stiffness was calculated from the slope of a straight line fitted to the loading data between 200N and 800N.

7.3 CONCEPTUAL DESIGN

7.3.1 Design Specification

The development of a new end-effector is an evolutionary process where each design and subsequent iteration aims to be an improvement on the previous. In this instance the success of each end-effector will be determined by the following parameters:

- Ground contact time
- Ground reaction force profile shape
- Ground contact area or 'footprint'

The following paragraph summarises the requirements used to define a Product Design Specification (PDS) (Pugh 1991) that has been carried out with specific directive triggers for an end-effector design. A full version of the PDS can be found in appendix 1.

The purpose of the design is to enable the emulation of the human during the foot-ground contact phase for walking. As such it is expected to be able to withstand the associated loadings; multiple repetitions of 850 N (±50 N) at a rate of 200 kN/s. The end-effector needs to be attached to the faceplate of the robot through a circular plate (diameter 160mm), using two eight 10mm bolts. It also has to be a sensible weight and small enough to fit within the desirable work envelope, identified in Chapter 6.

7.3.2 Design Concepts

Part of the design process was to come up with a number of conceptual design ideas that could be evaluated and the best taken forward as the final design solution, the concept designs generated for the end-effector are presented in figure 7.3.1. One of the main issues with the original system was the length of ground contact and the fact that the robot was having to drive the end-effector through the contact, requiring large amounts of work and robot movement. The fastest joint of the robot is joint 6 (section 4.2), it has been hypothesised that ground contact times could be reduced by making joint 6 one of the prime movers during the footstrike. This opens up the possibility to generate the force

profiles through rotation about a fixed point. The principle of using a linear bearing and a slide is to reduce the dependence on the robot to generate the high loading rates observed in human gait potentially allowing the force peaks to be achieved quicker.

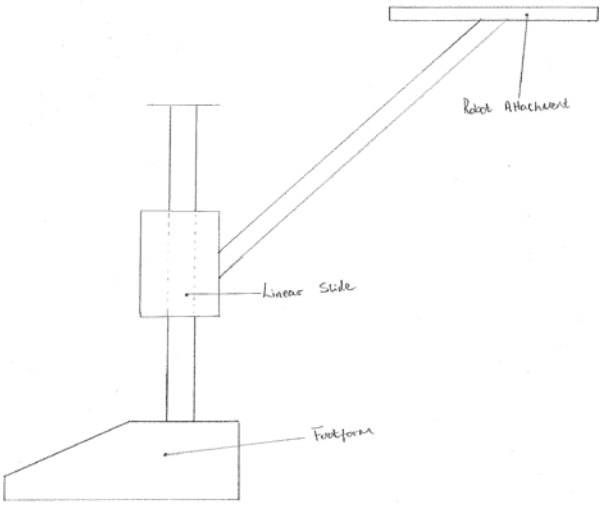

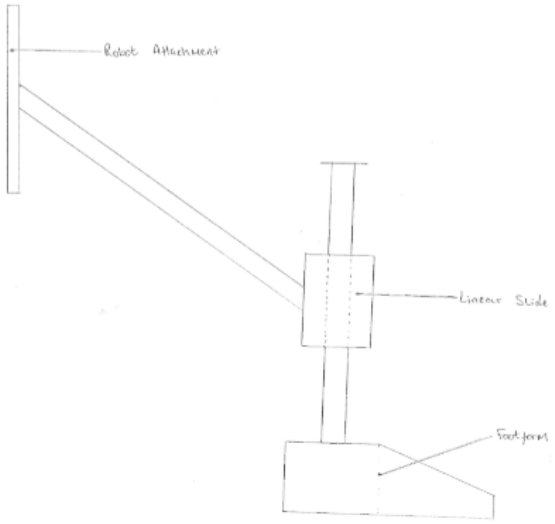

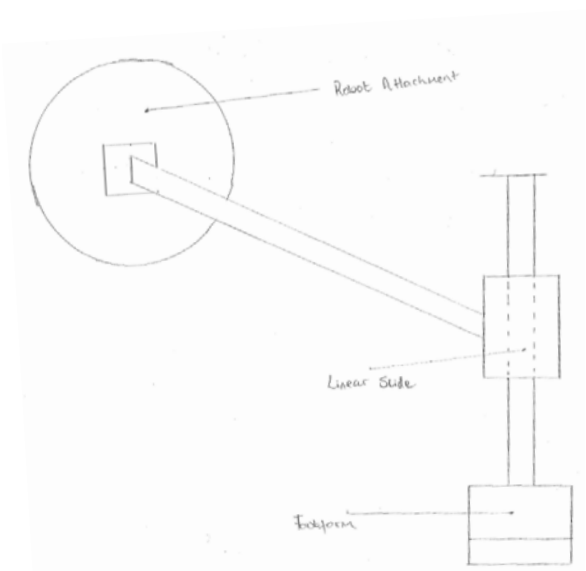

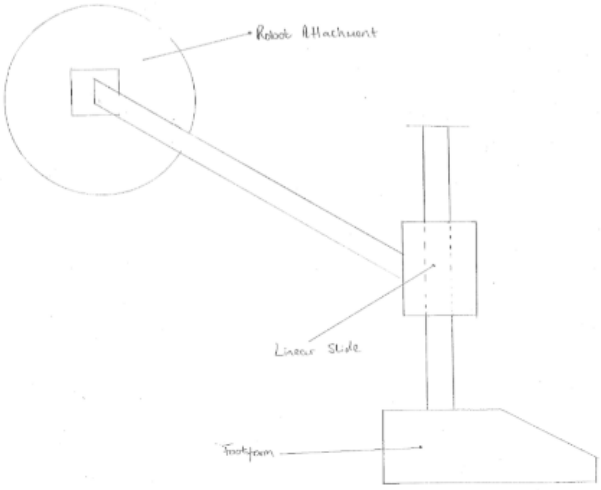

Continued.

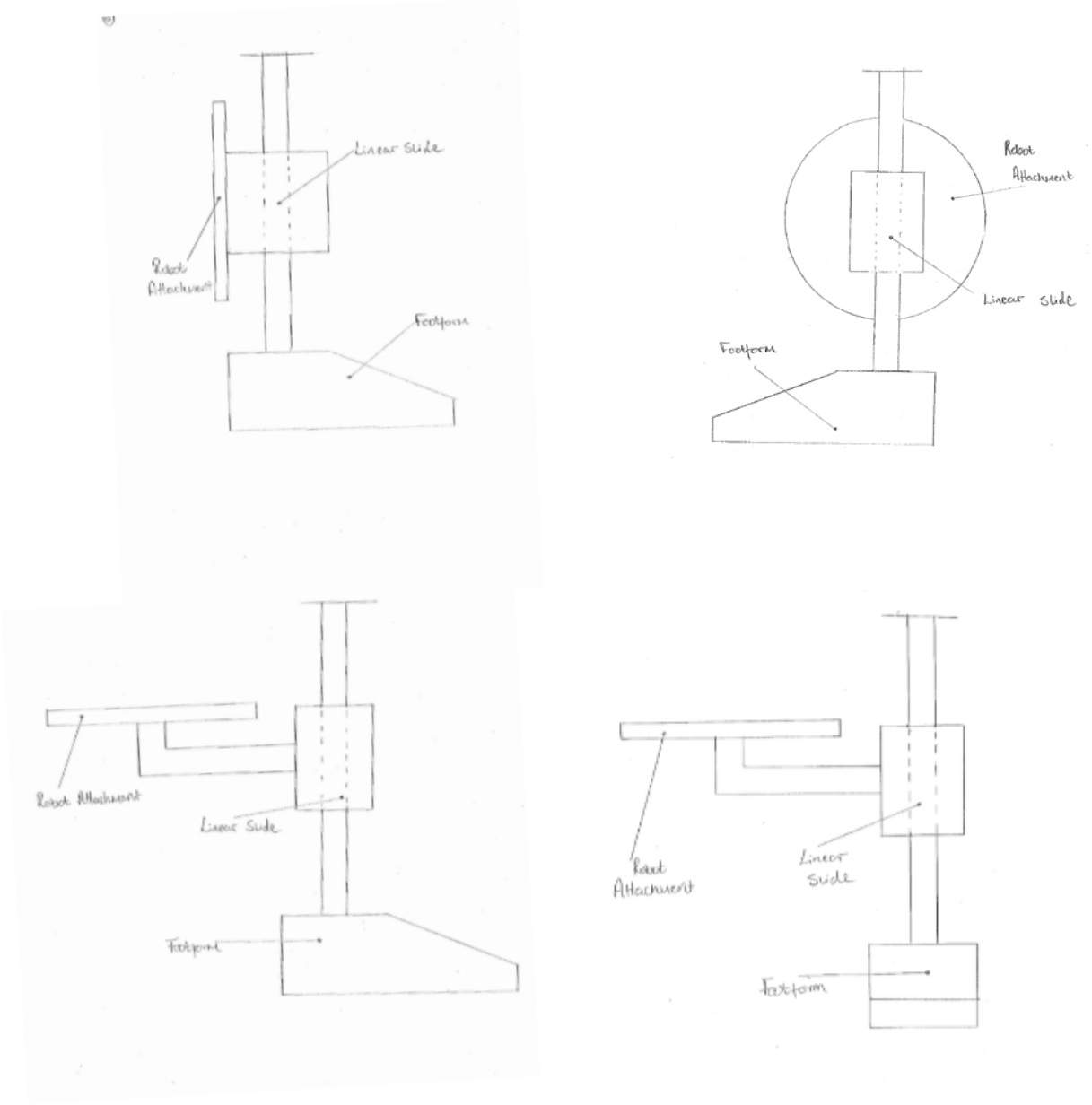

Figure 7.3.1 – A selection of potential design concepts, based on using the principle of a linear bearing and a slide. Each design is made up of a robot attachment, the linear slide and a footform.

After consideration of the conceptual designs, two concepts were chosen (figure 7.3.2) for prototype manufacture and were then tested similarly to the original end-effector (documented in sections 7.3.3 & 7.3.4). Both designs consist of a linear slide bearing which restricts the movement of a hardened steel keyed bar to one dimension. Initially both prototypes were mounted with a high density foam footform (UK size 9) which can be threaded onto the keyed bar, this footform was deemed best at this stage of the process as it incorporates a much greater level of compliance compared to the original end-effector. This allows for a greater margin for error in the process of exploring the performance of each design iteration. As the foot moves away from the ground contact, the linear bearing will slide up the bar, adding rotation to the compliant footform, eventually lifting the foot off the ground from a toe-off position.

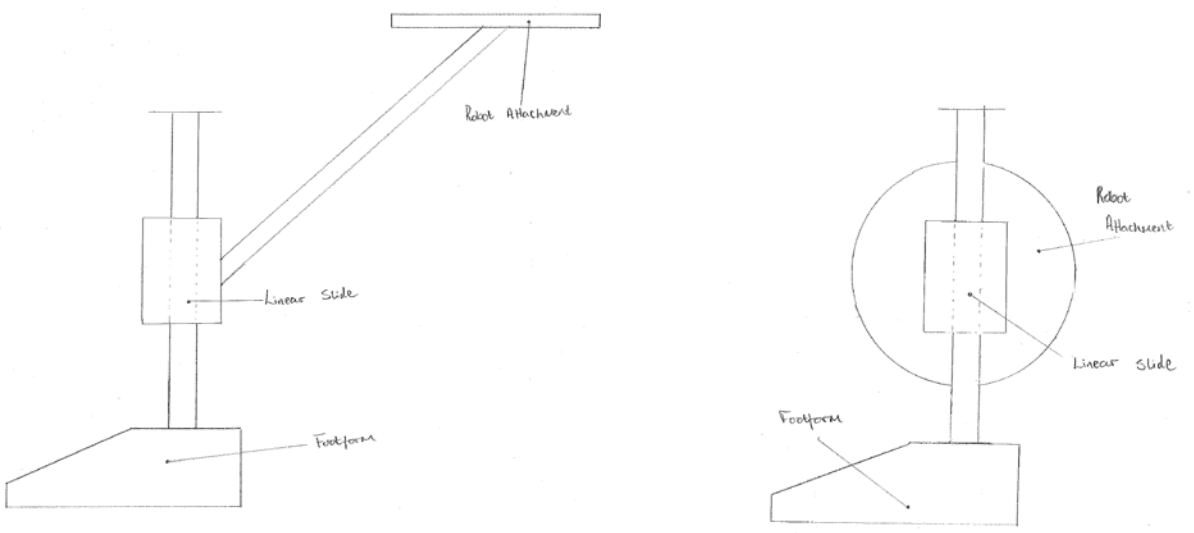

Figure 7.3.2 – The two design concepts that were chosen to be taken forward to prototype phase.

Each of these designs were tested to investigate **(1)** how they influenced the requirements on each robot joint to complete the footstrike emulation; and **(2)** the ground contact time and vertical force profiles for the footstrike emulation.

7.3.3 Design Concept One

The prototype for design concept one (figure 7.3.3) is made up of a steel bar (280mm in length) protruding anteriorly and inferiorly from the centre of the mounting plate at an angle of 55 degrees; the other end attaches to a linear slide bearing (50mm x 90mm x 60mm). The footform is situated anteriorly and inferiorly from the mounting plate which is parallel to the plantar aspect.

Figure 7.3.3 – The prototype of design concept one (6.2 kgs).

As with the original end-effector, the plantar aspect of the footform is parallel to the faceplate of the sixth joint of the robot and as such when subjected to the robot tests, the robot movement is similar to that of the original end-effector. The heel of the footform was programmed with human kinematic data (Chapter 3), and was offset to create a ground contact on the force platform.

Visual analysis of the movement shows that the majority of the joints are in use with the robot seeming to move 'up and over' the end-effector (figure 7.3.4). This is reflected in the ground contact time of 1-1.3 seconds which is similar to that of the original end-effector Ronkainen *et al* 2010 – section 2.4.1.

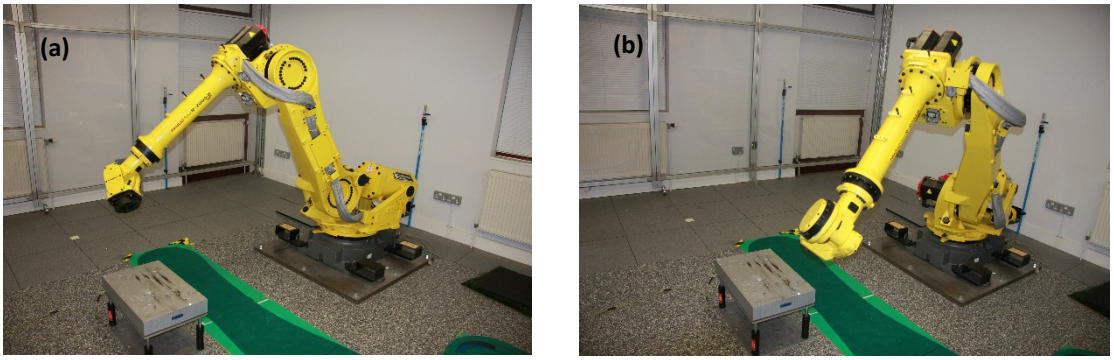

Figure 7.3.4 – A visual analysis of the robots movements for design concept one, for **(a)** ground contact and **(b)** toeoff.

One of the main innovations of this end effector is compliance, however, control over the compliance proved difficult, this is reflected in the vertical ground reaction forces (figure 7.3.5), which have numerous peaks at low magnitudes (~100-250N). The linear bearing appears to be damping the system resulting in the low force magnitudes and 'bouncing' the footform resulting in numerous force peaks. The similar contact time coupled with the multiple force peaks at low magnitudes indicates that this design isn't a great improvement on the original end-effector.

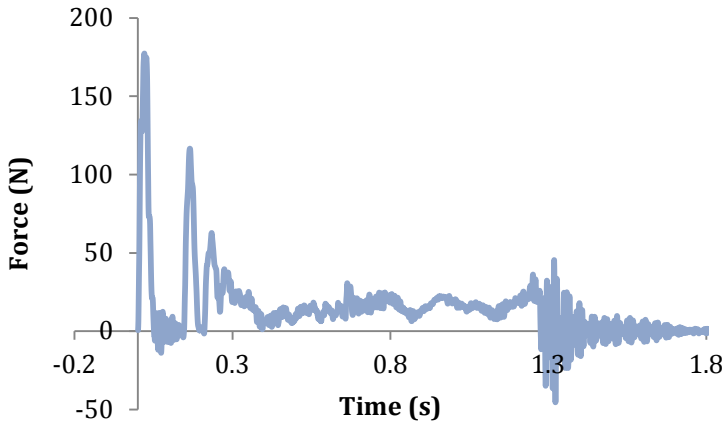

Figure 7.3.5 - The vertical ground reaction forces for a robot footstrike with design concept one.

7.3.4 Design Concept Two

The second design concept (figure 7.3.6) has the linear slide bearing directly attached to the mounting plate, which is orientated perpendicular to and much closer to the plantar aspect of footform, it is thought that this will reduce the movement requirement on some of the more proximal (and slower) joints of the robot table 4.2.1.

Figure 7.3.6 – The prototype of design concept two.

As before the heel of the footform was programmed to move through ground contact with the human kinematic data collected in Chapter 3. The way in which the end-effector is mounted to the robot results in a completely different movement to that of any previous end-effector (figure 7.3.7). The robot as a whole has to move less in order to direct the footform through the same trajectory. Rotation about the linear bearing helps to facilitate this. The majority of the motion is facilitated by the 6^{th} joint of the robot (one of the fastest joints), helping to increase the motion speed.

Figure 7.3.7– A visual analysis of the robots movements for design concept two, for **(a)** ground contact and **(b)** toeoff.

One noticeable effect is a significant reduction in ground contact time 1.2s to 0.6s. As before the vertical ground reaction forces (figure 7.3.8) have a number of peaks at low magnitudes, this can be attributed to there still being no compliance control there is still a clear need for damping

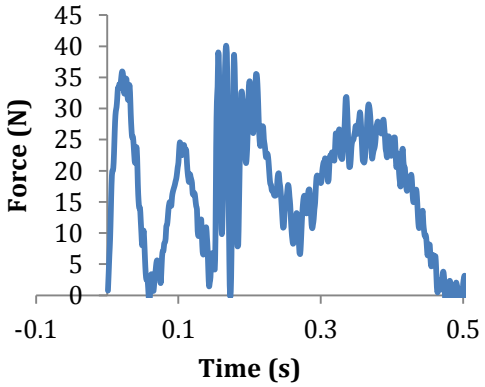

Figure 7.3.8 - The vertical ground reaction forces for a robot footstrike with design concept two.

7.4 DESIGN SELECTION

Following analysis of each of the selected design concepts, it was decided that design concept 2 would be taken forward, with a number of slight alterations intended to improve it further. Results from the characterisation of the original end-effector (section 7.2.3) indicate that the Blatchford prosthetic is an adequate footform representation for the new end-effector, despite the Blatchford heel spring being stiffer than the human heel pad.

7.4.1 Design Alteration

The design allows for a biofidelic component, comprised of a number of foam discs, to be positioned on either side of the linear slide. This adds resistance to the movement of the footform (in both directions) as opposed to it moving freely along the bar. The entire system is subjected to a pre-load by using an aluminium tube and washer combination. Although there is still compliance in the design the intention is to reduce the total number of force peaks, created by the foot 'bouncing' on the force plate the reaction between the footform and the ground is allowed to play more of a role in vertical ground reaction force generation. The resistance provided by this area is intended to represent the lower leg of a human (during the walking gait) and thus needs to have a stiffness value of 10-30 kN/m, and be able to attain vertical ground reaction forces of 850 N (±50 N) over a period of 0.1 seconds (the initial loading phase). The material properties of a variety of different foam discs was investigated with the intention of identifying the optimum material and thickness required.

A variety of foam samples (low density polyethylene, high density polyethylene, high rigidity polyethylene & ethylene vinyl acetate copolymer) were selected for initial consideration through a series of mechanical tests. Using the Instron ElectroPuls E3000 (Instron Systems; Norwood, MA), fitted with a 5KN load cell and two flat plates (130mm & 150mm diameter respectively) (figure 7.4.1) each sample, with differing stack heights, were compressed with varying levels of displacement in an attempt to provide a result that fell within the target stiffness range of 25.± 4kN/m, shown by Arampatzis *et al*. (1999). Each sample was subjected to repetition testing (20 cycles), intended to replicate the effect of repeated

footstrikes. Compression to the determined displacement was achieved in 0.1 seconds, totally unloaded in 0.3 seconds with a rest period of 0.8 seconds giving a total cycle time of 1.2 seconds which is similar to the gait cycle time for walking. The stiffness of each sample (with corresponding disc number) was recorded by dividing the total displacement by the maximum force attained. An individual sample was then selected for further prolonged testing to the same protocol in increments of up to 1,000 cycles.

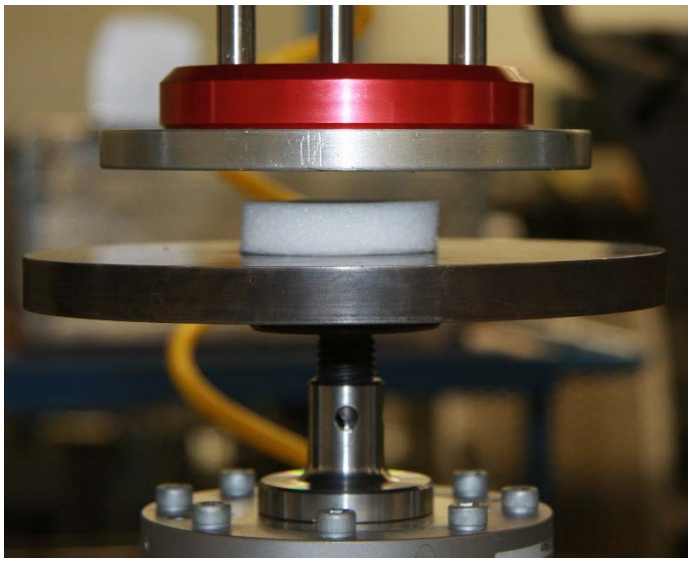

Figure 7.4.1 – An example of a foam sample on the Instron ElectroPuls, prior to mechanical testing.

Table 7.4.1. The compression and stiffness data for the adequate foam samples that achieved stiffness values in the range 10-30 kN/m.

Sample Name	Number of pads	Displacement (mm)	Force range (N)	Stiffness, k (KN/m)
High Density Polyethylene 60	8	50	650 - 800	13 - 16
	7	45	620 - 940	13 - 20
Low Density Polyethylene 45 (10mm)	4	34	840 - 850	24 - 25
	5	44	805 - 840	18 - 19
	6	50	740 - 860	14 - 17
		52	820 - 915	15 - 17
Low Density Polyethylene 45 (6mm)	9	49	800 - 845	16 - 17
	8	40	845 - 880	21 - 22
	7	33	800 - 820	24 - 24
Low Density Polyethylene 33	6	52	750 - 820	14 - 15
		53	750 - 920	14 - 17
	5	42	760 - 840	18 - 20
High Rigidity Polyethylene 80	3	25	791 - 920	31 - 36
	4	30	865 - 960	28 - 32
		27	641 - 690	23 - 25
		29	790 - 880	27 - 30
	5	38	730 - 830	19 - 21
		39	760 - 880	19 - 22
Ethylene Vinyl Acetate Copolymer 50	7	50	790 - 860	15 - 17
	6	40	700	17
		42.5	900 - 920	21 - 21
	5	35	850 - 865	24 24
Ethylene Vinyl Acetate Copolymer 30	9	55	825 - 935	15 - 17
	8	47	850 - 910	18 - 19

Table 7.4.1 shows the foam samples that fall within the target stiffness, for a given load. There are a number of samples that fit within the desired range, but it was decided that the best approximation to a human was the 10mm thick low density polyethylene 45 foam with 4 discs. The stiffness of 25kN/m at an applied load of 840-850N is a good representation of the results shown by Arampatzis. et al. (1999). This sample combination was tested to a longer period of cyclical loading (1000 repetitions) for further assessment.

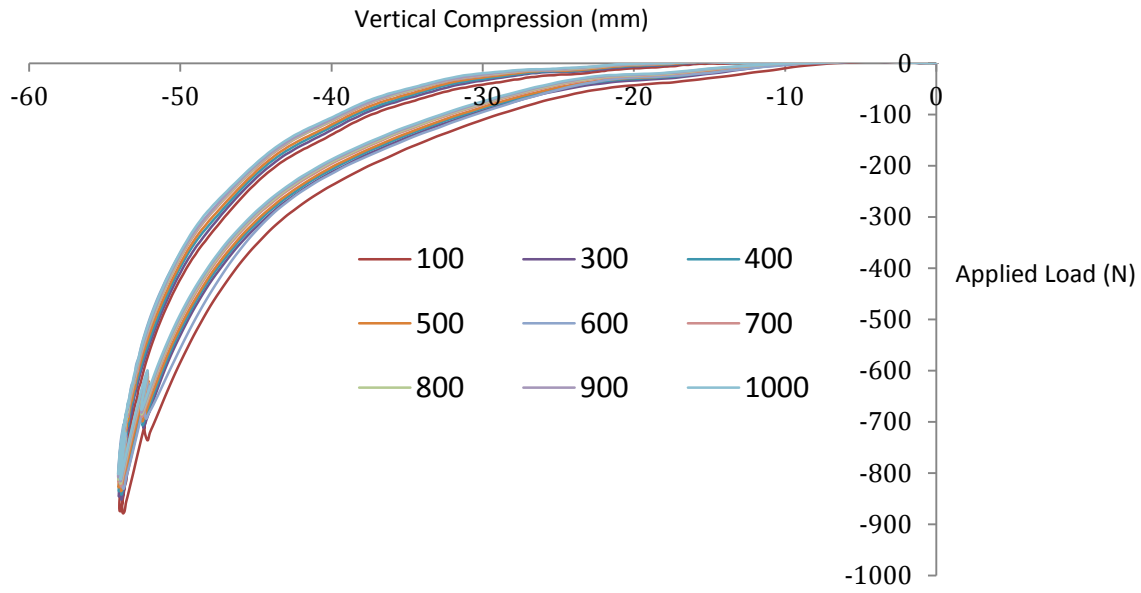

Figure 7.4.2. A chart showing applied load against compression distances for the selected foam sample, at interval's of 100 cycles for a total of 1000 cycles.

Figure 7.4.2 demonstrates that the properties of the selected foam sample don't change markedly over the repeated loading. There is a slight drift as the number of cycles increases, but providing regular maintenance and replacement, this shouldn't be an issue. These results provide the conclusion that the 10mm thick low density polyethylene 45 foam with 4 discs either side of the linear bearing can be used in cyclical testing with high levels of repetition, in making up the biofidelic component of the end-effector.

The above information has contributed towards the creation of a final design solution (Figures 7.4.3 & 7.4.4).

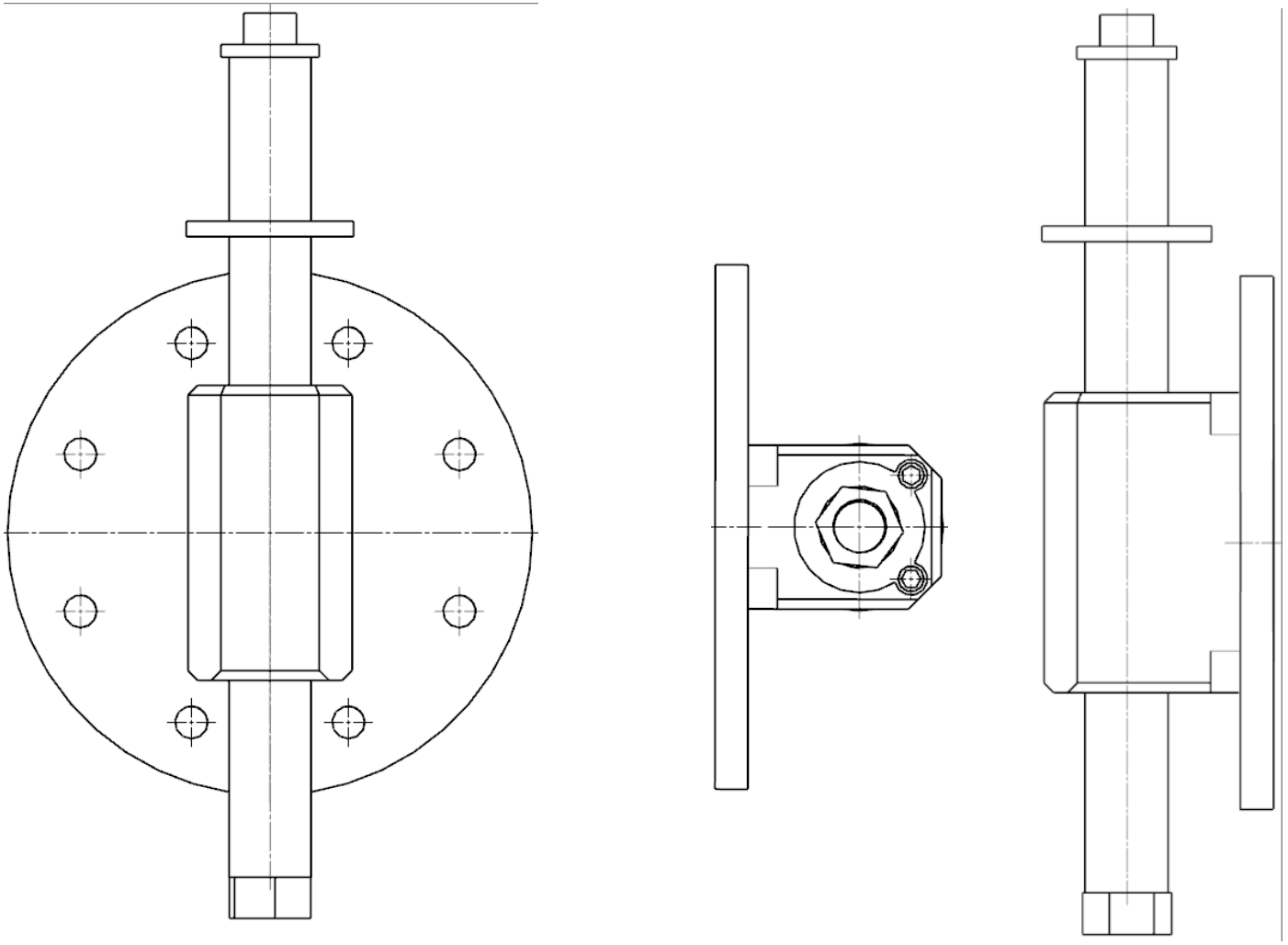

Figure 7.4.3 – Technical drawings of the final design selection, consisting of robot attachment and linear slide bearing.

Figure 7.4.4 – The final design solution. Consisting of biofidelic sections (with applied pre-load), robot attachment and linear bearing.

7.4.2 Design Validation

As a validation for the design selection and alterations it was subjected to the same robotic test protocol as each of the concepts (section 7.2.), as the mounting orientation is the same – the overall robot movement is unchanged from the second design concept.

The vertical ground reaction forces have fewer peaks and has a more desirable shape and size to that of the human profile (figure 7.4.5).

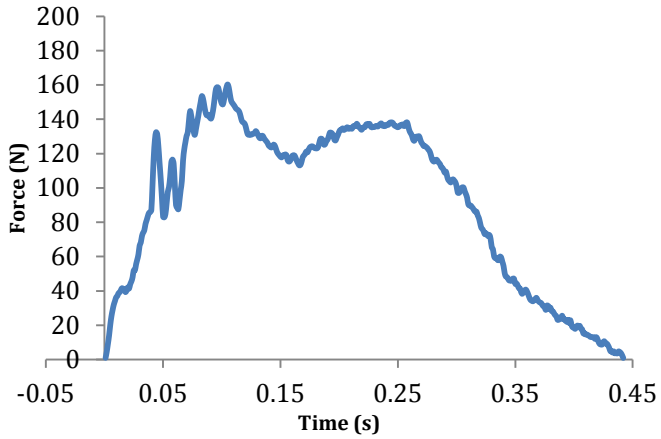

Figure 7.4.5 - The vertical ground reaction forces for a robot footstrike with the final design solution.

Table 7.4.2 provides a comparison matrix of the different end-effector designs investigated in this chapter, each marked against a number of factors to consider in the design that were introduced in section 7.1.

Table 7.4.2 – A comparison of all of the end-effectors against the design directive triggers.

+ = Improvement ***0 = No Change*** ***- = Worse***	***Original End-effector***	**Design Concept One**	**Design Concept Two**	**Final Selection**
Ground contact time	0	0	+	+
Overall robot movement	0	0	+	+
Compliance	0	+	+	+
Peak vertical ground reaction force	0	-	-	0
Number of vertical ground reaction force peaks	0	-	-	0
Biofidelity	0	+	+	+
Novel application of GRF	0	+	+	+
Total Improvements	**0**	**3**	**5**	**5**

Analysis of each subsequent design iteration has shown improvements against the previous at each stage. The final design selection has shown significant improvement against all other options.

7.5 CONCLUSIONS

This chapter has addressed the aim of developing and testing a new end-effector design intended to improve the emulation of the human gait using the robot and is specifically focused on addressing research question three of this thesis. The need for change was reinforced after evaluating the original end-effector and the footstrikes that it was able to produce. Despite it being able to generate adequate vertical ground reaction force magnitudes, there was insufficient loading rate and ground contact time emulation. Having visually analysed the robot movement, it was clear that the limitation of the original end-effector included the footform being driven through ground contact by the robot, and the robot having to move up and over the area of ground contact involving contribution from multiple joints including the slower proximal joints.

A number of design concepts were generated, from which two prototypes were made. Each design iteration was benchmarked against the previous in a number of areas. A selection was made and a number of alterations made to improve it further. The final design solution (figure 7.4.2) is biofidelic both in terms of the footform and built in compliance. It has also introduced a new way of generating the required motion. This end-effector is to be used in subsequent human gait emulation tests on the robot (Chapter 9), with the intention of improving upon the performance of the original end-effector.

CHAPTER 8

ROBOT CELL DESIGN AND OPTIMAL FORCE PLATFORM LOCATION

8.1 INTRODUCTION

To emulate the foot-ground interaction, a number of parameters were identified in Chapter 3 as being most relevant to a successful emulation, one of which was the ground contact time. A typical human running ground contact is ~0.2 seconds *(Hunt et al 2001)*. Previous attempts to emulate the running footstrike have had a number of issues in achieving this ground contact time, for example, Ronkainen *et al* 2008 could only achieve 1.2 seconds on the same robot as used in this study.

As shown in Chapter 7, altering the design of the end-effector, can give shorter ground contact times, down to 0.6 seconds. However, this is still 2-3 times longer than the typical human running footstrike.

The location of ground contact within the robot cell influences the spatial operation of the robot which, similarly to the redesigned end-effector in Chapter 7, may also influence the ground contact time. There may be options to reduce the ground contact time further by optimising the ground contact location within the cell, i.e. moving the force platform relative to the robot. When the robot cell was originally set up, the force platform was fitted to a raised platform and positioned in the middle of the cell directly in front of the robot. The purpose of this was to allow easy

observations of the end-effector movement and no consideration was given to how this position may influence the performance of the footstrike emulation. Therefore, an optimisation of this position may further improve the ground contact time and hence the footstrike emulation. Physical optimisation achieved by moving the force plate and programming the robot for each new position is likely to be a time consuming task, compared to virtual optimisation using the computer software RoboGuide. Relocating the force plate and altering the programmes within the virtual environment can be achieved quickly and easily.

In Chapter 6 it was shown that although RoboGuide lacks accuracy in simulation it does demonstrate the same kinematic trends as the physical robot. Therefore, a reduction in footstrike contact time in RoboGuide can be expected to translate into a reduction in the physical robot contact time, although the magnitudes of change may differ. Therefore, RoboGuide is a useful tool to investigate the optimal force plate location before making any changes to the physical location.

8.1.1 Aims

- To determine whether or not relocating the force plate within the robot cell, and therefore changing the spatial operation of the robot, has the potential to reduce the ground contact time and, thus, improve the emulation performance of the robot.

8.1.2 Objectives

The above aims will be achieved through the following objectives:

- To simulate the footstrike in RoboGuide for a range of force plate locations to establish where the contact time is closest to the human footstrike, for each end-effector.
- To validate the results by repeating the process for a select few of these trials on the physical robot.
- To relocate the force platform, if beneficial, for use in subsequent investigations.

8.2 METHODOLOGY

The methods are split into two stages: optimisation using RoboGuide and validation of the results on the real world robot.

Stage 1 – RoboGuide – optimisation of force plate location

The computer software RoboGuide, as introduced in Chapter 6, was used to simulate the human footstrike in a virtual environment and NX5 [unigraphics] (Siemens PLM Software; CA, USA) was used to recreate the physical robot cell within the virtual RoboGuide environment. CAD models of the Force Plate (Kistler, Switzerland; 9281CA), original end-effector and linear bearing end-effector (Chapter 7) were created and imported into RoboGuide (Figure 8.2.1). The end-effector model does not contain all of its physical counterpart, however, all of the dimensions, alignments and key features are accurate.

Shod human running footstrike data, collected in Chapter 3, was programmed into RoboGuide. The heel of the end-effector CAD model was used as the Tool Centre Point (TCP), i.e. the centre point of rotation for all of the robots movements. The programme was made up with fourteen co-ordinate points (each programmed with maximum smoothing – CNT100). The ground contact phase was made up of ten evenly time spaced co-ordinate points and there were two points located on either point of the contact phase, intended to bring the footform into and away from the ground contact phase. The velocities were those of the human data, except in instances where the velocity exceeded 2000mm/s (the maximum programmable velocity of the robot), in which case 2000mm/s was used.

The first part of the investigation centred around trials using the original end-effector (the original end-effector used in Chapter 7). The initial footstrike occurred with the force platform in its original position within the robot cell. Using the timer feature embedded within RoboGuide the time taken for the entire programme to complete its entire movement (run time) was documented; an average and standard deviation of five repetitions was obtained following four subsequent repeats in the same location.

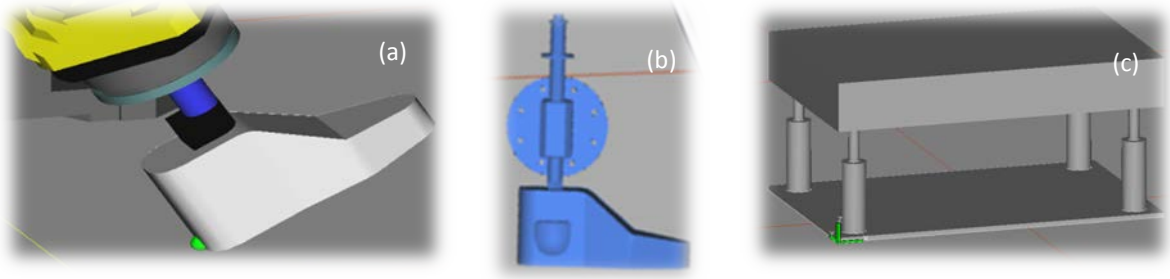

Figure 8.2.1: (a) The imported CAD model of the shod original end-effector; **(b)** The imported CAD model of the shod linear bearing end-effector and **(c)** The imported CAD model of the Kistler Force platform.

After finding the time for the original position, the effect of relocating the force platform within the cell was investigated. A grid of potential locations was identified covering an area of 1.5m x 1.5m x 1m (covering a viable work envelope in front of the rigidly fixed robot), there were 49 potential locations for each of the three height levels (figure 8.2.2). The platform and footstrike location were re-positioned and tested for each of the different locations, five run times were recorded for each location, to obtain a mean and standard deviation. The mean run time for each position was added to a colour coded map of the space, thus giving a visual representation of whether or not there was an improvement in total programme run time against that of the original location.

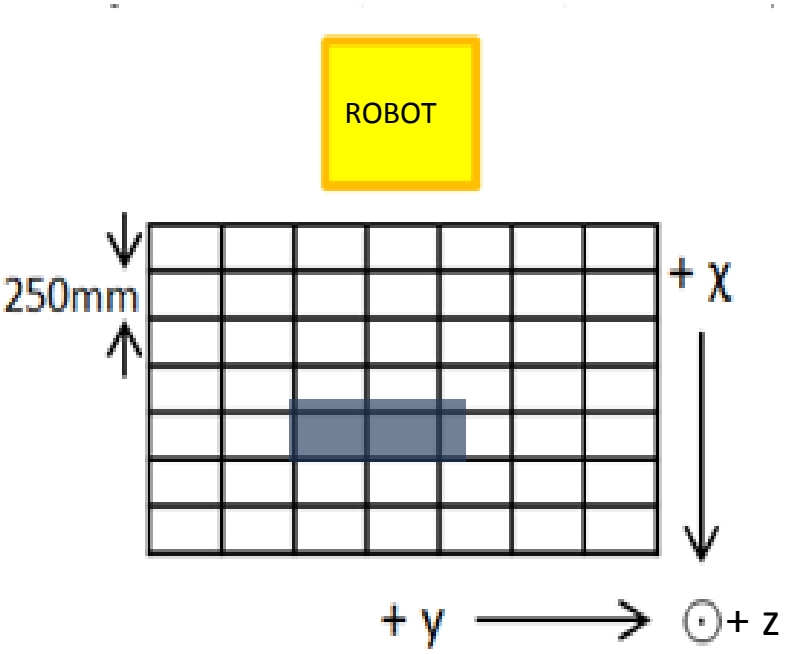

Figure 8.2.2: A schematic showing the layout of the potential force platform locations. The hatched area shows the original location of the force platform. In addition to the 49 locations illustrated, this was repeated at two further z values (+500mm and +1000mm from the original). The 147 (7 x 7 x3) potential new locations cover a volume of 1.5m x 1.5m x 1m.

Once the best and worst locations (based on motion time) had been determined, further analysis into each was carried out. Using a built in tool within RoboGuide and with the aid of digitising using Image Pro Plus (Bethesda, UK), joint angles for each of the 6 robot joints were calculated. These were then graphically plotted against each other, identifying potential optimal robot joint angles.

Following the trials with the original end-effector, the whole process was repeated with the linear bearing end-effector (Chapter 7).

Stage 2 – Real world validation of RoboGuide Optimisation

Once the results for virtual optimisation for each end-effector had been obtained, the fastest and slowest location for each end-effector at each height were selected for emulating on the physical robot. These emulations served as a validation for the virtual optimisation programme. Identical programming parameters were inputted into the robot for each of these locations. The robot movement was recorded using a high-speed video

camera (Photron FastCam, SA 1.1, 1000Hz; - Bucks, UK) recording at 1000Hz (shutter speed – 0.001/sec), from which an overall movement time for the programme was identified. These were then compared to the corresponding RoboGuide values to validate the optimal position obtained in RoboGuide prior to any force platform repositioning. The original force platform location was also tested, however, to avoid inconsistencies with the other locations, the force platform was removed.

Other than alerting the user to contact, RoboGuide is unable to simulate an interaction with a surface, therefore the validation on the physical robot was performed without relocating the physical force platform to each location, i.e. using mid-air running.

8.3 RESULTS

Stage 1 – RoboGuide – optimisation of force plate location

Figure 8.3.1 shows the total RoboGuide run time in seconds for the human footstrike motion using the original end-effector and various force platform locations.

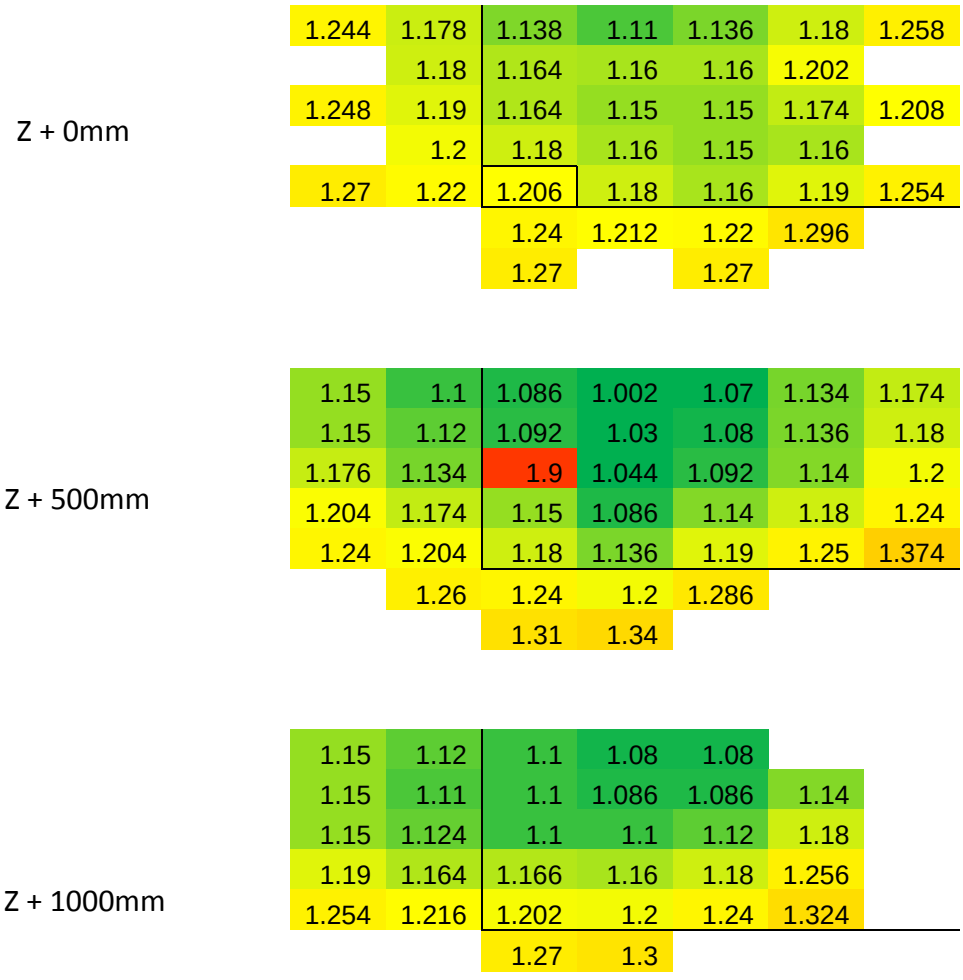

Figure 8.3.1: Map of the run times (seconds) for the different force platform locations and the original end-effector. Green on the scale represents an improvement on the original location and red is slower. The solid rectangle at z + 0mm represents the original force platform location. Not all of the potential locations are covered

The percentage time difference between the original location and each of the other locations investigated, with the original end-effector, is shown in figure 8.3.2.

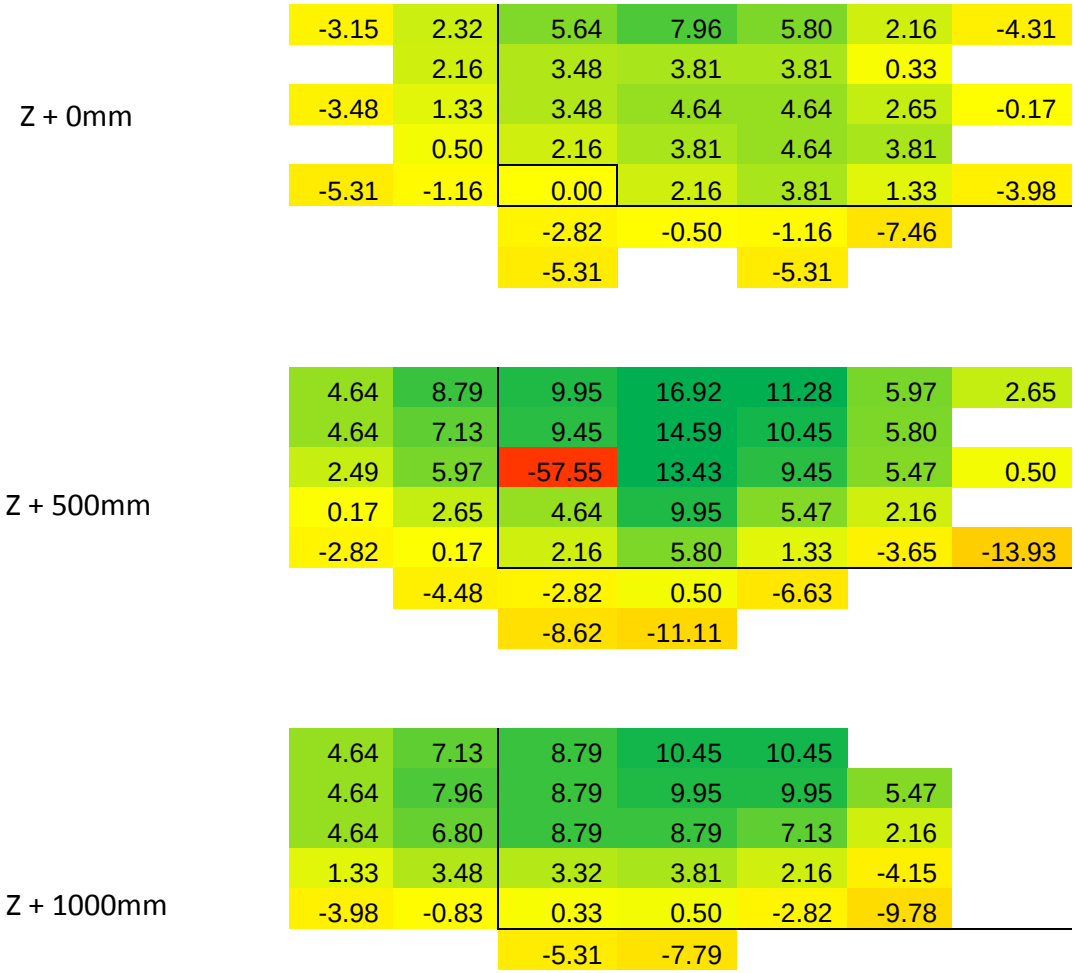

Figure 8.3.2: Map showing the percentage changes in run time for the different force platform locations against the original end-effector, a negative percentage means a slower time and a positive percentage represents a faster time. Green on the scale represents an improvement on the original location and red is slower.

Figure 8.3.3 shows the RoboGuide run cycle time in seconds for the human motion footstrike using the linear bearing end-effector, and various force platform locations.

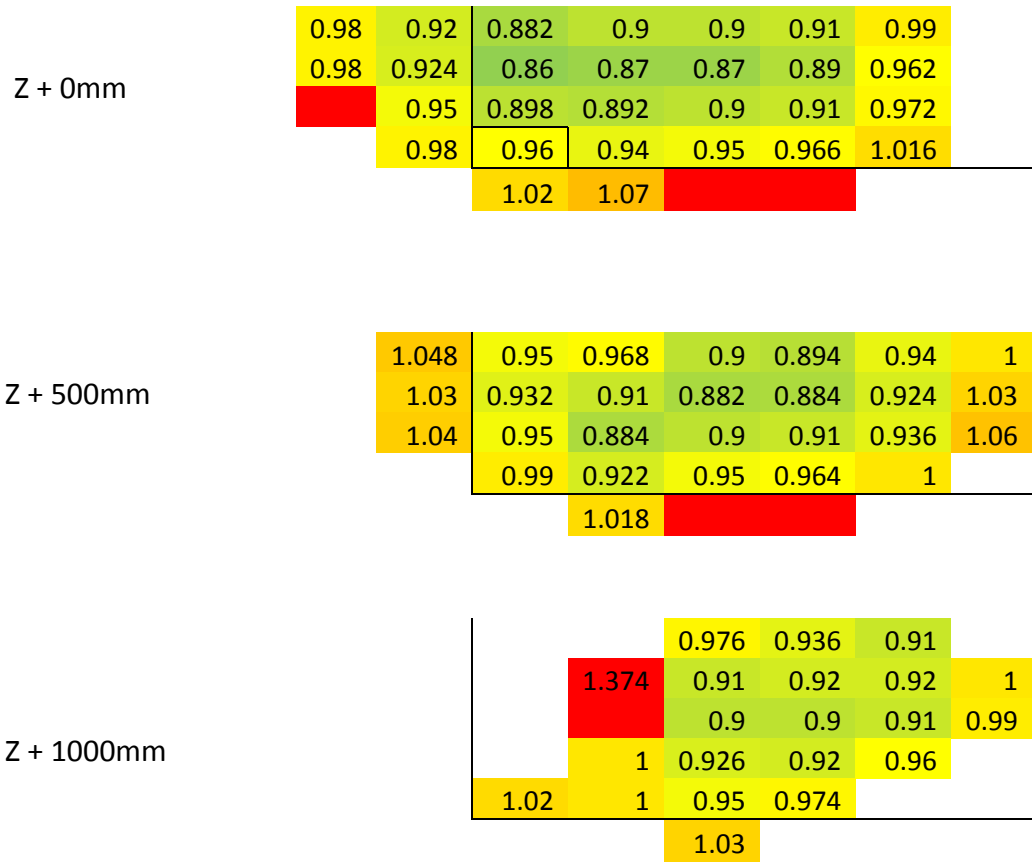

Figure 8.3.3: Map of the run times (seconds) for the different force platform locations and the linear bearing end-effector. Green on the scale represents an improvement on the original location and red is slower.

The percentage time difference for the emulated motions, with the linear bearing end-effector, at the various potential force platform locations are shown in figure 8.3.4. As before the map is colour coordinated, in the same way as the times.

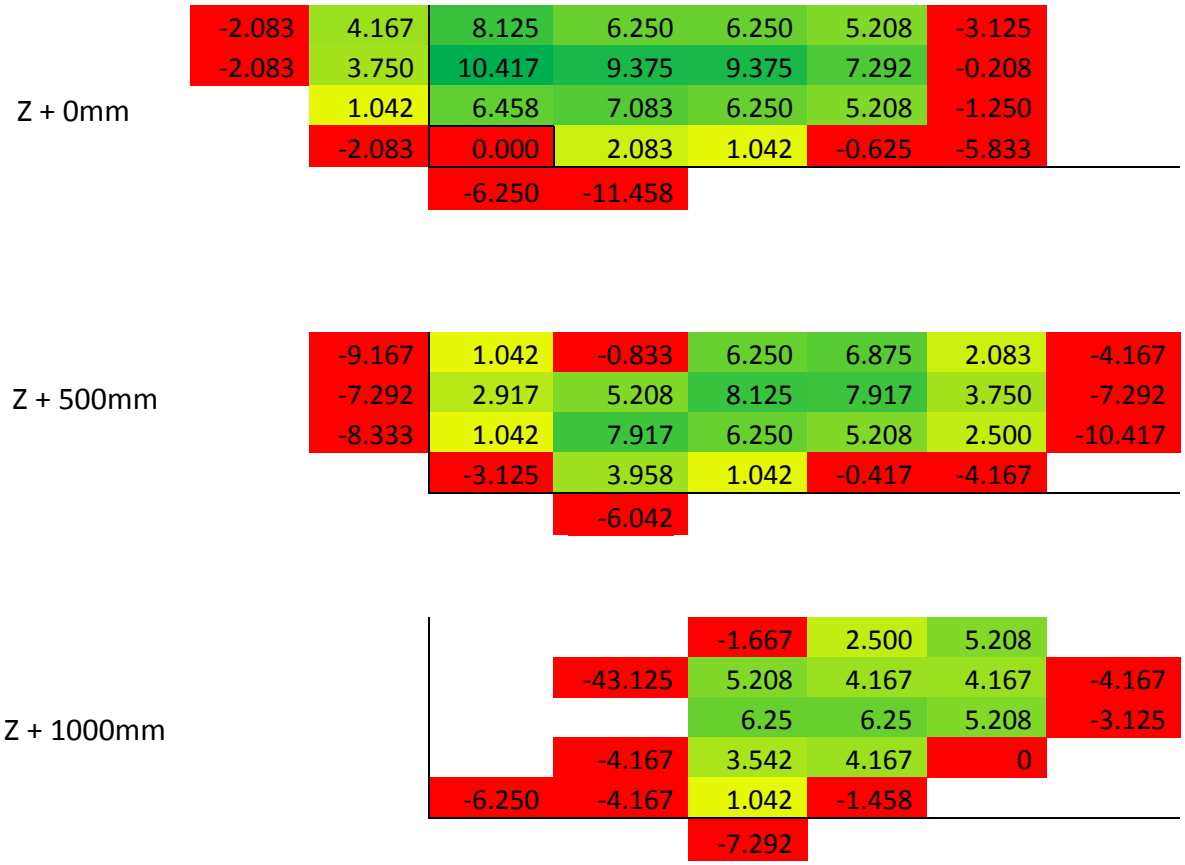

Figure 8.3.4: Map showing the percentage changes in run time for the different force platform locations with the linear bearing end-effector, a negative percentage means a slower time and a positive percentage represents a faster time. Green on the scale represents an improvement on the original location and red is slower.

After investigating the potential positions for the force platform it was decided to investigate the robot joint angles (table 8.3.1) for original, best and worst force plate locations, for each of the robot joints highlighted in figure 8.3.5. This helped to understand joint positions that helped or hindered performance. The results would indicate that there is no individual robot joint that has a role in making the location optimal. It is more likely that how the joints work in relation to each other and throughout the entire movement will have an influence on the outcome.

Table 8.3.1 The angles in degrees of each robot joint relative to its neutral position for original, best and worst location for each end-effector. The position of each joint is shown in figure 8.3.5. The values shown are for those where the footform is in mid-stance.

	Original			**Linear Bearing**		
	Original (0,0,0)	Best (-1182, 0, 500)	Worst (-500, -1000, 500)	Original (0,0,0)	Best (-500, 0, 0)	Worst (-750 250, 1000)
Joint 1	178.09	172.87	142.20	176.18	173.34	188
Joint 2	33.32	-50.19	14.93	29.98	12.32	-41.09
Joint 3	86.34	121.03	102.64	68.11	56.74	127.74
Joint 4	0	0	0	0	0	-54.15
Joint 5	-44.40	-77.38	-63.81	61.52	72.34	12.59
Joint 6	5.24	7.65	37.87	-15.17	-15.49	38.90

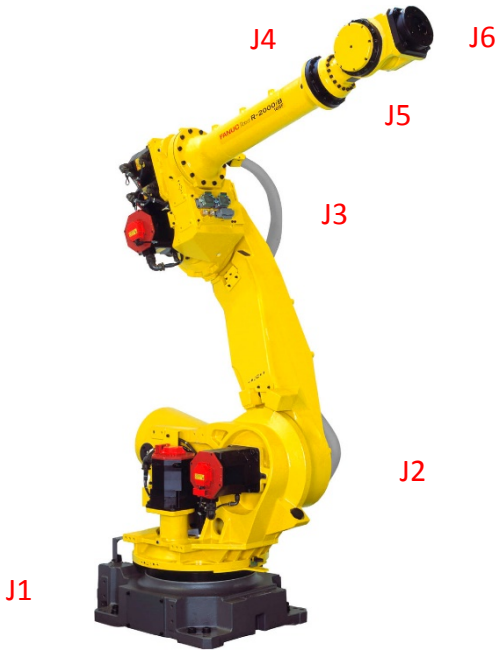

Figure 8.3.5: The location of each joint (1-6) on the FANUC robot. Joint 1 is the most proximal and joint 6 is the most distal.

Stage 2 – Real world validation of RoboGuide Optimisation

The next stage was to conduct a real world physical validation of the RoboGuide optimisation results. The cycle times for the test locations validated on the real world robot using the original end-effector, are given in figure 8.3.6. As expected, although different, the trends are similar for the actual times. The quickest location on RoboGuide is also the quickest on the physical robot and represents a 24% improvement on the original force plate location (better than the 17% improvement observed for this location in RoboGuide).

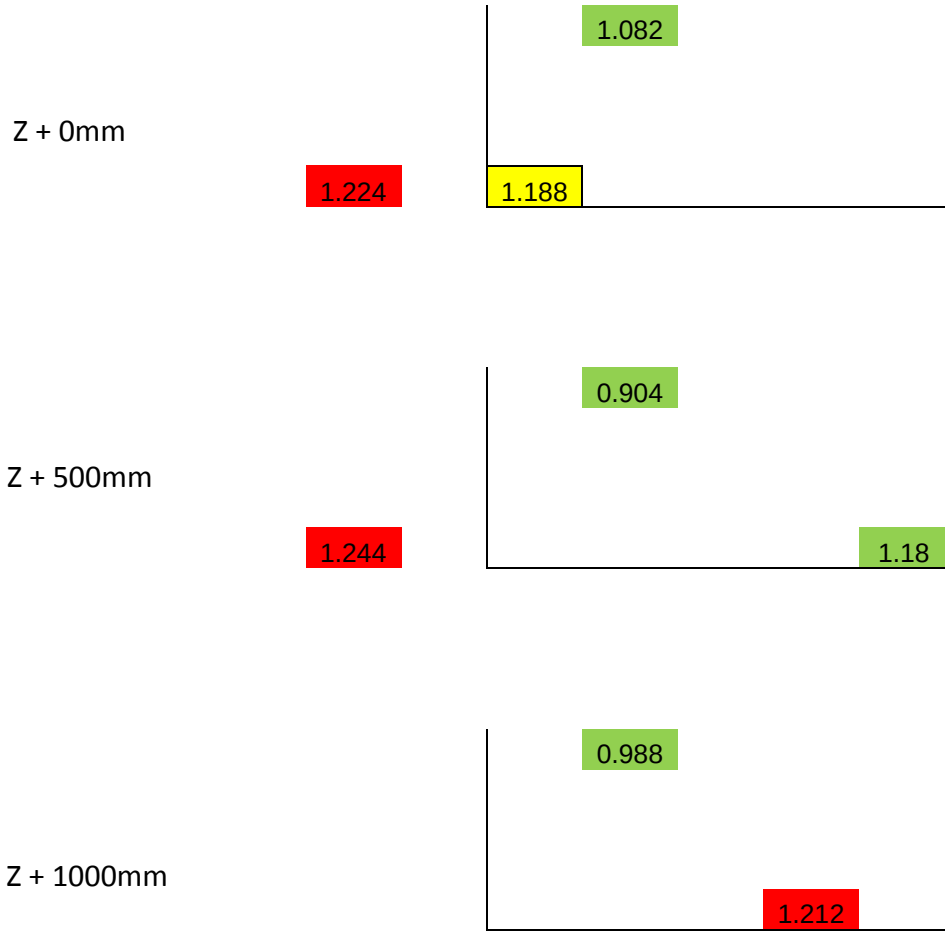

Figure 8.3.6: Map showing cycle times (seconds) for various force platform locations using the original end-effector, for selected locations on the robot. Green on the scale represents an improvement on the original location and red is slower.

The cycle times for the linear bearing test locations validated on the real world robot, are given in figure 8.3.7. Again as expected, although different, the trends are similar for the actual times. The quickest runtime on the physical robot occurred at a different location compared to RoboGuide and represented a small 3% improvement compared to the original location.

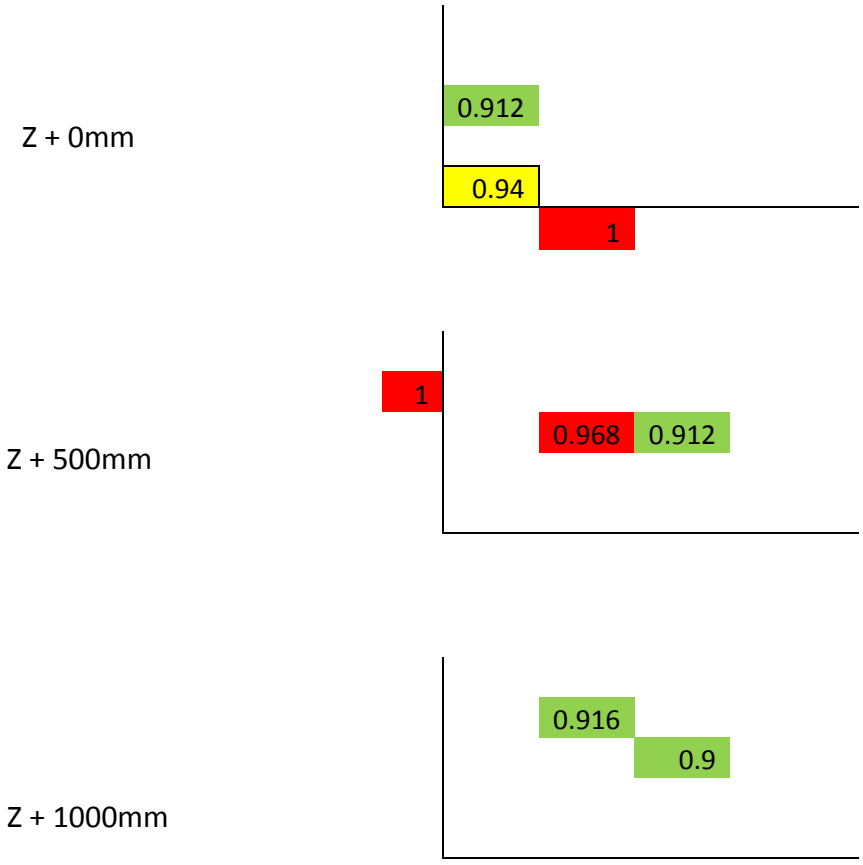

Figure 8.3.7: Map showing cycle times (seconds) for various force platform locations using the linear bearing end-effector, for selected locations on the robot. Green on the scale represents an improvement on the original location and red is slower.

8.4 DISCUSSIONS

This chapter investigated whether the total run time for footstrike emulation programme could be improved through relocation of the force platform within the robot cell. Initially the virtual environment of RoboGuide was used to assess how the time may vary for a range of force platform locations throughout the cell. Moving the force platform to a new location and making alterations to the programmes accordingly can be achieved far easier in a virtual environment than the physical one. The ability to create CAD models of the robot end-effector and cell furniture allowed for a full virtual recreation of the real world environment and the ability to easily change and move these features is very advantageous in applications such as this.

Stage 1 – RoboGuide – optimisation of force plate location

When looking at the run time maps, one of the most noticeable things was that there were a number of potential force platform locations, which gave an improved runtime on the original. For the original end-effector and at each vertical location map, the pattern appeared to be that the most optimal times occurred as the force platform was moved towards the robot (-x) and in the direction of the motion (+y), (figures 8.3.1 & 8.3.2). As the force platform was raised from its original location to the middle and upper levels, the run times were, on average, quicker than those at the original level closest to the ground.

For the original end-effector, the optimal location was with the force platform raised by 500mm, moved closer to the robot by 1000mm (-x) and in the direction of the motion 250mm (+y) from the original location resulting in an approximate 17% reduction in runtime. Had these results been for the new end-effector design then force platform relocation would have been more justified, but in this instance it was not deemed necessary. Also, the original force platform location falls within a region of improvement, however it is at the periphery.

There is one major anomaly in run time located at (-750, 0, 500), where the time is 0.72s slower than the original. Out of all of the locations tested, this was by far the slowest and is located adjacent to the region of 'more optimal' times, i.e. all of the regions around the anomaly are much quicker than the original time. It is uncertain why this location was so poor, but it may be the case that, the joints of the robot were orientated in such a way that make it difficult for the movement to be performed quickly.

A parallel investigation was also carried out to be able to draw comparisons in run time between the original end-effector and the linear bearing end-effector, (figures 8.3.2 and 8.3.4). The design of the linear bearing end-effector required a different mounting angle and orientation therefore a different footstrike programme to the original end-effector was used to move the footform through the ground contact phase. Comparisons between the two end-effectors were less reliable but still help with the overall aim of finding the optimal force platform location for each respective end-effector. As with the original end-effector, there were many different locations that provided a shorter cycle time than the original location. However, the differences are not to the same magnitude as the original end-effector (up to a 10% improvement compared to 17% for the original). The original linear bearing run time was faster than the original end-effector location, due to the reduced kinematic demand on the more proximal joints of the robot. This kinematic option reduces the gains to be made through force platform relocation.

The linear bearing end-effector again showed a tendency for the quicker run times to be located closer to the robot. Unlike the original end-effector, the most optimal locations appear to be on the same level as the original force platform location and raising the force platform level leads to fewer locations where the times are better.

The angles for each of the robot joints (table 8.3.1) indicated that there was no stand out angle for an individual joint that would lead to an improved overall run time. Instead it was more likely that optimal times were achieved by a combination of joint angles and how they work with each other to drive the footform through the movement. Thus making optimal

force platform position dependent upon the end-effector that is to be used and therefore the orientations adopted by the robot to run the programme.

Stage 2 – Real world validation of RoboGuide Optimisation

A select number of locations from the RoboGuide testing were also tested on the robot (figures 8.3.6 and 8.3.7) i.e. the best and worst location at each height for each end-effector. As expected the results showed a similar trend in run times between RoboGuide and the robot, however there were differences in the values of the times. The results reinforced that relocating the force platform can produce a reduction in run time. Indeed, for the original end-effector the percentage of the improvement was larger for the robot than for RoboGuide (24% vs 17%). For the linear bearing end-effector the improvements were much smaller than those on RoboGuide (<3 % vs 10%), presumably due to the reduced kinematic demand for this end-effector. The original location for this end-effector initially provided a quicker cycle time than that of the original.

At each of the investigated locations a value for standard deviation was obtained from the average of 5 repetitions. For the majority of cases the standard deviation was 0, and always equal to or greater than 0.0055 seconds. This reinforces the repeatability of the virtual simulation, physical emulations and the precision of the measurement tools used.

The outcomes from stages 1 and 2 have indicated that there are different optimal force platform locations depending on which end-effector is used. The nature of the linear bearing design means that the robot is orientated differently and drives the footform differently to the original end-effector, so it is not surprising that the optimal force platform location differ. The tests carried out in stage 2 validated the findings of Chapter 7, i.e. that the robot orientation and movement due to the new linear bearing end-effector design are an improvement on the original methods in terms of run time. However, with such a small improvement in total run time at the optimal location (<4%), force platform relocation was not deemed necessary, the required effort does not outweigh any improved output particularly since the improvement is so much smaller than the difference between robot

and human. Furthermore the gains are negligible compared to those made through the new end-effector design changes.

The major limitation of this study is that it would have been more desirable to document the ground contact time (a variable used in human and robot footstrike analysis). However there was no accurate way of recording this on RoboGuide or for mid-air running of the robot.

8.4 CONCLUSIONS

The primary aim of this chapter was to investigate the potential of relocating the force platform within the robot cell to reduce ground contact time in footstrike emulation to closer to the value for the human footstrike and thereby address research question three of this thesis. The physical robot environment was mirrored within RoboGuide, the running footstrike programmed, and repeated at various locations within the robot. Cycle times were compared between locations, and for the two differing end-effectors. The following conclusions were drawn:

- For both end-effectors, there were a number of force platform locations, that gave faster run times than the original and these tended to be grouped together in easy to define regions. The most optimal times occur as the force platform is moved closer to the robot (-x) and in the direction of the motion (+y).
- From validating the RoboGuide results at a number of positions on the robot, it was confirmed that improvements in run time would be achieved through force platform relocation. The potential improvements remained greater for the original end-effector (17%) than the linear bearing end-effector (10%), which also had more varied results.
- Despite the above findings it was decided that the force platform would not be relocated, as the gains in total run time were negligible for the linear bearing end-effector (3%).

CHAPTER 9

EMULATION OF THE SHOE-GROUND INTERACTION DURING THE GROUND CONTACT PHASE OF HUMAN WALKING

9.1 INTRODUCTION

The primary aim of this thesis is to investigate the potential of using a 6 degrees-of-freedom industrial robot to emulate the ground contact phase of human gait. The chapters leading up to this point have laid the foundations for how this might be achieved, from the collection and documentation of human kinematic data (Chapter 3) to the understanding of the robot programming and resultant movement (Chapter 5) and the design of an end-effector of support human gait emulation (Chapter 7). Based on this work, and the previously identified challenges in emulating running gait using this robot (Ronkainen *et al* 2010), the decision was made to initially focus on walking.

The biomechanics of the ground contact phase of walking were presented in Chapters 2 and 3. In brief the footstrike can be broken down into touch down (where the heel first contacts the ground), mid-stance (where the foot rolls over to flat) and toe-off; with a total ground contact time of approximately 0.6 seconds. The vertical ground reaction forces display two peaks of a little over bodyweight. The first peak occurs while the weight is on the rearfoot and the second 'pushoff' peak is in the second half of stance. In the context of applying the

current research to footwear testing, the key variables determining the success of the emulation were considered to be applying the correct load and loading rate to the correct part of the shoe throughout stance.

In this chapter the human kinetic and kinematic data for walking (Chapter 3) were used to define the programmed movement data for the robot and/or validate the resulting kinematics and kinetics.

The robot is kinematically controlled and the following human data were used to fully programme the robot to emulate the sagittal plane walking movement:

- ❖ Heel trajectory
- ❖ Resultant heel velocity
- ❖ Foot angle

The following human data were used to validate the resulting gait emulation:

- Ground reaction forces (vertical and anterior-posterior)
- Loading rate (vertical)
- Centre of pressure position (anterior-posterior)
- Ground contact time
- The programmed kinematics (listed above).

The outcomes of investigations that characterised the robot movement and evaluated RoboGuide (Chapters 5 and 6); suggested that direct use of the human kinematics may not be the optimal means to emulate human gait. This was a major factor in the design process for the new end-effector (Chapter 7), where the concept of rotating the footform about a fixed point was introduced. So, as well as programming the robot using the human kinematics, rotation about a fixed point was also investigated; it was hypothesised that this would reduce the 'footprint' (i.e. the anterio-posterior distance that the shod footform is in contact with the ground) and ground contact time, whilst investigating a different way of applying the ground reaction forces. During human walking gait, there are three main rotation points which account for much of the foot movement during ground contact; from the point of ground contact through midstance the main point of rotation is the heel. After

this the centre of rotation moves forward to the metatarsal phalangeal joint (MPJ) and after this the centre of rotation moves to the distal toes (section 2.2). Since the heel and MPJ rotations account for the majority of ground contact these were the focus for programming the robot. By simplifying the programmed ground contact movement to a rotation about a fixed point may allow fewer points to be used and the ground contact time to be reduced.

Hence, two methods of programming the robot to emulate human walking were considered: **1.** Direct application of the human kinematic data. **2.** Rotation about a fixed point (the heel for the initial phase of stance and the MPJ for the latter phase).

9.1.1 Aims

- The overall aim of this chapter is to use the FANUC R-2000iB robot to emulate the ground contact phase of human walking.

9.1.2 Objectives

The above aim was achieved through the following objectives:

- To develop robot programmes for the walking emulation based on using the human kinematic data directly (with both original and new-end-effector designs); applying a rotation about the heel; and applying rotation about the MPJ.
- To compare the output kinematics and kinetics from each programmes to the human walking data presented in Chapter 3.

9.2 METHODOLOGY

The experimental methodology for this chapter is presented in the following sub-sections, documenting equipment used, data collection and processing methods.

9.2.1 Footstrike Data

The primary kinematic and kinetic walking footstrike data presented in this chapter was collected from trials carried out using the FANUC R-2000iB robot; the human kinematic and kinetic data used for programming the robot and validating the output is that collected in Chapter 3. The new end-effector design, as described in Chapter 7, was used for all of the robotic testing and the Blatchford prosthetic footform was fitted with the same asics Gel running shoe as used in the human testing.

9.2.2 Equipment

All of the foot-ground interactions took place with the end-effector footform impacting the force platform (Kistler, Switzerland; 9281CA) located in the middle of the robot cage recording at 2000 Hz. The platform has been designed to 'drop away' should the impact force exceed 100kN, helping to prevent damage to either the force plate and/or robot. A tripod mounted highspeed camera (Photron Limited Europe, UK; Fastcam SA-1 675K-MK1) was used to record footage of the trials at 500Hz with a pixel resolution of 1024x1024 and a shutter speed of $1/500^{th}$ of a second. The camera was set up perpendicular to the direction of motion, parallel with the anterior-posterior line of the force platform, and filmed the ground contact phase of each footstrike in the sagittal plane (Figure 4.2.3). The camera field of view was approximately 0.8 x 0.8m.

9.2.3 Data Collection

The anatomical areas of interest on the Blatchford footform and end-effector were marked using spheres, 14mm in diameter, covered in retro-reflective tape and mounted on small discs that could be adhered to the footform using double-sided tape. The use of these markers ensured that the tracked kinematics were in the same location as those tracked on the human using the VICON motion analysis system (Chapter 3). The retro-reflective tape also made the markers easy to pick out during the digitisation process. Repeated impacts with the force plate can sometimes make the markers fall off, so to ensure consistent re-attachment the location was first identified with a marker pen. Where applicable, the same marker set as described in Chapter 3 was used and a full list of markers and their locations are shown in figure 9.2.1.

Figure 9.2.1 - The anatomical positions of the VICON markers (not all are visible) for the robot fitted with the linear end-effector. The marker locations are as follows: **1.** Hallux **2.** Medial metatarsal (not shown) **3.** Lateral metatarsal **4.** Medial calcaneus (not shown) **5.** Lateral calcaneus **6**. Medial malleolus (not shown) **7.** Lateral malleolus **8**. Heel **9.**Centre of the end-effector.

9.2.4 Robot Programmes

All of the robot trials were carried out under shod conditions with the robot emulating the human walking gait. There were two main methods of programming the robot in this process:

1. **Human kinematic data method:** The kinematic and kinetic information collected for the foot and heel marker in Chapter 3 was used to programme the heel position,

velocity of the end-effector heel and foot orientation (sagittal plane). Further to this, an additional programme was created where the position and orientation at initial ground contact was used as a reference to establish the vertical offset (50mm) required to match the magnitude of the impact peak of the vertical ground reaction force from the human data.

2. **Rotation method:** The rotation method was used to generate two programmes; *(a)* rotation about the heel with the intention of emulating the first half of ground contact (touchdown through to midstance) and *(b)* rotation about the MPJ with the intention of emulating the second half of ground contact (midstance through to toe-off). The rotations occurred in the sagittal plane of motion, with the respective centre points of rotation positioned on the longitudinal centre-line of the plantar aspect of the foot. For the heel rotation method, a range of starting positions (off the force platform) were programmed to investigate the effect of differing approach angle trajectories of the footform on the emulation characteristics. A similar process was carried out for the final positon in the MPJ rotation method.

The programmes created using the above process were done as described in Chapter 4, each programme is shown in more detail over the following pages tables 9.2.1, 9.2.2 and 9.2.3. The two-dimensional positional co-ordinates of the heel (y & z), in relation to the point of ground contact (0, 0), are shown along with the angle of the plantar aspect of the foot relative to the ground and heel resultant velocity. Also shown is an image of the robot and footform at each of the programmed points. The results of Chapter 5 led to the conclusion that the most appropriate smoothing level for footstrike emulation is maximum smoothing i.e. ‘CNT100’.

Table 9.2.1 – The robot programme and corresponding footform positions for the robot programmed with human kinematic data. Shaded cells represent the area of ground contact.

Human kinematics				
Point #	**x (mm)**	**z (mm)**	**Velocity (mm/s)**	**Angle (°)**
1	COL DETECT OFF			
2				
3	-357.24	72.154	2000	15
4	-258.468	62	2000	15
5	-174.466	59.23	2000	17.606
6	-102.464	42	2000	21.691
7	-48.001	22	1730	24.357
8	-13.847	8.308	807	24.844
9				
10	0	0	1723	22.547
11	36.924	9.231	46	-31.108
12	46.155	24.923	206	-36.602
13	114.464	120.012	2000	-48.835
14	243.698	204.928	2000	-63.125
15				
16	300.931	227.082	2000	-70.361
17	355.394	242.775	1750	-79.512
18	416.319	251.083	1500	-89.353
19	481.859	254.775	1250	-100.143
20				
21	COL DETECT ON			
22				
23	-57.016	371.305	1000	42.895
24	-357.24	72.154	1000	15
END				

Table 9.2.2 – The robot programme and corresponding footform positions for the robot programmed with a fixed point of rotation at the heel. Shaded cells represent the area of ground contact.

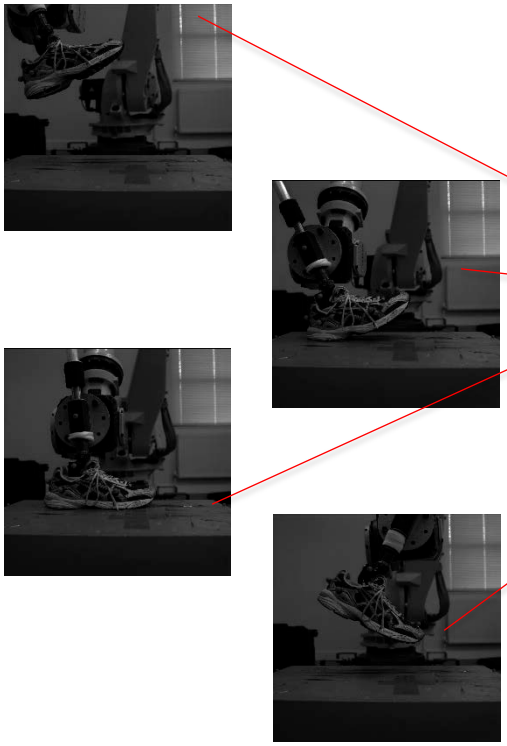

Rotation about the heel				
Point #	x (mm)	z (mm)	Velocity (mm/s)	Angle (°)
1	COL DETECT OFF			
2				
3	0.009	198.993	600	23
4				
5	0	0	600	23
6	0.01	0.013	10	-10.749
7				
8	0.033	276.314	600	-10.749
9				
10	COL DETECT ON			
11				
12	-125.929	198.993	600	-10
END				

Table 9.2.3 – The robot programme and corresponding footform positions for the robot programmed with a fixed point of rotation at the MPJ. Shaded cells represent the area of ground contact.

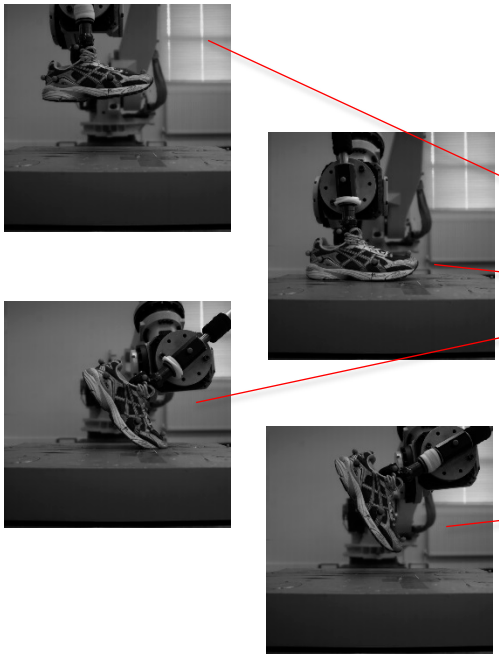

Rotation about the MPJ				
Point #	x (mm)	z (mm)	Velocity (mm/s)	Angle (°)
1	COL DETECT OFF			
2				
3	0	191.695	600	23.103
4				
5	0	0	600	23.103
6	0.03	-0.037	10	-74.917
7				
8	-49.88	134.134	600	-86.992
9				
10	COL DETECT ON			
11				
12	-24.197	134.133	300	86.992
END				

9.2.5 Data Processing

The force data (medio-lateral, anterior-posterior and vertical ground reaction forces) and centre of pressure data which was initially captured within the BioWare software (Kistler, Switzerland), was exported to Microsoft Excel for graphical analysis. The ground contact phase on the force platform was determined using the vertical ground reaction force data, with a threshold of 10N identifying the period of contact.

Each high-speed video file was cropped to include only the ground contact phase and the areas immediately prior to and following contact. These video files were then subsequently down-sampled to every 10^{th} frame (i.e. 50Hz) and exported for Image digitisation using the Image Pro software (Media Cybernetics, Inc; MD, USA). Manual digitisation techniques were used to track the position of the centre of the markers, which were then converted into co-ordinate data (measured in mm) and exported to Microsoft Excel, whereupon heel velocity and foot orientation were calculated. The data was then imported to MatLab, for graphical representation (The Mathworks; Natick, MA, USA)

Evaluation of the emulation was based on a comparison of the following parameters with those form the human data collection (Chapter 3):

- Ground reaction forces (vertical and anterior-posterior)
- Loading rate (vertical)
- Centre of pressures (anterior-posterior plane)
- Ground contact time.
- Heel marker position (sagittal plane)
- Angles of the plantar aspect (using the markers at the heel and lateral MPJ) of the foot relative to the ground.

The afore mentioned kinematics and kinetics of the robot footstrikes were compared to those of the human footstrike data (Chapter 3), this was able to determine the success of the emulation or 'goodness of fit'. This was achieved through visually comparing the results profiles and numerically comparing parameters such as peak force magnitude, loading rates and kinematics of key footstrike instances. This is explored further in the following sections.

9.3 RESULTS

9.3.1 Ground Reaction Forces

The vertical and horizontal ground reaction forces for all of the robot programmes against real human data are shown in figures 9.3.1 – 9.3.4

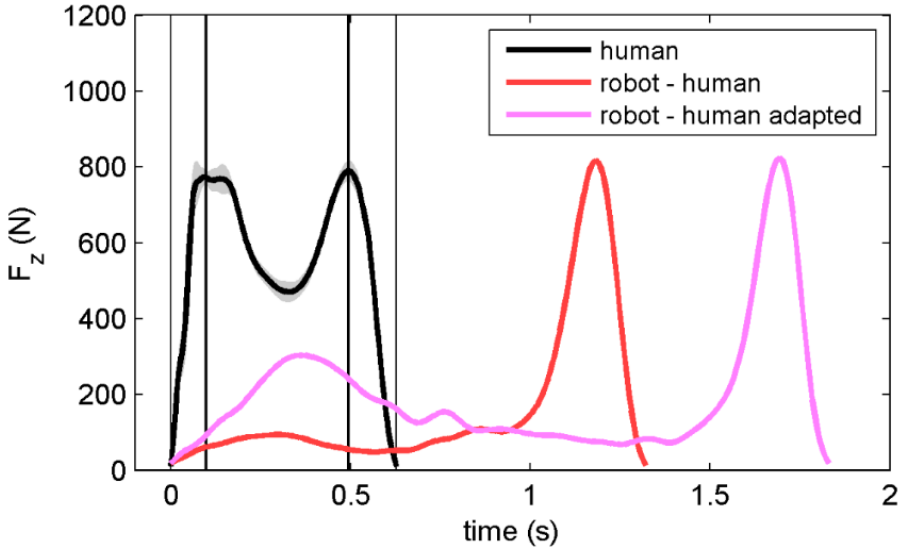

Figure 9.3.1 – The vertical ground reaction forces for the real world human and the robot programmed with human kinematic data. The pink trace represents the adapted programme with impact point vertically offset downwards by 50mm to match the magnitude vertical ground reaction force peak of the human data. The thick vertical lines represent the two vertical ground reaction peaks for real human data and the thin vertical lines represent touchdown and toeoff for real human data.

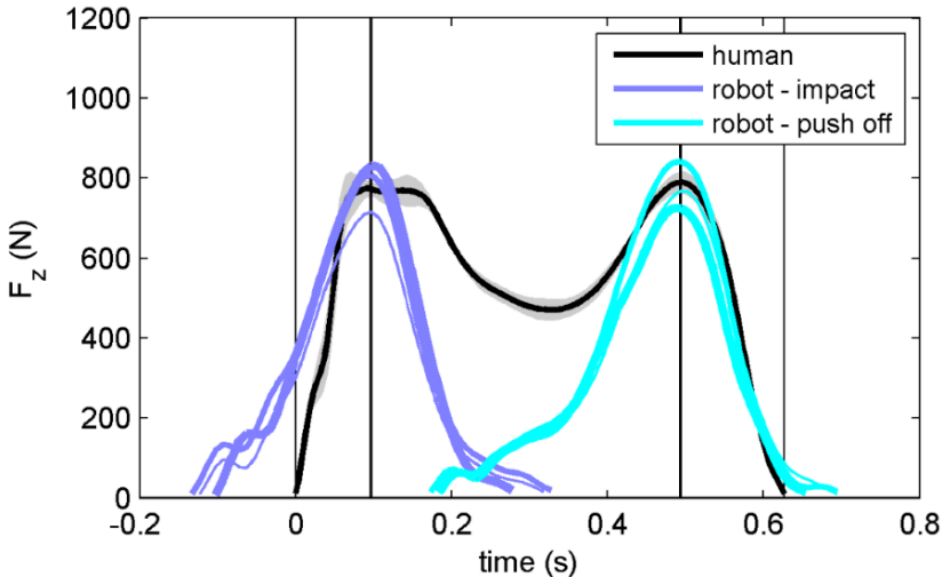

Figure 9.3.2 – The vertical ground reaction forces for the real world human and the robot programmed with rotations about the MPJ and heel. The thinner rotation traces represent the different start and finish positions respectively, the thinner the trace the more removed the position. The vertical lines represent the two vertical ground reaction peaks (thick) and touchdown/toeoff (thin) for real human data.

Programming the robot with human kinematic data (figure 9.3.1) was unable to generate an adequate impact peak. Second peak magnitudes were acceptable; however the ground contact time was too large. Programmes with a fixed point of rotation (figure 9.3.2) were able to achieve the magnitudes of the respective peaks with desirable loading rates. The ground contact times of these programmes were also much closer to the target value.

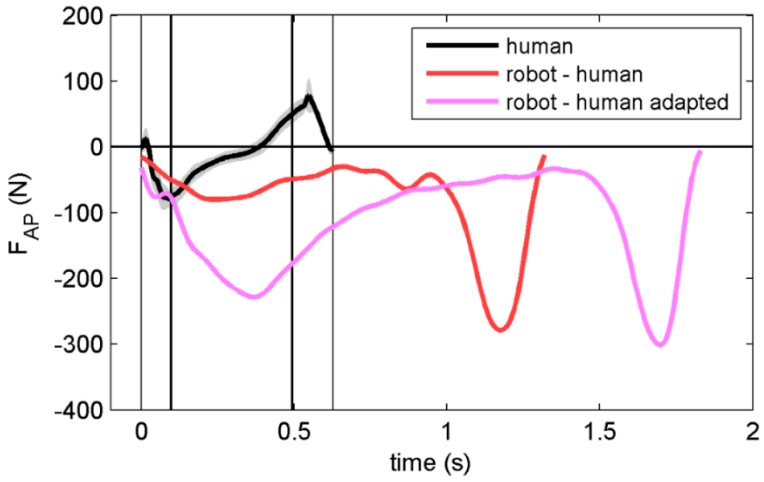

Figure 9.3.3 – The horizontal ground reaction forces for the real world human and the robot programmed with human kinematic data. The pink trace represents the adapted programme with impact point vertically offset downwards by 50mm to match the magnitude vertical ground reaction force peak of the human data. The vertical lines represent the two vertical ground reaction peaks (thick) and touchdown/toeoff (thin) for real human data.

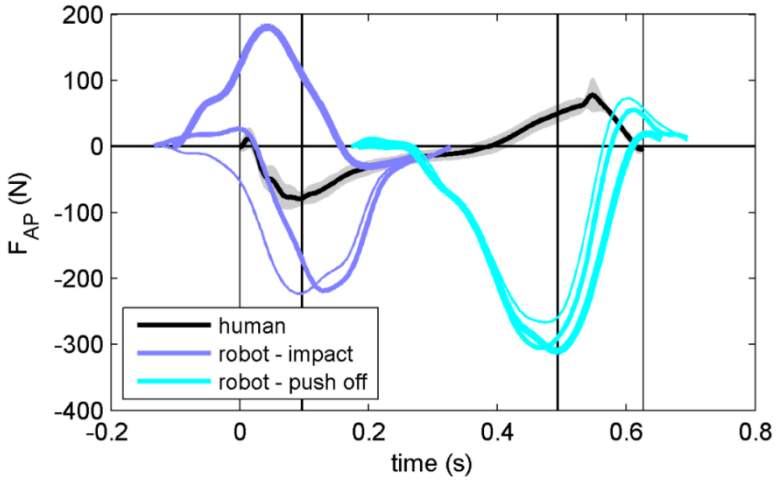

Figure 9.3.4 – The horizontal ground reaction forces for the real world human and the robot programmed with rotations about the MPJ and heel. The thinner rotation traces represent the different start and finish positions respectively, the thinner the trace the more removed the position. The vertical lines represent the two vertical ground reaction peaks (thick) and touchdown/toeoff (thin) for real human data.

The anterio-posterior forces for all of the robot programmes (figure 9.3.3 and 9.3.4) struggle to match the real human data with force magnitudes that are too large and show no indication of generating a propulsive force as the contact moves from midstance to toeoff.

9.3.2 Centres of Pressure

The centres of pressure for all of the robot programmes against real human data are shown in figures 9.3.5 and 9.3.6.

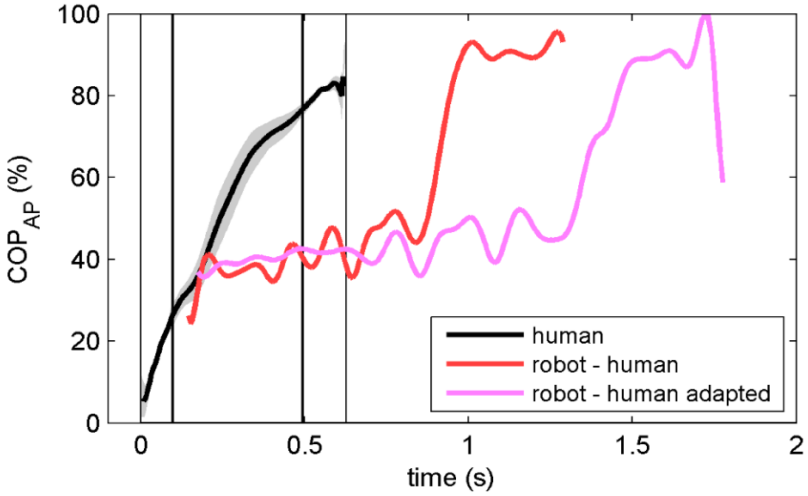

Figure 9.3.5 – The centres of pressure as a percentage of the anterio-posterior distance along the shod foot for the real world human and the robot programmed with human kinematic data (0% is the heel and 100% the toe). The pink trace represents the adapted programme with impact point vertically offset downwards by 50mm to match the magnitude vertical ground reaction force peak of the human data. The vertical lines represent the two vertical ground reaction peaks (thick) and touchdown/toeoff (thin) for real human data.

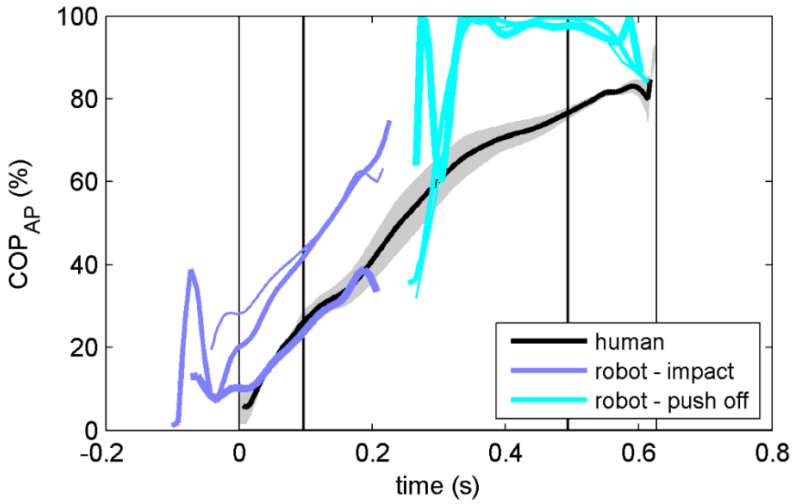

Figure 9.3.6– The centres of pressure as a percentage of the anterio-posterior distance for the real world human and the robot programmed with rotations about the MPJ and heel (0% is the heel and 100% the toe). The thinner rotation traces represent the different start and finish positions respectively, the thinner the trace the more removed the position. . The vertical lines represent the two vertical ground reaction peaks (thick) and touchdown/toeoff (thin) for real human data.

The human kinematic profiles aren't able to successfully emulate the positions of the centre of pressure on the shoe with the CoP remaining on the rear foot for too long. The CoP for the rotation programmes, specifically the rotation about the heel, are a much better emulation. The emulation is not as accurate for the rotation about the MPJ, which sees the CoP being too close to the anterior aspect of the footform.

9.3.3 Footform kinematics

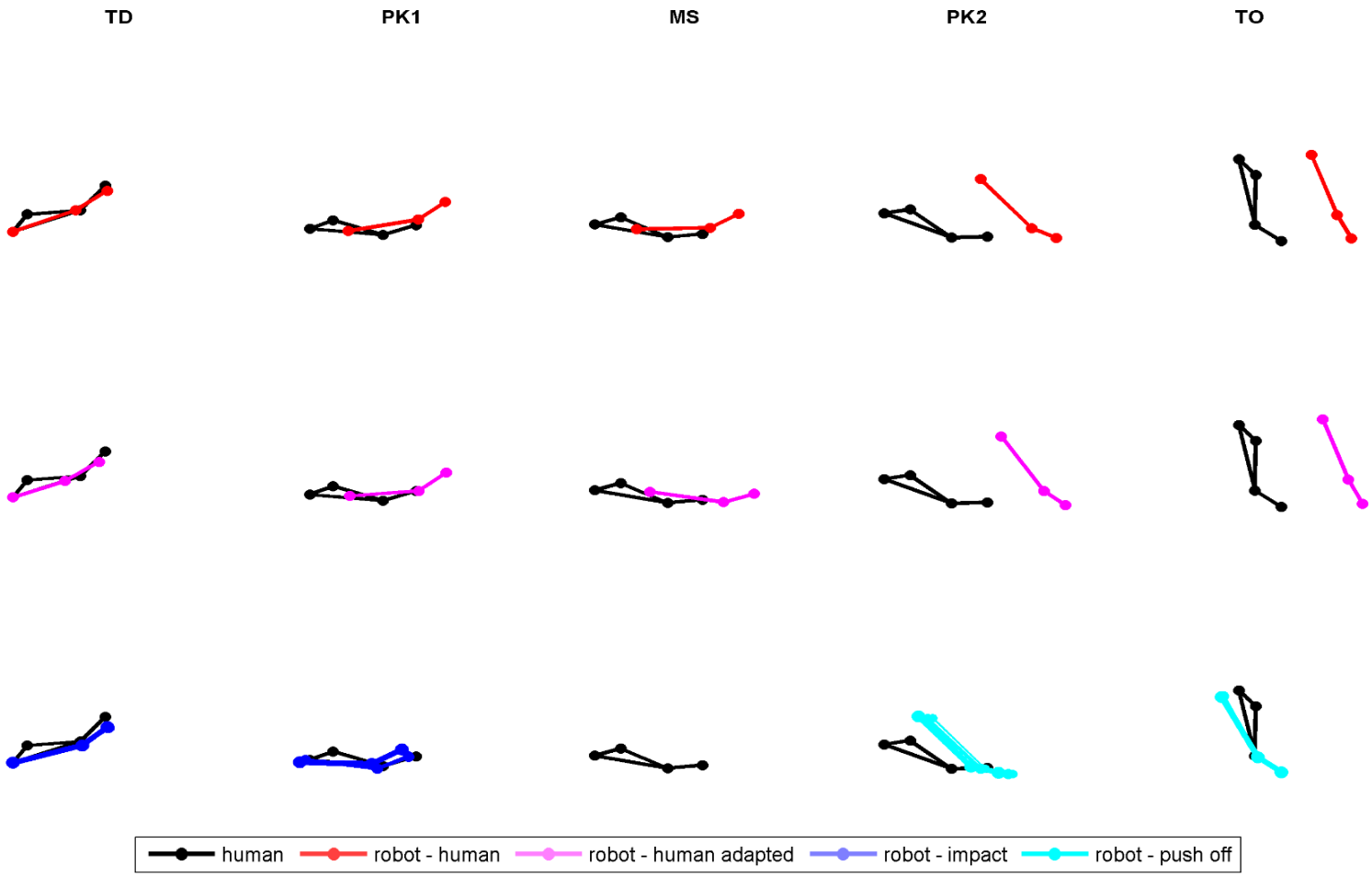

Figure 9.3.7– A schematic showing the position and orientation of the real human footform against each of the robot programmes at the main points of the ground contact phase; **TD –**touch down, **PK1 –** Peak 1 (impact peak), **MS –** Midstance, **PK2 –** Peak 2 and **TO –** Toeoff. The heel marker for each robot programme was matched to that of the real human at the initial point of ground contact.

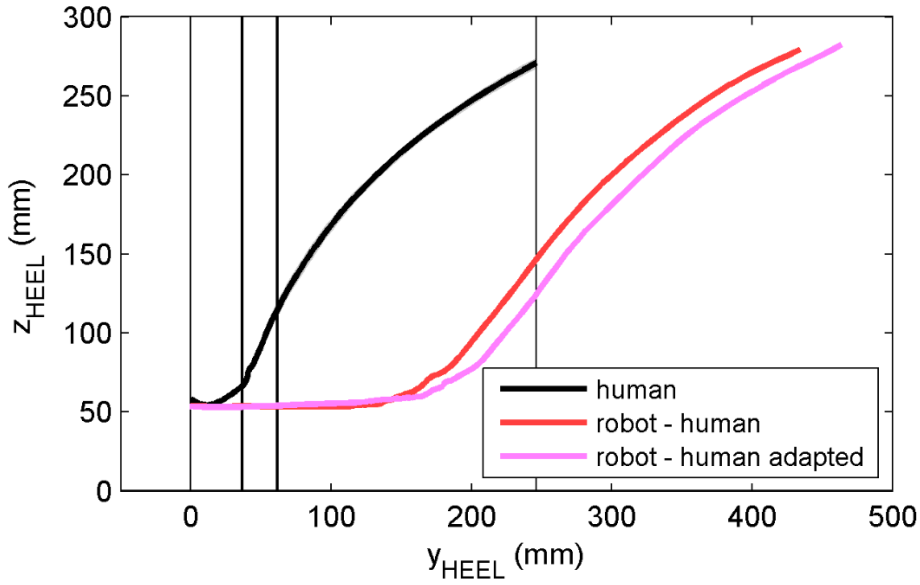

Figure 9.3.8 – The two dimensional position of the heel in the sagittal plane for the real world human and the robot programmed with human kinematic data. With impact point vertically offset downwards by 50mm. The vertical lines represent the two vertical ground reaction peaks (thick) and touchdown/toeoff (thin) for real human data.

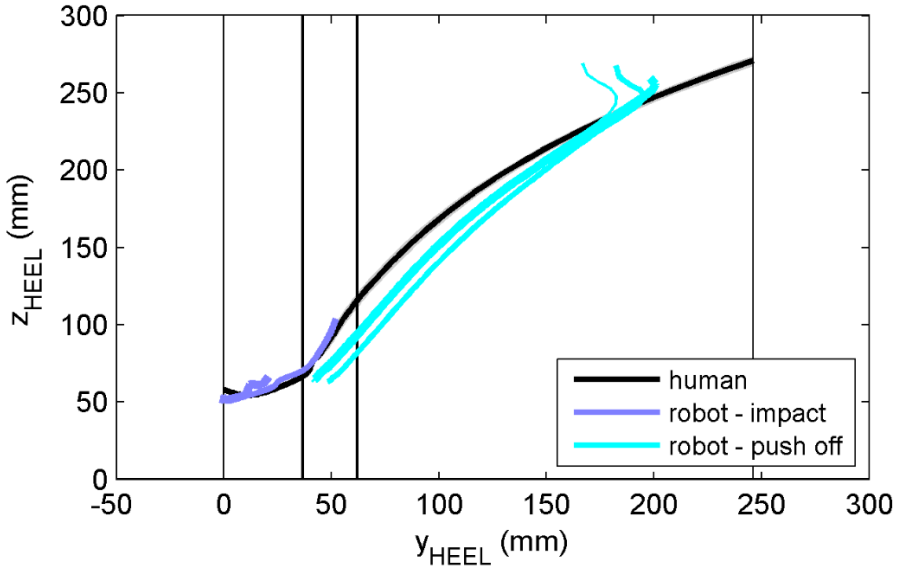

Figure 9.3.9– The two dimensional position of the heel in the sagittal plane for the real world human and the robot programmed with rotations about the MPJ and heel. The thinner rotation traces represent the different start and finish positions respectively, the thinner the trace the more removed the position. . The vertical lines represent the two vertical ground reaction peaks (thick) and touchdown/toeoff (thin) for real human data.

Figures 9.3.7 – 9.3.9 show the heel position during the robot footstrike compared to that of the human. The main finding is that the footprint for the human kinematic programmes is too large while that for the programmes with a fixed point of rotation is much closer to the real human footprint.

9.3.4 Footform angles

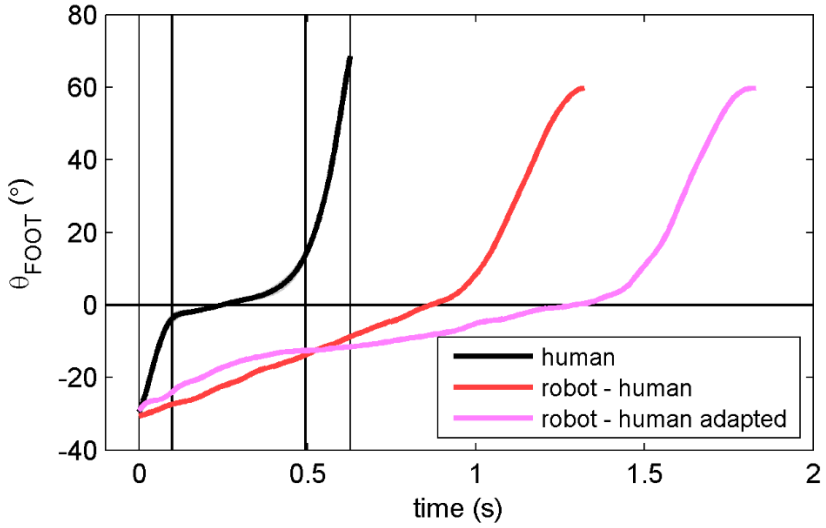

Figure 9.3.10 – A representation of the angle of the footform relative to the ground for the real world human and the robot programmed with human kinematic data. The pink trace represents the adapted programme with impact point vertically offset downwards by 50mm to match the magnitude vertical ground reaction force peak of the human data. The vertical lines represent the two vertical ground reaction peaks (thick) and touchdown/toeoff (thin) for real human data.

.

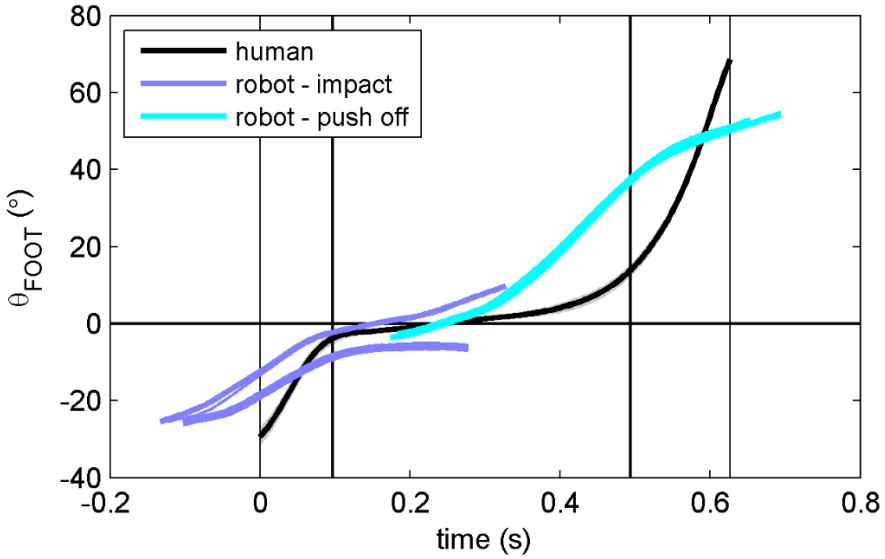

Figure 9.3.11 – A representation of the angle of the footform relative to the ground for the real world human and the robot programmed with rotations about the MPJ and heel. The thinner rotation traces represent the different start and finish positions respectively, the thinner the trace the more removed the position. The vertical lines represent the two vertical ground reaction peaks (thick) and touchdown/toeoff (thin) for real human data.

The foot angle relative to the ground and MPJ angle for the robot programmes compared to the real human data are shown in figures 9.3.10 – 9.3.12.

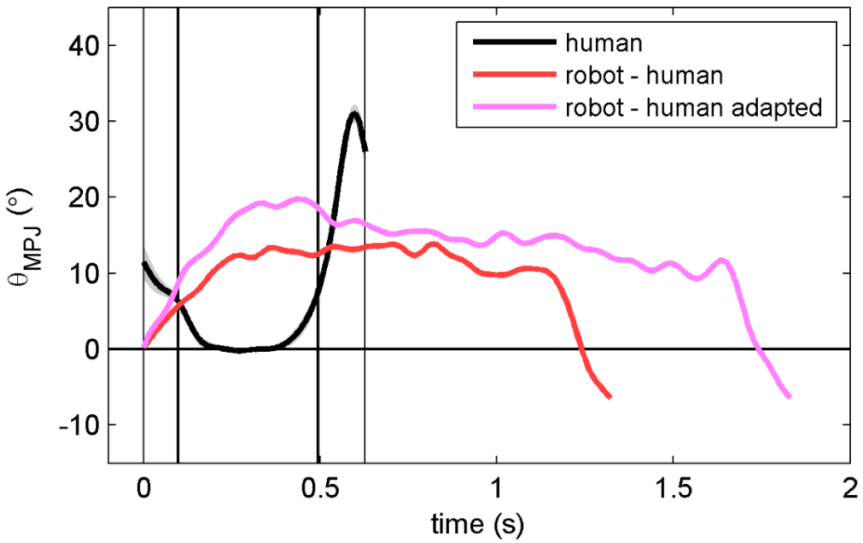

Figure 9.3.12 – A representation of the angle of the MPJ for the real world human and the robot programmed with human kinematic data The pink trace represents the adapted programme with impact point vertically offset downwards by 50mm to match the magnitude vertical ground reaction force peak of the human data. The vertical lines represent the two vertical ground reaction peaks (thick) and touchdown/toeoff (thin) for real human data.

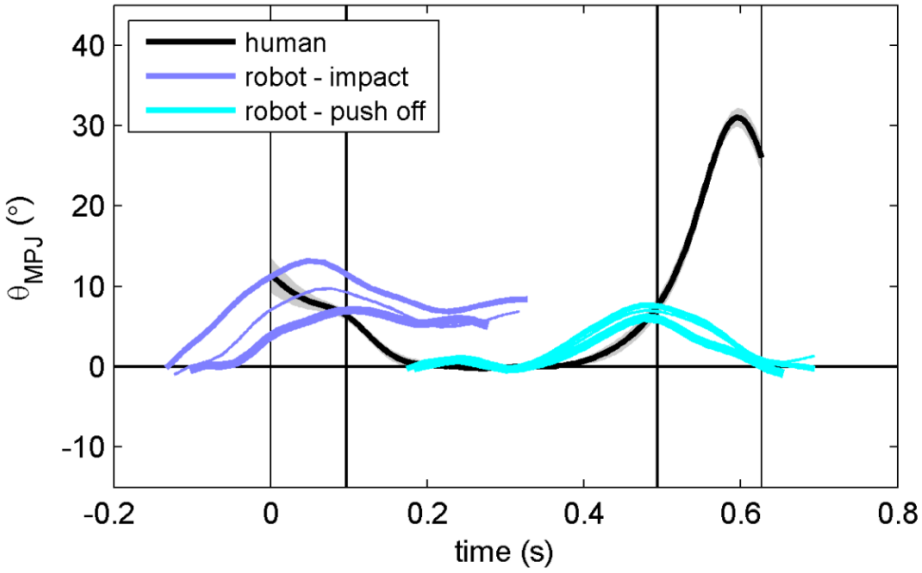

Figure 9.3.13 – A representation of the angle of the MPJ for the real world human and the robot programmed with rotations about the MPJ and heel. The thinner rotation traces represent the different start and finish positions respectively, the thinner the trace the more removed the position. The vertical lines represent the two vertical ground reaction peaks (thick) and touchdown/toeoff (thin) for real human data.

All of the robot programmes provide a very poor representation of the MPJ angle. The foot angle during the first phase of ground contact is better emulated when programmed with a rotation about the heel compared to the human kinematic programmes. With less flexion occurring at the MPJ compared to the real human gait (figure 9.3.11).

A summary of the remaining kinematic and kinetic features is given in table 9.3.1.

Table 9.3.1 – A summary of the remaining key kinematic and kinetic features for each of the robot and real human footstrikes. Values coloured in red represent a good emulation of the real human value.

Parameter	Robot Programmes									Real Human	
	Human Kinematics	Human Kinematics (increased impact peak)	Rotation about the heel			Rotation about the MPJ					
			Start -0mm	Start -50mm	Start -100mm	Finish -0mm	Finish -50mm	Finish -50mm			*SD*
Timings (s)											
VGRF Peak 1	0.32	0.36	0.22	0.24	0.22	n/a	n/a	n/a		**0.1**	*0.04*
VGRF Midstance	0.58	1.26	0.4	0.46	0.44	0	0	0		**0.33**	*0.02*
VGRF Peak 2	1.18	1.7	n/a	n/a	n/a	0.32	0.32	0.32		**0.49**	*0.01*
VGRF Toeoff	1.34	1.84	n/a	n/a	n/a	0.48	0.52	0.52		**0.63**	*0.01*
Max. Loading Rate (N/s)	4469	286	6090	4658	4732	3987	5190	4171		**11025**	*1548*
Footprint (m)	0.54	0.57	0.29	0.32	0.32	0.31	0.28	0.27		**0.36**	*0*
Forces (N)											
Vertical Peak 1 max.	95	304	831	807	715	n/a	n/a	n/a		**794**	*32*
Vertical midstance max.	49	69	n/a	n/a	n/a	n/a	n/a	n/a		**470**	*26*
Vertical Peak 2 max.	818	826	n/a	n/a	n/a	725	842	767		**790**	*27*
Braking max.	-279	-302	-30	-219	-223	-311	-305	-267		**-83**	*13*
Propulsive max.	-13	-6	181	27	1	19	56	73		**79**	*26*
Velocity at ground contact (m/s)											
Heel	0.68	0.01	0.19	0.15	0.08	0.18	0.12	0.14		**0.7**	*0.11*
MPJ	0.82	0.71	0.33	0.35	0.23	0.18	0.21	0.24		**1.21**	*0.11*
Toe	0.72	0.64	0.29	0.28	0.22	0.2	0.24	0.23		**1.69**	*0.09*
Velocity at midstance (m/s)											
Heel	0.05	0.05	0.07	0.06	0.07	0.87	0.76	0.71		**0.08**	*0.02*
MPJ	0.12	0.07	0.11	0.08	0.09	0.33	0.27	0.26		**0.02**	*0.01*
Toe	0.18	0.08	0.19	0.22	0.21	0.12	0.1	0.08		**0.05**	*0.01*
Velocity at toeoff (m/s)											
Heel	0.73	1.02	0.61	0.51	0.52	0.28	0.53	0.55		**3.33**	*0.14*
MPJ	0.75	0.99	0.66	0.3	0.3	0.4	0.48	0.55		**2.05**	*0.14*
Toe	0.66	0.9	0.64	0.18	0.18	0.39	0.42	0.45		**1.39**	*0.11*

9.4 DISCUSSION

The overall aim of this chapter was to use the FANUC R-2000iB robot to emulate the ground contact phase of human walking. Using the knowledge gained in the previous chapters of this thesis; the above aim was addressed by programming the robot in ways; **1.** Directly using the real human kinematic data (Chapter 3) and **2.** To move with a pure rotation about the plantar aspect of the footform, either the heel or the MPJ, during the ground contact phase. All footstrikes were conducted using the new end-effector design outlined in Chapter 7, which has been deemed an improvement on the original.

The level of emulation success has been evaluated through comparisons to the real human data collected in Chapter 3. One of the main reasons for wanting to produce an accurate footstrike emulation is to be able to use the system and protocol put together in this thesis as an accelerated wear device for testing footwear. In this regard, the kinetics of the robot footstrike, and the location of force application to the shoe, have been deemed the most important factors in assessing the success of the robot footstrike. The results of each parameter (for each robot condition) are discussed in further detail in the subsequent sections, with precedence given to the important kinetic factors.

9.4.1 Ground Reaction Forces

Keller *et al* (1996) show that the target vertical ground reaction force trace for the walking gait is an m-shape with the impact peak and active peak having a force magnitude of a little over bodyweight (which in this example is approximately 800N), the trough in between these peaks occurs during midstance where the weight moves from the rearfoot to forefoot region. The ability to emulate the rates and magnitudes of the two peaks was given priority, it is these features which most affect the wear on the shoe and the lower forces which are more evenly distributed are not as important in comparison. This is also common practice in simple

mechanical tests used in industry (Newton Running 2013). It is for that reason that the robot programmes for the human kinematic data were vertically offset into the ground until an adequate force magnitude (for the second peak) was achieved (figure 9.3.1).

Programming using the real human data resulted in a vertical ground reaction profile with no real impact peak; because of this it was decided to manually alter the programme with a larger vertical offset at ground contact to try and generate an impact peak. An offset of 50mm increased the impact peak to approximately 300N, however, this was at the expense of an increased ground contact time. The loading rate of this smaller peak was also insufficient, it takes five times as long to achieve a much lower force. It can be concluded that entire vertical ground reaction force emulation is not readily achieved through programming the robot with human kinematics alone or through simple manipulation of the human kinematics.

Figure 9.3.2 shows the vertical ground reaction forces for the programmes instructed to rotate about the heel and MPJ respectively. As with human kinematic programme they were offset into the ground until the adequate force magnitude was achieved, the time stamp of the force peaks were matched to those of the real human data. The premise behind this method was that each programming method was meant to concentrate on a specific half of the footstrike emulation. The results would indicate that this technique has been more successful in emulating the vertical ground reaction forces, this time the forces acting on the heel during the impact peak have been achieved. The slight downside is the that loading rate (table 9.3.1) may be slightly low (by a factor of approximately 2) and the unloading rate too fast, but this is still a vast improvement on direct use of human kinematics. As with the human kinematic method the magnitude and loading rates of the second peak are a good match for the MPJ rotation. As shown in figure 9.3.2, these force traces can be plotted as a combination, where it is visually apparent how much of an improvement this technique gives in terms of profile matching. As well as the lower loading rate, the forces during midstance (the trough) are not accommodated for. The main reason for this is because it is made up of two different profiles and the

forces will inevitably tend towards 0N. If the forces traces had been plotted to start at the same time, as opposed to matching the peak forces, the midstance region would have a better emulation; but as already discussed, the peak forces and where they act are the most important factors with the trough given less priority as the lower forces are spread out over a larger area. Perhaps going forward it would be pertinent to investigate the potential of creating a single robot programme in which the fixed point of rotation changes half way through moving anteriorly from the heel at touchdown to the MPJ at toeoff.

In the real human data (Chapter 3), the anterio-posterior ground reaction force data is made up of two phases, the negative braking is the effect of the foot hitting the ground and the positive propulsion phase which is a consequence of the foot pushing off the ground, in both cases the magnitude doesn't exceed 100N. Previous studies (Ronkainen *et al* 2010) have had little success in emulating this aspect of the ground reaction forces, and the results indicate only limited improvement in the current study. For the robot programmed with human kinematic data (figure 9.3.3) the entirety of anterio-posterior force trace is negative (braking phase), this is because the robot constantly drives the footform through the programmed movement in a posterior-to-anterior direction. There is no dynamic interaction with the ground where there would be a propulsive phase during push-off (section 3.2.1.4), the footform is just pulled away from the ground contact.

The anterio-posterior ground reaction forces produced by the rotation programmes also struggle to match the real human data. For the heel rotation, as the heel is positioned directly above the point of ground contact, a propulsive force is generated (~175N) which goes against what would be expected. The most logical reason for this is that the footform is moving against the direction of motion as it rotates through the motion. These findings are repeated, but on a smaller scale, as the starting position moves back by 50mm and when the footform is 100mm back from the original start point there is no propulsive force at all. Moving the start position back does result in a desired braking force, however, the magnitudes are still too large (~200N). As with the human kinematic robot programme the rotation

about the MPJ mainly produces a braking force (~300N), the human data suggests that a propulsive force should be generated (~100N) as the foot flexes and pushes away from the ground. As before this would suggest that the footform is being moved through the motion as opposed to dynamically interacting with the ground. There is a small area at the end of the MPJ rotation where a propulsive force is being generated, this is happening right at the end of the toe-off phase where the footform is under enough flexion to push in the direction it has come from. This is more prevalent for the programmes with an end point that is positioned further back in the sagittal plane. The lack of a propulsive phase is a clear limitation and for both types of programme may be attributed to the end-effector, as the footform moves from midstance into toe-off the linear slide and built in compliance may act to alleviate the force against the direction of motion. However, this may be negligible, as generating a propulsive force has always been an issue – even when an end-effector with no compliance was used.

Two methods through which the anterio-posterior forces may be improved in future iterations of this work are:

1. Include horizontal compliance (similar to the vertical compliance in the new end-effector design, Chapter 7) which has reduced the magnitudes of these forces.
2. Re-design the footform to include rotational springs at the ankle and MPJ to store and return energy during the ground contact, thereby increasing the push off forces.

9.4.2 Ground Contact Times

The ground contact time for the robot when it is programmed with real human kinematic data is 1.34 seconds, which is more than double that of the target (214%) human value of 0.63 seconds. The discrepancy is even larger for the programme that has been modified to have a more substantial impact peak; as mentioned the shape of this profile is closer to that of the target but the ground contact time is 1.82 seconds – a difference of nearly 300%.

These differences in ground contact time would appear to be an improvement on the 600% documented by Ronkainen *et al* 2010, but it must be remembered that was an attempt to emulate running, which is associated with much shorter ground contact times (typically 0.2 seconds). This helps to justify the decision to attempt to emulate walking before running, with a potential advancement over the previous work in the observation that the output was closer to the target set by the input. Despite this, the ground contact time using the human kinematic data remains a major limitation and justification that programming the robot in this manner may not be the best approach.

One of the main contributing factors to the increased footprint and therefore ground contact time was the influence of robotic smoothing. As already discussed, maximum levels of robotic smoothing were applied with the aim of producing the fastest and smoothest trajectory. However, this action has an adverse effect on the trajectory of the footform; the trajectory of the human heel in the sagittal plane, for example, is in the form of a 'v-shaped' trough, the application of smoothing turns this into a shallower 'u-shaped' trough which cuts out the lowest point of the 'v'. This means that in order to achieve adequate vertical ground reaction force magnitudes the entire programme had to be vertically offset downwards. With a shallower motion trajectory this means that more of the trajectory is involved in the ground contact phase resulting in a greater ground contact time and larger footprint.

The previous statement can be corroborated by analysing the ground contact times of the robot programmes based on the rotation about an individual point (figures 9.3.2 and 9.3.4). As previously mentioned, the time of maximum peak force for each rotation movement has been matched to its respective peak on the human profile. Although the ground contact times still haven't been matched the differences are much smaller than those of the robot programmed with human kinematic data. The heel rotation programme appears to have an extra 0.1 seconds at the start of the motion and the MPJ rotation takes slightly longer to finish. However, the unloading rates appear to be well matched between the robot and human data and the additional time is attained with very little force acting on the footform. When the

two profiles are combined, the robot has a ground contact time of approximately 0.2 seconds longer than the human data, this difference of 128% is a vast improvement upon previous attempts made using the robot. Start position for the heel rotation programme and finish position for the MPJ rotation programme had negligible effect on ground contact time.

9.4.3 Centre of Pressure

The centre of pressure (CoP) is an indication of where the forces are acting on the footform and is an important parameter to consider (Rodgers 1998). Figures 9.3.5 and 9.3.6 show the centre of pressure acting on the footform for each of the robot programmes as a percentage of foot length (0% is the heel and 100% is the toe). The human kinematic profiles aren't able to successfully emulate the positions of the centre of pressure on the shoe. The trend is for the position of the CoP to remain on the rearfoot for too long before moving rapidly to the forefoot and toes for the final point of ground contact. The CoP is never near the posterior aspect of the heel indicating that the initial impact occurs further towards the centre of the foot compared to human walking.

Although they are still not an exact emulation, the CoP for the rotation programmes, specifically the rotation about the heel, are a much better emulation. After matching the points of maximum force it is already known that the heel rotation profile contacts the ground early, however the relationship between the CoP and the heel is consistent with the human results. The emulation is not as accurate for the rotation about the MPJ, there are good matches at midstance and toe-off but trace deviates from the human between these phases, with the CoP moving closer to the toe. This is due to the footform being much stiffer than the human foot at the MPJ and thus much lower flexion occurs at this point. This causes the forces to move rapidly to the most distal part of the footform and similarly the CoP. Despite the previous statement and although there is still room for improvement, the CoP's for the rotation programmes are much more biofidelic than those of the human kinematic programmes.

9.4.4 Footform Kinematics

Figure 9.3.7 is a schematic showing the kinematics of the footform of each robot programme relative to the real human foot at each of the main points of ground contact. Each instance documents the two-dimensional position of the markers at the heel, MPJ and toe. This helps to visualise the orientation of the foot, the angle of the MPJ and its position in the anterio-posterior direction for each programme. One of the most notable features is that for the human kinematic programmes, the size of the footprint is much larger than that of the human subject (figure 9.3.8). It is clear that this trend starts to develop early on in the ground contact phase. The footprint for real human walking is 0.36m which compares to the human kinematic robot programmes producing a footprint of 0.54m and 0.57m respectively (table 9.3.1). As previously mentioned in Chapter 5 this can be attributed to robotic smoothing and the effect of having to vertically offset the programme downwards to achieve adequate force magnitudes. Emulation of the two-dimensional trajectory was much more successful for the programmes with a fixed point of rotation, as shown in figure 9.3.9.

As already alluded to, there have been difficulties in generating a propulsive force, the fact that there is very little MPJ flexion for the human kinematic programmes at toe-off may be a considerable factor. The human kinematic programmes provide a very poor representation of the MPJ angle (figure 9.3.12), it is too small initially, too large in the middle part of ground contact and too small at the end. The MPJ angle produced by the rotation programmes (figure 9.3.13) also fail to fully emulate the human subject. As before the angles appear to remain constant at between 10 and 20 degrees until the end of ground contact. It appears the carbon blade fibre representing the forefoot is much stiffer around the MPJ (section 7.2) compared to the human foot (section 3.1).Considering the angle of the plantar aspect of the foot relative to the ground, the human kinematic profiles have a much slower transition to the foot being flat at midstance. The footform doesn't appear to be in this phase for as long as the human before moving into the final phase with a much more biofidelic foot angle, this trait is also shown in figure 9.3.10. The angles of the foot during the first phase of ground are better emulated when programmed with a

rotation about the heel figure 9.3.11, with a very close angle match at the point of the first peak and with a more realistic period of the footform being flat in midstance. This is less so the case for the rotation about the MPJ where the foot angles appear to be too large compared to the human subject. This is because the programme has been instructed to rotate past the suggested value in order to generate sufficient vertical ground reaction forces, a parameter that has been deemed more important in assessing wear patterns on the shoe. However, it never exceeds the human value at toeoff so could therefore be increased further.

As part of the overall evaluation of the robots ability to emulate human gait it is important to see how it compares to other existing robotic test devices (section 3.4.1). The lack of available data makes it difficult to draw comparisons with the pedatron and Stewart platform. It is also difficult to conduct a direct comparison with the work of De Raeve *et al* (2014) due to a further lack of data, however this has been reported to have good kinematic and vertical ground reaction force emulation. Starker *et al* (2013) appear to have had similar levels of success to the work outlined in this thesis, with accurate emulation of vertical ground reaction forces with less control over their loading rates. In some cases this was achieved through manual adaptation of the programmes, as was the case in this investigation. They also appear to have had less success in emulating horizontal ground reaction forces with larger than expected magnitudes and single phase profiles evident. In a follow up investigation Starker *et al* (2014) used a tilt table to emulate the human running gait. They had difficulties in doing this at full seed and as such could only emulate features whilst running at 60% of running velocity, this problem is not too dissimilar to that encountered by Ronkainen *et al* (2010) when using the FANUC. The adidas wheel wear machine (WWM) investigated by Mara (2007) attempts to emulate the human running gait. Although it is able to attain force magnitude and loading rates, there are numerous force peaks that follow an un-typical shape over a long time period (figure 3.4.2). There appear to be similar issues as shown when using the human kinematic data programme. The rotation programmes for the FANUC produce more realistic virtual ground reaction forces than the WWM.

9.5 CONCLUSIONS

The primary aim of chapter was to use the FANUC R-2000iB robot to emulate the ground contact phase of human walking and thereby directly address research question four of this thesis. The success of the emulation was based primarily on the match of the vertical and anterio-posterior ground reaction forces, loading rate and centre of pressure position between the robot and the human data. Based on the results presented the following conclusions can be drawn:

- When the robot is programmed directly with the human kinematic data the success of the emulation is relatively poor; the ground contact time is too long with an increased footprint size and poor ground reaction force profile replication. Specifically the lack of an impact peak and very large braking forces throughout.
- Using the rotation method each of the respective vertical ground reaction forces have been matched. The loading rate of the impact peak is too low, but the loading and unloading rates of the second peak are a good match. When combined it is shown that it is difficult to match the midstance trough of the force profile, but this is acceptable as most of the force acting on the shoe are at the peaks as opposed to a lower force being spread more evenly.
- The anterio-posterior ground reaction forces have proved difficult to emulate, the magnitudes are larger than they should be and tend to be braking throughout, with very little evidence of a propulsive force being applied.
- Compared to the human kinematic programmes the rotation method produces a ground contact time that is significantly closer to that of the real human time. The same can also be said for the size of the footprint, which is significantly reduced for the rotations programmes compared to the human kinematic programmes and are much closer to the target.
- Despite not being a wholly accurate emulation of the human footstrike, it can still be claimed that the outcome of this study is as good as, or better than

what has been done before both at Loughborough University and more broadly.

- It can be suggested that in its current set-up, the capabilities of the robot have been reached. Introducing an improved footform with MPJ and/or ankle compliance and possibly horizontal compliance the key suggestions to further improve the emulation.

CHAPTER 10

CONCLUSIONS

10.1 INTRODUCTION

The overall aim of this thesis was to investigate using a FANUC R2000*i*-B six degrees-of-freedom (6 DoF) industrial robot to emulate the ground contact phase of human gait The work documented in the previous chapters has linked together to form a body of work that has intention of achieving this aim.

10.1.1 Aims

This Chapter aims to assess the success of the previous Chapters in meeting the overall thesis aim; whilst outlining its limitations and any areas of potential improvement.

10.1.2 Objectives

The above aim will be achieved through the following objectives:

- To assess the research questions outlined in Chapter 1 and how successfully they have been addressed.
- To introduce potential areas of future work that can strengthen the potential of using the FANUC to emulate human gait.

10.2 RESEARCH QUESTIONS

In Chapter 1 (page 4), four research questions were introduced. By addressing these questions, adequate steps would be taken to achieve the overall thesis aim of emulating the human gait. The following sections outlines the success in addressing each research question.

10.2.1 Research Question One

What are the biomechanical features that need to be emulated and what are typical values for them?

Research question one is primarily addressed in Chapter 2 and Chapter 3, the gathered information was also used to support the subsequent research questions. A comprehensive review of current literature was presented in Chapter 3, one of the main topics was the interaction between the foot and ground during gait. From this information a list of key kinematic and parameters were identified as being important in both programming the robots movements and evaluating its outcomes. In terms of using the robot for durability testing of footwear the vertical and anterio-posterior forces, vertical loading rate and point of force application were considered as key to evaluating the success of the emulation.

The above premise was taken further in Chapter 3 which aimed to measure the kinematics and kinetics of the gait of one human subject. The collected data was used in programming the robot, as described in Chapter 4 and as a validation for the output robot kinetics and kinematics (Chapter 9).

10.2.2 Research Question Two

What are the capabilities of the robot and what are the intricacies of its operation?

Research question two is answered by Chapters 4, 5 and 6; all three are chapters concentrated on the robot and its operation. The work of Ronkainen *et al* (2010) emphasised the fact that it was important to have an understanding of the robots basic operating principles and performance capabilities before using for more complex tasks.

In Chapter 2 the FANUC robot was introduced, with an explanation on how it is programmed. The concept of robotic smoothing is first introduced, which is fully investigated in Chapter 5 where its effect is documented alongside that of velocity and the number of programmed co-ordinate points. It was found that the output kinematics of the robot were influenced by all three variables, indicating that the features within the control system and the way in which the robot is programmed affect the resultant motion.

Chapter 6 assessed the relationship between the robot and the computer software RoboGuide for both complex and simple movements. The main conclusion was that RoboGuide was able to simulate simple two-dimensional movements but was less successful in more complex movements such as a human heelstrike running. The features identified in Chapter 5 are also a factor when programming the robot using RoboGuide. These findings led to the conclusion that RoboGuide has only limited use in supporting the wider thesis aim. Despite this, it was still relevant in supporting subsequent research questions.

10.2.3 Research Question Three

How can the robot set-up be configured to emulate the ground contact phase of the human gait?

Chapters 7 and 8 document the process of optimising the robot set-up for best emulating human gait which directly addresses research question three. Chapter 7 aimed to designed develop and test a new robot end-effector, the need for which became apparent upon evaluating the original end-effector. A number of design concepts were introduced and benchmarked against the former in a number of areas. The final design solution (figure 7.4.2) is biofidelic both in terms of the footform and built in compliance, it also introduced a new way of generating the required motion. This end-effector was then used in the final gait emulation tests on the robot (Chapter 9).

Chapter 8 investigated the potential of relocating the force platform within the robot cell to reduce ground contact time in footstrike emulation to closer to the value for the human footstrike. This RoboGuide based analysis found that there were alternate force platform locations that may provide a quicker movement time compared to the original location. However, the optimum location differed for the original and new end-effector designs. The results were then validated on the real robot. Despite these findings it was decided that the force platform would not be relocated, as the gains in total run time were negligible for the linear new bearing end-effector.

10.2.4 Research Question Four

To what degree can the robot be used to accurately emulate human gait?

The outcomes of research questions one to three were all used to assist in the investigation conducted in Chapter 9 which addresses research question four. The aim of the overall thesis is mirrored in the aim of Chapter 9 which was to use the FANUC R-2000iB robot to emulate the ground contact phase of human walking. The success of the emulation was based primarily on the match of the vertical and anterio-posterior ground reaction forces, loading rate and centre of pressure position between the robot and the human data. The primary conclusion was that when the robot is programmed directly with the human kinematic data the emulation is poor; the ground contact time is too long with an increased footprint size and poor ground reaction force profile replication. Specifically the lack of an impact peak and very large braking forces throughout. Using a rotation about a fixed point on the footform gait emulation was improved.

Vertical ground reaction force magnitudes were well matched, the loading rates were much closer to the human values, however, the horizontal forces remained difficult to emulate. Ground contact time was significantly closer to that of the real human times was the footprint. Furthermore, when compared to existing robotic devices for footstrike emulation the current results appear as good as or better than what has previously been achieved.

10.3 SUMMARY

The thesis research questions have been addressed with various degrees of success. Which in turn has led to the partial fulfilment of the overall thesis aim of using the FANUC robot to emulate human gait. The approach involved gaining an understanding of the biomechanical features of human gait that can be used to help programme the robot. Before emulation could begin the robots set-up was optimised to maximise the potential outcomes.

The emulation quality was lower when the robot was programmed with human kinematic data as opposed to a rotation about a fixed point. This method has also showed an improvement on the previous work of Ronkainen *et al* (2010) specifically in the area of ground contact time, loading rates and areas of force application, all important parameters when assessing the wear of footwear in industry.

There are a number of other test devices that attempt to emulate the human gait, i.e. the pedatron, the WWM, KUKA and ABB 6 DoF industrial robots (section 4.2.1). There are some aspects in which the FANUC represents an improvement on these, for example vertical ground reaction force and ground contact time, and there are some aspects where little or no advancements have been made, for example horizontal ground reaction forces. Referring back to figure 1.2.1 in Chapter 1, the FANUC still has a long way to move along the scale to be able to reproduce an accurate human gait emulation. At this stage it fits onto the scale alongside the existing mechanical devices.

At the commencement of this PhD the novelty of the work lay in the fact that an off the shelf six DoF industrial robot for footwear testing has not previously been explored. Although footstrike emulation using similar robots has since been attempted by a number of other institutions (De Raeve *et al* 2014 and Starker *et al* 2014) with varying degrees of success. The specific approaches taken have differed, for example end-effector designs (figure 2.4.3 and figure 2.4.5), as well as the application focus (use within the medical sector for example). Furthermore, despite still being in its infancy, the novelty of the current thesis remains valid.

10.4 FUTURE WORK

Upon completion of this thesis it is apparent that the FANUC has not been able to wholly satisfy the initial aim of emulating the human gait. There have been some successful emulation aspects, but there have also been some short comings. However, these short comings have not been to such a degree that that they cannot be overcome in the future and as such there is still potential for the FANUC to be able to emulate human gait going forward.

In its current set-up, the capabilities of the robot appear to have been reached, altering this may prove to be more fruitful. A logical starting point for subsequent work would be to improve the footform used as part of the end-effector outlined in Chapter 7. The improved design could have compliance at the MPJ or ankle joints and potentially a horizontal compliance. These additions would hopefully improve the ground reaction force emulation, with potential for aiding the transition from midstance to toeoff. One of the major limitations to the current system is the lack of propulsive force that is generated, making the footform more biofidelic may improve this. It may also allow for alterations to be made to the robot trajectory, with less emphasis on the robot pulling the footform through ground contact as opposed to a more dynamic interaction with the ground.

A further improvement to the footform/end-effector configuration could be to add weight to the top of the linear slide. This alteration may make it easier to achieve the first peak of the vertical ground reaction force profile with more adequate loading rates, reducing the requirement for a large vertical offset at ground contact, this is especially the case for the robot programmed with real human kinematic data. This addition may also improve the chances of achieving a propulsive force as it would be pushing the footform into the ground at toeoff as opposed to the robot solely pulling it away.

The most positive aspects of footstrike emulation occur when the robot is programmed to rotate about a fixed point at either the heel or MPJ, these best represent the two halves of the ground contact phase. In some instances the results have been merged to document the relationship to an entire footstrike. The nature of programming the robot means that only one centre point of rotation can be applied to each programme. Moving forward it may be worthwhile investigating the ease at which this feature can be overridden and allow for the creation of a programme in which the centre point of rotation would move from the heel to the MPJ half way through.

Once the emulation process has become more accurate, it would be of interest to see the effects of instructing the robot to perform multiple footstrikes in succession, similar in focus to the work of Ronkainen *et al* (2010). This would bring the robot in line with what is required of an accelerated wear device for testing footwear and thus improve its potential for being used in the athletic footwear industry. In addition, alternative footstrikes could be considered since the current work has been based on the data from a single typical young healthy adult male.

Other sports applications could be investigated and benefit from some of the general understanding of the robots capabilities developed within this thesis.

REFERENCES

ABB Robotics, 2014. *IRB 6640 Product Overview.* [Online]
Available at:
http://www.abb.co.uk/product/seitp327/df458c1c0223a1aec1257363006dd9b3.aspx?productLanguage=us&country=GB
[Accessed July 2014].

Aerts, P., Ker, R. F., DeClercq, D. and Ilsley, D. W. (1996). "The effects of isolation on the mechanics of the human heel pad." Journal of Anatomy 188: 417-423.

American Standard for Testing Materials (ASTM).,(200). ASTM F1614-99 (2006) 'Standard Test Method for shock Attenuating Properties of Materials Systems for Athletic Footwear [Online] Available at:
http://enterprise.astm.org/filtrexx40.cgi?+REDLINE_PAGES/D395.htm
[Accessed 30 July 2014].

Arampatzis, A., Bruggemann, G-P. and Klapsing, G. M. (2000). "Control Of Leg Stiffness And Its Effect On Mechanical Energetic". *18 International Symposium on Biomechanics in Sports.*

Bates, B. T., Osternig, L. R., Sawhill, J. A. and James, S. L. (1983). "An assessment of subject variability, subject-shoe interaction, and the evaluation of running shoes using ground reaction force data." Journal of Biomechanics 16(3): 181-191.

Baycroft, C. M. and Culp, V. (1993). "Running Shoes - Design Facts and Functional Fantasies." Chiropratic Sports Medicine 7(1): 6-8.

Bobbert, M. F., Yeadon, M. R. and Nigg, B. M. (1992). "Mechanical analysis of the landing phase in heel toe running." Journal of Biomechanics 25(3): 223-234.

Bojsenmoller, F. (1979). "Calcaneocuboid joint and stabillity of the longitudinal arch of the foot at high and low gear push off." Journal of Anatomy 129(AUG): 165-176.

Buschmann, W. R., Jahss, M. H., Kummer, F., Desai, P., Gee, R. O. and Ricci, J. L. (1995). "Histology and histomorphometric analysis of the normal and atrophic heel fat pad." Foot & Ankle International 16(5): 254-258.

Canoso, J. J., Liu, N., Traill, M. R. and Runge, V. M. (1988). "Physiology of the retrocalcaneal bursa." Annals of the Rheumatic DIiseases (The EULAR Journal) 47(11): 2.

Cavagna, G. A. (1977). "Storage and Utilization of Elastic Energy in Skeletol Muscle." Exercise and Sports Science Reviews 5: 89.

Cavanagh, P. R. and Lafortune, M. A. (1980). "Ground reaction forces in distance running." Journal of Biomechanics 13(5): 397-406.

Challis, J. H., Murdoch, C. and Winter, S. L. (2008). "Mechanical Properties of the Human Heel Pad: A Comparison Between Populations." Journal of Applied Biomechanics 24(4): 377-381.

Chase, A. W. (2009). "The anatomy of a running shoe." Competitor: 40-40.

Cheung, J. T. M., Zhang, M. and An, K. N. (2006). "Effect of Achilles tendon loading on plantar fascia tension in the standing foot." Clinical Biomechanics 21(2): 194-203.

Cole, G. K., Nigg, B. M., Fick, G. H. and Morlock, M. M. (1995). "Internal loading of the foot and ankle during impact in running." Journal of Applied Biomechanics 11(1): 25-46.

Cole, G. K., Nurse, M., Miller-Young, J. and Hawes, M. (2001). “Functional zones of the shoe.” Technical report in conjunction with adidas - G. K. Cole. Calgary, University of Calgary - Kinesiology.

Declercq, D., Aerts, P. and Kunnen, M. (1994). "The mechanical characteristics of the human heel pad during foot strike in running - an in-vivo cineradiographic study." Journal of Biomechanics 27(10): 1213-&.

Denoth, J. (1986). “Load on the Locomotor System and Modelling. Biomechanics of Running Shoes.” B. M. Nigg. Champaign, Illinois, Human Kinetics: 110-112.

De Raeve, E., Saey, T., Muraru, L. and Peeraer, L. (2014). “The use of a robotic gait simulator for the development of an alignment tool for lower limb prostheses.” *4th Congress of the International Foot and Ankle Biomechanics Community,* 7(1).

Dickinson, J. A., Cook, S. D. and Leinhardt, T. M. (1985). "The measurement of shock-wave following heel strike while running." Journal of Biomechanics 18(6): 415-422.

Drake, R. L., Vogl, W. and Mitchell, A. W. (2005). Gray's Anatomy for Students, Elsevier Churchill Livingstone. pp: 557-584.

Endo Lite. *The Elite VT (image reproduction).* [Online]
Available at: www.endolite.co.uk
[Accessed November 2011].

FANUC-Robotics. (May 2010). from http://www.fanucrobotics.co.uk/en/Products/Software/SIMULATION%20and%20DEVELOPMENT/Roboguide.aspx.

FANUC,. *RJ3 Programming Manual.* s.l.:FANUC Robotics (2009).

Ferrandis, R., Garcia, A. C., Ramiro, J., Hoyos, J. V. and Vera, P. (1994). "Rearfoot motion and torsion in running - the effects of upper vamp stabalizers." Journal of Applied Biomechanics 10(1): 28-42.

Floyd, R. T. (2007). “Manual of Structural Kinesiology.” New York, McGraw-Hill Highe Education.

Frederick, E. C. (1989). The Running Shoe: Dilemmas and Dichotomies in Design. The Shoe in Sport. B. Segesser and W. Pforringer. London, Wolfe Publishing ltd.

Frederick, E. C., Hagy, J. L. and Mann, R. A. (1981). "The prediction of vertical impact force during running." Journal of Biomechanics 14(7): 498-498.

Gerritsen, K. G. M., van den Bogert, A. J. and Nigg, B. M. (1995). "Direct dynamics simulation of the impact phase in heel-toe running." Journal of Biomechanics 28(6): 661-668.

Giakas, G. Baltzopoulos, V., (1997). "Time and frequencey domain analysis of ground reaction forces during walking: an investigation of variability and symmetry". *Gait and Posture,* Volume 5, pp. 189-197.

Gibbs, P. J. (2006). Advanced modelling of sports footwear. PhD Thesis - Sports Technology Institute. Loughborough, Loughborough University. Doctor of Philosophy

Glaister, B. C., Bernatz, G. C., Klute, G. K. and Orendurff, M. S. (2007). "Video task analysis of turning during activities of daily living." Gait & Posture 25(2): 289-294.

Glaister, B. C., Schoen, J. A., Orendurff, M. S. and Klute, G. K. (2007). "Mechanical behavior of the human ankle in the transverse plane while turning." Ieee Transactions on Neural Systems and Rehabilitation Engineering 15(4): 552-559.

Graaff, V. d. (1998). Human Anatomy, McGraw Hill.

Hansen, A H., Childress, D, S., Miff, S. C., Gard, S. A., Mesplay, K. P. (2004). "The human ankle during walking: implications for design of biomimetic ankle prosthesis". *Journal of Biomechanics,* Volume 37, pp. 1467-1474.

Hasegawa, H., Yamauchi, T. and Kraemer, W. J.; (2007). "Footstrike Patterns of Runners at the 15-KM Point During an Elite- Level Half Marathon". *Journal of Strength and Conditioning Research,* 21(3), pp. 888-893.

Hay, J. G. (1993). The Biomechanics of Sports Techniques, Prentice Hall.

Hennig, E. M. and Milani, T. L. (1995). "In-shoe pressure distribution for running in various types of footwear." Journal of Applied Biomechanics 11(3): 299-310.

Hennig, E. M., Valiant, G. A. and Liu, Q. (1996). "Biomechanical variables and the perception of cushioning for running in various types of footwear." Journal of Applied Biomechanics 12(2): 143-150.

Hicks, J. H. (1954). "The mechanics of the foot .2. The plantar aponeurosis and the arch." Journal of Anatomy 88(1): 25-&.

Higginson, B. K. (2009). "Methods of Running Gait Analysis." Current Sports Medicine Reports 8(3): 136-141.

Hilgers, M. P., Mayer, B. and Walther, M. (2009). "Current Trends in Athletic Shoe Design." Athletic Therapy Today 14(6): 4-8.

Hubbard, J. (2009). Private Communication - Description of the SATRA Pedatron

Hunt, A. E., M. Smith, R., Torode, M. and Keenan, A.-M. (2001). "Inter-segment foot motion and ground reaction forces over the stance phase of walking." Clinical Biomechanics 16(7): 592-600.

Jahss, M. H., Michelson, J. D., Desai, P., Kaye, R., Kummer, F., Buschman, W., Watkins, F. and Reich, S. (1992). "Investigations into the fat pads of the sole of the foot - anatomy and histology." Foot & Ankle 13(5): 233-242.

Jin X. and Yang X. (2009). *Off-Line Programming of a Robot for Laser Re-Manufacturing.* Tsinghua Science and Technology 14(1): 186-191.

Johnson, T. E. (1996). Running and Court Shoe. Sports and Fitness Equipment Design. E. F. Kreighbaum and M. A. Smith. Champaign, IL, Human Kinetics: 15-30.

Ker, R. F. (1996). "The time-dependent mechanical properties of the human heel pad in the context of locomotion." Journal of Experimental Biology 199(7): 1501-1508.

Ker, R. F., Bennett, M. B., Kester, R. C. and Alexander, R. M. (1989). "Foot strike and the properties of the human heel pad." Journal of Engineering in Medicine 203: 191-196.

Kistler. "Product Information." Retrieved May 2010, from http://www.kistler.com/gb_en-gb/131_Productfinder_ForceSensors/F1000/Product-Finder-Force.html.

Kogler, G. F., Solomonidis, S. E. and Paul, J. P. (1996). "Biomechanics of longitudinal arch support mechanisms in foot orthoses and their effect on plantar aponeurosis strain." Clinical Biomechanics 11(5): 243-252.

KUKA Robotics, (2014). *KR 150 R2700 EXTRA.* [Online]
Available at: http://www.kuka-robotics.com/united_kingdom/en/products/industrial_robots/high/extra/kr150_r2700_extra/start.htm
[Accessed July 2014].

Ledoux, W. R. and Blevins, J. J. (2007). "The compressive material properties of the plantar soft tissue." Journal of Biomechanics 40: 2975-2981.

Liu LX. Yang X. *et al.* (2011). *Planning Strategies for Surface Hardening by Laser Robot.* Advanced Materials Research 383-390: 6324-6328.

Mann, R. A., Moran, G. T. and Dougherty, S. E. (1986). "Comparative electromyography of the lower-extremity in jogging, running and sprinting." American Journal of Sports Medicine 14(6): 501-510.

Mara, G. E. (2007). Boundary Conditions for the Virtual Testing of Athletic Footwear. Sports Technology Institute. Loughborough, Loughborough University. Doctor of Philosophy: 300.

McClay, I. S., Robinson, J. R., Andriacchi, T. P., Frederick, E. C., Gross, T., Martin, P., Valiant, G., Williams, K. R. and Cavanagh, P. R. (1994). "A Profile Of Ground Reaction Forces In Professional Basketball." Journal of Applied Biomechanics 10(3): 222-236.

Mills, N. J. (2003). Running Shoe Materials. Materials in Sports Equipment. M. Jenkins. Cambridge, Woodhouse Publishing Ltd.: 65-99.

Monckton, S. P. and Chrystall, K. (May 2002). “Design and Development of an Automated Footwear Testing System.” IEEE International Conference on Robotics & Automation, Washinton DC, IEEE.

Munro, C. F., Miller, D. I. and Fuglevand, A. J. (1987). "Ground Reaction Forces a Reexamination." Journal of Biomechanics 20: 147-155.

Newton Running, (2013). *Greater Shoe Efficiency - Test Methods.* [Online]
Available at: http://www.newtonrunning.co.uk/why/shoe-tests.html
[Accessed July 2014].

Nigg, B. M., Bahlsen, H. A., Luethi, S. M. and Stokes, S. (1987). "The influence of running velocity and midsole hardness on external impact forces in heel toe running." Journal of Biomechanics 20(10): 951-959.

Nigg, B. M. and Herzog, W., Eds. (2005). Biomechanics of the Musculo-skeletal System, Wiley.

Novacheck, T. F. (1998). "The Biomechanics of Running." Gait & Posture 7: 77-95.

Odenwald, S., (2006). Test Methods in the Development of Sports Equipment. *The Engineering of Sport 6,* Volume 2, pp. 301 - 306.

Oleson, M., Adler, D. and Goldsmith, P. (2005). "A comparison of forefoot stiffness in running and running shoe bending stiffness." Journal of Biomechanics 38(9): 1886-1894.

Oando. *The Ossu Ceterus.* [Online]
Available at: http://www.oandp.com/articles/news_2002-04-30_27.asp
[Accessed November 2011].

Otto Bock. *The Otto Bock Trias.* [Online]
Available at:
http://corporate.ottobock.co.uk/cps/rde/xchg/ob_uk_en/hs.xsl/1998.html
[Accessed November 2011].

Pain, M. T. G. and Challis, J. H. (2001). "The role of the heel pad and shank soft tissue during impacts: a further resolution of a paradox." Journal of Biomechanics 34(3): 327-333.

PRWeb, 2013. *Global Athletic Footwear Industry Analyzed by Transparency Market Research.* [Online]
Available at: http://www.transparencymarketresearch.com
[Accessed 21 October 2013].

Pugh, S., (1991). Total Design - Integrated Methods for Successful Product Engineering. In: Harlow, ed. s.l.:Pearson Education Ltd., pp. 44-65.

Reber, L., Perry, J. and Pink, M. (1993). "Muscular control of the ankle in running." American Journal of Sports Medicine 21(6): 805-810.

Rome, K., Webb, P., Unsworth, A. and Haslock, I. (2001). "Heel pad stiffness in runners with plantar heel pain." Clinical Biomechanics 16(10): 901-905.

Ronkainen, J., Roberts, M., El-Kati, R., Roberts, B., Forrester, S. and Fleming, P. (2008). Replicating Human Running: Implementation of A 6 Degree of Freedom Industrial Robot in the Sports Domain, Loughborough University Institute of Sports Technology.

Root, M. L., Orien, W. P. and Weed, J. H. (1977). "Normal and abnormal function of the foot." Clinical Biomechanics Corporation.

SATRA-TECHNOLOGY-CENTRE (2009). Test Equipment Catalogue, SATRA: 1.

Scott, S. H. and Winter, D. A. (1990). "Internal forces at chronic running injury sites." Medicine and Science in Sports and Exercise 22(3): 357-369.

Shorten, M. (2009). "Plantar pressure distribution and footwear design. ." Footwear Science 1 (88-90.).

Standring, A., Ellis, H., Healy, J. C., Johnson, D. and Williams, A., Eds. (2005). Gray's Anatomy, Elsevier Churchill Livingstone.

Starker, F., Dennerlein, F., Balb, F. and Schneider, U. (2013). Simulation des Prothesen-gangs mittels eines.Sech-Achs-Roboters. *Prothetik*

Starker, F., Dennerlein, F., Balb, F. and Schneider, U. (2014). A Method for Sports Shoe Machinery Endurance Testing: Modification of ISO 22675 Prosthetic Foot Test Machine for Heel-to-toe Running Movement.. *The Engineering of Sport 10,* Volume 72, pp. 405-410.

Stefanyshyn, D. J. and Nigg, B. M. (1997). "Mechanical Energy Contribution of the Metatarsophalangeal Joint to Running and Sprinting." Journal of Biomechanics 30: 1081-1085.

Stewart, D. (1995). A Platform with 6 Degrees of Freedom. Institute of Mechanical Engineering, Proceedings. 180 I, no 15: 371-385.

The Stewart platform (image), web link, reproduced from: http://www.robotik.jku.at/joomla16/index.php/forschung/research-projects/stewart-gough-plattform

VICON. "Product INformation - NEXUS." Retrieved May 2010, 2010, from http://www.vicon.com/products/.

Weijers, R. E., Kessels, A. G. H. and Kemerink, G. J. (2005). "The damping properties of the venous plexus of the heel region of the foot during simulated heelstrike." Journal of Biomechanics 38(12): 2423-2430.

Weijers, R. E., Mameren, H. V., Walenkamp, G. H. and Hout, J. A. A. M. V. D. (2003). "Changes of the soft tissue of the forefoot during loading: a volumetric study." Foot 12: 70-75.

APPENDIX 1

PRODUCT DESIGN SPECIFICATION FOR NEW END-EFFECTOR

Part of the process for designing the new end-effector in Chapter 7 was the creation of a product design specification. As described by Pugh (1991), this was created with specific directive triggers for the design. A summary of this was shown in section 7.3 and the full version is outlined below:

Performance: The purpose of the device is to enable the end-effector as a whole to emulate the role of the human leg and foot complex during the foot-ground contact phase for walking. The device is to be loaded to up to 850N (±50N) over a period of 0.1 seconds, the unloading period is approximately 0.3 seconds followed by a 0.8 seconds period where the only applied load is due to the gravitational pull of the linear slide and foot. This total of 1.2 seconds is the time that it takes for one for one complete gait cycle. A small level of can be applied to these times, so long as the overall cycle time remains at 1.2 seconds. As part of repetition trials, the device will be subjected to multiple footstrike cycles, it is anticipated that the device will be subjected to the same parameters as above with little recovery time between each.

Environment: The product is to be stored and operational at room temperature, with normal pressures and humidity levels. Loading forces of up to 3000N at a loading rate of 200KN/s with the associated vibrations are expected. Any parts that will have an inhibited performance due to dust and dirt should be protected or easy to clean.

Maintenance: Regular checks and detailed services are readily available; with brief visual checks taking place prior to almost every use. To simplify processes tasks such as joint lubrication should be made as easy as possible.

Size: The product must be mounted onto the sixth joint of the robot with a circular plate (diameter 160mm), using two-eight 10mm bolts (20mm in length), through boltholes separated at 45 degrees located 60mm from the centre of the plate. The product needs to be of a size so that when attached to the robot, the robot itself and end-effector remain within the desirable work envelope, as identified in chapter 8.

Weight: The robot is capable of manipulating 165Kg, excess/needless weight may compromise the force generation, so weight should be kept to a minimum, without affecting strength or durability.

Appearance/ Aesthetics: The initial design is not intended for public release, therefore there are no visual constraints, but there should be enough space to display the Loughborough University logo. The product must be able to hold a footform that has the ability to interact with the surface.

Materials: The use of existing readily available materials is preferable and they must conform to the 'Weight' and 'Environment' specifications (see relevant section). The materials should be, as much as possible, resistant to wear and tear and not be

dangerous to handle. For some sections the materials chosen will need to be as biofidelic as possible.

Lifespan: A life expectancy of 2 years is expected, however, It is likely that the product will evolve over time following subsequent investigations, it should be designed as best as possible, with realistic constraints allowing it to best fulfil the intended aims. The potential of future developments and changes should be factored into the design.

Storage: The device is to be stored in laboratory conditions, in some circumstances the device may be left attached to the robot for a period of time without use. There will be no limitations on shelf life, since the product is of a non-organic nature.

Testing: As this is a one off design, testing will be carried out in the conceptual design stage leading to subsequent design iterations, that conform to the PDS.

Patents: The device is novel, in the fact that it is key in helping to achieve human footstrike emulation using an industrial 6 degrees-of-freedom robot. There are no plans for a patent to be applied for, but this could change in the future.